สมบัติพลวัตรของดินทรายเชียงใหม่โดยการทดสอบแรงเฉือนอย่างง่ายแบบวัฏจักร

นาย ชกชาน เต

วิทยานิพนธ์นี้เป็นส่วนหนึ่งของการศึกษาตามหลักสูตรปริญญาวิศวกรรมศาสตรมหาบัณฑิต
สาขาวิชาวิศวกรรมโยธา ภาควิชาวิศวกรรมโยธา
คณะวิศวกรรมศาสตร์ จุฬาลงกรณ์มหาวิทยาลัย
ปีการศึกษา 2552

DYNAMIC PROPERTIES OF CHIANG MAI SAND USING CYCLIC DIRECT SIMPLE SHEAR TEST

Mr. Soksan Thay

A Thesis Submitted in Partial Fulfillment of the Requirements
for the Degree of Master of Engineering Program in Civil Engineering
Department of Civil Engineering
Faculty of Engineering
Chulalongkorn University
Academic Year 2009

Thesis Title	DYNAMIC PROPERTIES OF CHIANG MAI SAND USING CYCLIC DIRECT SIMPLE SHEAR TEST
By	Mr. Soksan Thay
Field of Study	Civil Engineering
Thesis Advisor	**Assistant Professor Suched Likitlersuang, D. Phil.**

Accepted by the Faculty of Engineering, Chulalongkorn University in Partial Fulfillment of the Requirements for the Master's Degree

.....Dean of the Faculty of Engineering
(Associate Professor Boonsom Lerdhirunwong, Dr. Ing.)

THESIS COMMITTEE

.....Chairman
(Associate Professor Supot Teachavorasinskun, D. Eng.)

.....Thesis Advisor
(Assistant Professor Suched Likitlersuang, D. Phil.)

.....Examiner
(Associate Professor Boonchai Ukritchon, Sc. D.)

.....Examiner
(Associate Professor Tirawat Boonyatee, D. Eng.)

.....External Examiner
(Assistant Professor Siam Yimsiri, Ph. D.)

ชกชาน เต: สมบัติพลวัตรของดินทรายเชียงใหม่โดยการทดสอบแรงเฉือนอย่างง่ายแบบวัฏจักร (DYNAMIC PROPERTIES OF CHIANG MAI SAND USING CYCLIC DIRECT SIMPLE SHEAR TEST) อ.ที่ปรึกษาวิทยานิพนธ์หลัก: ผศ.ดร.สุเชษฐ์ ลิขิตเลอสรวง, 105 หน้า.

เชียงใหม่เป็นจังหวัดที่สำคัญทางด้านเศรษฐกิจและวัฒนธรรมจังหวัดหนึ่งในภาคเหนือ ซึ่งตั้งอยู่ในบริเวณเสี่ยงภัยต่อการเกิดแผ่นดินไหว งานวิจัยนี้จึงเลือกทำการศึกษาสมบัติทางพลวัตรของดินทรายเชียงใหม่ด้วยการทดสอบแรงเฉือนอย่างง่ายแบบวัฏจักร พารามิเตอร์ที่สำคัญของดินทรายซึ่งใช้ในการวิเคราะห์แบบพลวัตรคือ โมดูลัสเฉือน และอัตราส่วนการหน่วง เครื่องมือทดสอบแรงเฉือนอย่างง่ายที่ใช้ทำการศึกษานี้เป็นแบบของสถาบันธรณีเทคนิคนอร์เวย์ที่อยู่ในห้องปฏิบัติการของภาควิชาวิศวกรรมโยธา จุฬาลงกรณ์มหาวิทยาลัย โดยถูกพัฒนาและปรับปรุงให้สามารถทำการทดสอบแบบวัฏจักรได้ เงื่อนไขการทดสอบเป็นแบบการควบคุมแอมพลิจูดความเครียด และควบคุมความเค้นประสิทธิผลตั้งฉากคงที่ ตัวอย่างดินทรายสร้างใหม่ถูกเตรียมด้วยวิธีตกตะกอนในน้ำโดยให้ใกล้เคียงกับสภาพการเกิดในธรรมชาติมากที่สุด โปรแกรมการทดสอบแรงเฉือนอย่างง่ายแบบวัฏจักรเลือกทำการศึกษาปัจจัยที่เกี่ยวข้องคือ ความหนาแน่นสัมพัทธ์ ความเค้นประสิทธิผลตั้งฉาก แอมพลิจูดความเครียด และความถี่ ผลการทดสอบชี้ให้เห็นว่า ค่าโมดูลัสเฉือน และอัตราส่วนการหน่วง ของดินทรายขึ้นกับ ค่าความเค้นประสิทธิผลตั้งฉาก และระดับความเครียด โดยที่ค่าโมดูลัสเฉือนลดลงเมื่อระดับความเครียดเพิ่มขึ้น ในทางตรงข้ามค่าโมดูลัสเฉือนเพิ่มขึ้นตามค่าความเค้นประสิทธิผลตั้งฉากที่เพิ่มขึ้น ส่วนพฤติกรรมฮิสเทอริซีสซึ่งอธิบายด้วยค่าอัตราส่วนการหน่วงมีค่าเพิ่มขึ้นตามการเพิ่มของความเครียด และมีค่าลดลงตามความเค้นประสิทธิผลที่เพิ่มขึ้น ผลการศึกษายังนำไปเปรียบเทียบกับงานวิจัยในต่างประเทศหลายแหล่ง

ภาควิชา วิศวกรรมโยธา ลายมือชื่อนิสิต .....

สาขาวิชา วิศวกรรมโยธา ลายมือชื่อ อ.ที่ปรึกษาวิทยานิพนธ์หลัก .....

ปีการศึกษา 2009

507 07092 21: MAJOR CIVIL ENGINEERING
KEYWORDS: DYNAMIC PROPERTIES/CYCLIC DIRECT SIMPLE SHEAR/ CYCLIC RESPONSE/ UNDRAINED TEST/WATER PLUVIATION METHOD

SOKSAN THAY: DYNAMIC PROPERTIES OF CHIANG MAI SAND USING CYCLIC DIRECT SIMPLE SHEAR TEST. THESIS ADVISOR: ASST. PROF. SUCHED LIKITLERSUANG, D. ENG., 105 pp.

Chiang Mai province is located in northern part of Thailand, wherein low to medium earthquake can occur. Therefore, this research aims to present an assessment of dynamic properties of Chiang Mai sand using cyclic direct simple shear test. Two of the most important parameters of dynamic properties in any dynamic analysis related to soils are shear modulus and damping ratio. The monotonic direct simple shear apparatus, which is developed at Norwegian Geotechnical Institute by Bjerrum and Landva, is modified to cyclic direct simple shear so as to be able to determine dynamic properties of Chiang Mai sand. Drained (constant normal stress) tests are carried out with saturated sand sample reconstituted by water pluviation method, which can closely replicate the in-situ fabric of natural sand deposits. In this study, relative density, vertical stresses, shear strain amplitude, and frequency are varied to observe their effect on sand dynamic properties. It can be concluded from the testing results that shear modulus and damping values mainly depend on vertical stress and shear strain. Shear modulus decreases with increasing shear strain amplitude. Oppositely, it increases with increasing vertical stress. The value of hysteretic damping increases with increasing shear strain amplitude. In contrast, when damping ratio decreases with increasing values of vertical stress. The experimental results of present study compared with previous investigations are found to be in fair agreement. All in all, this research is the first work focused on dynamic properties of Chiang Mai sand, which gives great distribution to the calculation of ground response during an earthquake. It also facilitates the following researchers who want to conduct further research on advanced soil laboratory testing about cyclic soil response in Chiang Mai as well as in Thailand.

Department : Civil Engineering Student's Signature Thay Soksan

Field of Study : Civil Engineering Advisor's Signature Sucheb Likitlersuang

Academic Year : 2009

ACKNOWLEDGEMENTS

I would like to express my deepest and sincerest appreciation and gratitude to my generous advisor, Assistant Professor Dr. Suched Likitlersuang for spending his precious times to show me the valuable instruction, advice, support, and encouragement during my study at Chulalongkorn University. I would like also to take this moment to apologize for all my mistakes that made him disappointed.

I honestly thank to AUN/SEED-Net (JICA) for financially support and officially coordinate for my study and to all the officers and staffs of AUN/SEED-Net for their helpfulness and kind cooperation.

Special thanks to my thesis committees: Associate Professor Dr. Supot Teachavorasinskun, Assoc. Prof. Dr. Boonchai Ukritchon, Assoc. Prof. Dr. Tirawat Boonyatee, Asst. Prof. Dr. Siam Yimsiri, for their extensive comments and constructive discussion on my thesis. Again, I would like to extend my gratitude to Mr. Pairoj Anantasethakul and Mr.Nirut Konkong for helping me modify the experimental apparatus.

I would appreciate to all the lecturers at the Department of Civil Engineering, Chulalongkorn University, for their prolific sources of knowledge, and wisdoms. In addition, I am definitely grateful to all helpful and kindly soil laboratory technicians, and my friends, especially Mr. Sochan Seng and Mr. Chitti P who offers me the data of seismic MASWM and downhole tests for my research.

Last but not least, I would show my profoundly gratitude and love to my family who always taking care, giving love and encouragement. They never let me down. Without them this thesis cannot be achieved.

CONTENTS

LIST OF TABLES

LIST OF FIGURES

CHAPTER I

INTRODUCTION

1.1 Background

Thailand lies in the interior of the Eurasian plate, with the boundary of the Burma microplate and Indian plate occurring to the west in the Andaman sea. This country was divided into six geographical regions, based on natural features including landforms and drainage, as well as human cultural patterns. They are, namely: Northern, Northeastern, Central, East, West and Southern Thailand. Among these regions, the northern part are situated in low to medium seismic risk zones. According to previous researches, there are a few active faults recently found in this region such as Chiang Mai and Chiang Rai provinces. These faults could possibly induce earthquakes of magnitude (M_L) of 5-6.5. It is evident from Figure B-1 (Appendix B) that Chiang Mai can be considered as moderate risk and moderately high risk zones equivalent to the Uniform Building Code (UBC) zone 2B and 3. For example, the earthquake with a magnitude of 5.1 was struck at 12:02 a.m. on Tuesday, December 12, 2006 in Mae Rim district, which is located near the city of Chiang Mai.

Chiang Mai, an area of 22,800 km^2, is situated about 700 km from north of Bangkok at latitude $17^0$15' N-$20^0$16' N and longitude $98^0$03' E-$99^0$33' E. Chiang Mai's land is covered by mountains and forests about 69.31%. Among the northern provinces of Thailand, Chiang Mai is chosen as the studied area because of the following reasons:

1. Closeness to the active faults.
2. Formation of loose to medium dense sand at shallow depth, which can cause liquefaction.
3. Attempt to enhance dynamic soil behavior in seismic zones. Although seismic design code has been enforced in the area since 1980, the fundamental knowledge on dynamic soil behavior has not been extensively attained.
4. The most densely populated areas in the north with a population of 1,603,220 in December 2004.

5. The chief economic center of the northern part, and the natural and tourist place of the country.

In view of foregoing reasons, the reliable dynamic properties of the sand have to be taken to avoid great damage caused by earthquake and provide the safety for local inhabitants. The direct simple shear (DSS) apparatus will be selected to conduct the laboratory test in this study because it is one of experimental apparatuses for determining the dynamic properties of cohesionless soils. The specimens can be prepared in accordance with in-situ stress state, which is more representative of the field condition. Other significance is that cyclic simple shear tests can be conducted for a wider range of strain amplitude from 10^{-2} to about 5%. This range is the general range of strain encountered in the ground motion during seismic activities.

1.2 Research Objectives

The objectives of this research are described as follows:

1. To evaluate the dynamic properties of Chiang Mai sand using DSS apparatus.
2. To estimate the effect of several parameters (vertical stress, shear strain amplitude, relative density, and frequency) on the shear modulus and damping ratio of sand.
3. To compare the experimental results from present study with previous investigations of both in field test and laboratory test. In field test, there are standard penetration test (SPT), Downhole test, and Multichannel Analysis of Surface Wave Method (MASWM).

1.3 Scope of Study

The scope of study is covered as outlines below:

1. Monotonic and cyclic DSS tests are conducted on Chiang Mai sands in order to figure out internal friction angle and dynamic properties of sand. The dry and saturated sand specimen will be used in the monotonic DSS test under drained and undrained condition, respectively. Furthermore, cyclic DSS test under drained constant normal stress condition is conducted on the saturated sand.

2. Reconstituted sand specimens are prepared using dry tamping method for dry sand and wet pluviation technique for saturated sand.
3. Although stress states in DSS test represent well for field situation, only horizontal stresses on the top and bottom can be measured. However, the lateral stresses induced by the rubber membrane cannot be determined from the experimental apparatus. Meanwhile there is nonuniformity of stress distribution on soil specimens in DSS test. This factor causes some influences on the stress-strain behavior of soil during testing.

1.4 Research Outcome

This research is the first work focused on dynamic properties of Chiang Mai sand, which gives great distribution to the calculation of ground response during an earthquake. It also facilitates the following researchers who want to conduct further research on advanced soil laboratory testing about cyclic soil response in Chiang Mai as well as in Thailand.

CHAPTER II
LITERATURE REVIEW

2.1 Introduction

In the past, most geotechnical researches were mainly concentrated on the determination of soil behavior under static load conditions such as the designs of building foundation and dam under static load condition. However, in the recent decades, many geotechnical engineers have had difficulties concerning the issues of earthquakes, vibrations of machinery, wave actions. As a consequence, the theoretical and experimental studies in the area of soil dynamics have taken great attention and progressed at a very rapid pace. Various researchers (Seed and Idriss, 1970, Silver and Seed, 1971, Dobry, 1987, Vucetic, 1993, Vanden Berghe, 2001; etc.,) have attempted to understand further the dynamic load characteristics on soils. Laboratory and field test procedures are used to predict the dynamic properties of soil.

The objective of this chapter is to position the present research relatively to the main research efforts determining the dynamic properties of sand using modified cyclic direct simple shear (DSS) test.

The chapter is divided in two main sections. The first section describes the three different field tests: the standard penetration test (SPT), the downhole test, and the multichannel analysis of surface wave method (MASWM). Some useful correlations able to estimate both the static and dynamic parameters of soil will be indicated. The second section discusses the two laboratory tests: direct shear box (DSB) and direct simple shear (DSS). The principles of DSB and DSS test are presented. An overview of stress strain behavior of DSB and DSS test under static loading condition are briefly shown to interpret the shear strength of soil (i.e, internal friction angles). In addition, cyclic properties of soil obtained from cyclic DSS test are illustrated. The following review does not pretend to be exhaustive. The ambition is to make the reader familiar with the different laboratory tests and the expected static and dynamic parameters of soil from these tests.

2.2 Field Tests

The objective of this section is to present the three different kinds of field tests: the standard penetration test (SPT), the downhole test, and the multichannel analysis of surface wave method (MASWM). The static and dynamic properties of soil can be evaluated based on some theoretical and empirical relationship.

2.2.1 Presentation to In-situ Tests

On the basis of field observations, it appears reasonable to standardize the field penetration number as a function of the input driving energy and its dissipation around the sampler into the surrounding soil that

$$N_{60} = N\frac{\eta_H \eta_B \eta_S \eta_R}{60} \quad \text{(2-1)}$$

Where N_{60} = standard penetration number, corrected for field conditions

N = measured penetration number

η_H = hammer efficiency (%)

$= 45\% \; for \; donut \; hammers$

$= 55\% \; for \; safety \; hammers$

$= 55\% - 83\% \; for \; automatic \; hammers$

Variations of $\eta_B, \eta_S, and \; \eta_R$, based on recommendation by Skepton (1986), are summarized in Table A-2.

In granular soils, the value of N is affected by the effective overburden pressure (σ_v'). For that reason, the value of N_{60} obtained from field exploration under different effective overburden pressures should be changed to

$$(N_1)_{60} = C_N N_{60} \quad \text{(2-2)}$$

Where C_N = correction factor

$$= \frac{2}{1+\frac{\sigma_v'}{P_a}}$$

σ_v' (kN/m^2) = vertical effective stress

P_a = atmospheric pressure

= 100 kN/m^2

Besides, downhole test is a method which determines soil stiffness properties by analyzing direct compressional and shear waves along a borehole down to about 30 m. Shear waves have to be generated at surface. A shear wave source (sledge hammer hit sidewise) is used at surface and a coupled receiver system is moved in the borehole. Travel times of the seismic waves are analyzed and seismic velocity is calculated. Shear wave velocity can be transformed to soil stiffness. The measurements can be performed below and above the groundwater table.

Furthermore, multichannel analysis of surface waves (MASW) is a relatively new approach which was developed by Park et al. (1999) and Xia et al. (1999). The main components of MASWM are geophones and seismograph. Geophones receive wave from seismic source caused by sledge hammer and send data to seismograph. This method provides more facilitation than downhole test because downhole test needs to drill the soil and spend a lot of time. It can also be used to locate and roughly delineate subsurface anomalies such as voids. A key advantage to this innovative seismic method is that it measures ambient seismic noise; therefore it can be used in noisy areas where seismic reflection and refraction cannot be used, such as construction zones and urban environments. The shear wave velocity and soil profiles at shallow depths can be obtained from MASWM. Therefore, the shear stiffness (G) of the ground can thus be calculated from the shear velocity when material density is known.

2.2.2 Correlations of In-situ Tests

In this part, some theoretical and experimental relationships obtained from the forgoing three in-situ tests will be pointed out to determine the vital parameters of static and dynamic properties of sand proposed by various authors.

The standard penetration number corrected for field conditions (N_{60}) can also be correlated (Seed et al., 1986) in the following form to predict the maximum shear modulus:

$$G_{max} = 3.6 \times 1000 \times (N_1)_{60}^{1/3} \times (\sigma_v')^{1/2} \quad \textbf{(2-3)}$$

The stiffness of soils can be found out from the theoretical relationship in function of shear wave velocity as follows:

Shear modulus of all types of soil

$$G_{max}\ (\frac{kN}{m^2}) = \rho v_s^2 \quad \textbf{(2-4)}$$

Young's modulus of all types of soil

$$E\ (\frac{kN}{m^2}) = 2(1+\mu)\rho v_s^2 \quad \textbf{(2-5)}$$

Where $\rho\ (t/m^3)$ = density of soil

v_s (m/s^2) = shear wave velocity

μ = Poison's ratio

2.3 Laboratory Tests

2.3.1 Introduction

After mentioning the three foregoing in-situ tests, this section will describe two types of laboratory tests: direct shear box (DSB) test and direct simple shear (DSS) test. The principles of these tests are introduced by comparing the advantages of these two tests. Next part of the section points out briefly the stress strain behaviors under monotonic loading. Some relationships and Morh's Coulomb models are used to interpret shear strength of sand. Last part of this section discusses in detail the cyclic soil properties obtained from cyclic DSS test.

2.3.2 Direct Shear Box (DSB) Test

A shear box is the simple apparatus to determine the shear strength parameters of soil in the drained conditions. The direct shear box can be tested with clay or sand. It consists of a horizontally split, open metal box. The soil is placed in the box, and one-half of the box is moved by shear stress (τ) relative to the other half, as shown in Figure 2-1. The principle stresses are allowed to rotate. The direct shear box (DSB) test is useful when a soil mass is likely to fail along a thin zone under plane strain conditions. Failure is constrained along a thin zone of the soil on the horizontal plane (AB) under constant normal stress (σ_v) according to ASTM D 3080. Generally, three

or more specimens are tested under different normal stress (σ_v) to determine the shear strengths of soil.

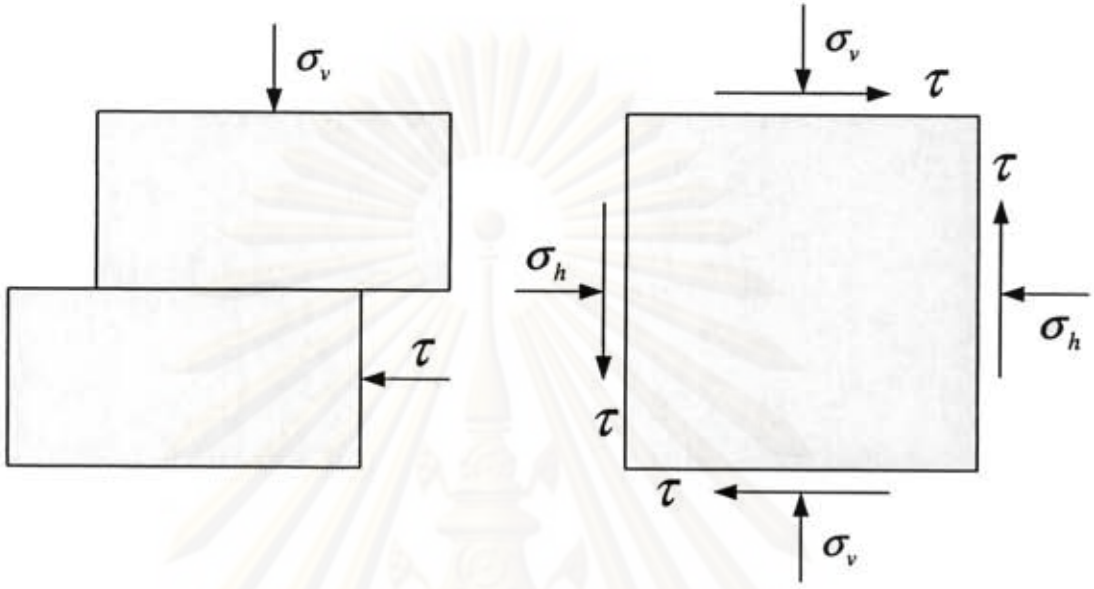

Figure 2-1 Stress states: (a) in DSB test; (b) in DSS test

Besides the advantages of the access to obtain the shear strengths of soil, this test also consists of some disadvantages. Airey, D.W. (1984) showed that the tilting of the top cap of DSB had a significant effect on both the peak and ultimate strengths. This effect makes the friction angle obtained from DSB test greater than that from DSS test. Additionally, non uniform shear stresses and displacements are greater in DSB test than DSS test. The assumption which soil fails a long horizontal plane is not realistic because the actual failure plane may not necessary to happen at horizontal direction. Furthermore, stress states in DSB test don't simulate the stress states in the field condition. However, the stress states in DSS test are simple shear stresses representative for real field situation.

2.3.3 Direct Simple Shear (DSS) Test

The Direct Simple Shear (DSS) apparatus, as shown in Figure 2-1, works on a similar principle to the direct shear box in that the top platen is moved horizontally with respect to the bottom platen. The principle stresses (σ_1 *and* σ_3) are allowed to rotate. Although these two apparatus consist of some similarity, DSS apparatus still has more

advantages than DSB. First, it is designed so that the sample is allowed to deform more uniformly than DSB which has problem of top cap tilting. Second, the stress states in DSS apparatus are simple shear stresses which closely represent stresses states in field condition. Third, this device can be conducted in drained or undrained condition, and in monotonic or cyclic loading tests. Excess pore-water pressures can be measured indirectly. Lastly, the soil specimen is consolidated to simulate natural aging of the soil before shearing.

2.3.4 Soil Properties under Monotonic Loading

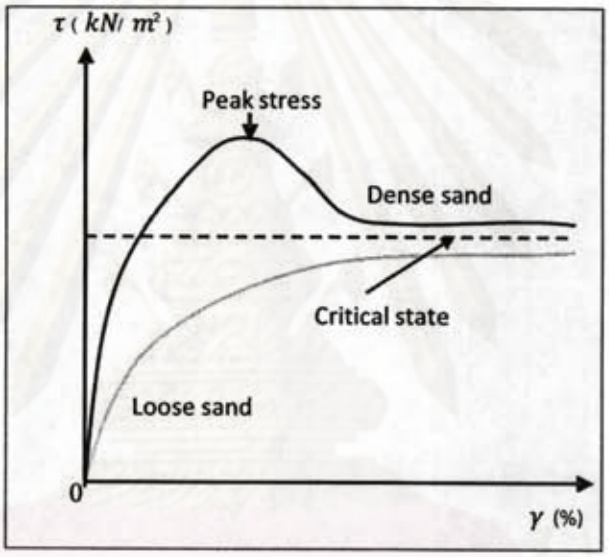

Figure 2-2 Stress-strain behavior of sand during monotonic loading

Figure 2-2 illustrates two types of soils, loose and dense sand. Loose sand curve shows gradual increase in shear stresses as the shear strain increases (strain hardening) until an approximately constant shear stress, which is called the critical state stress (τ_{cs}). The critical state is a state at which continuous shearing occurs without changes in shear stress and volume for a given normal effective stress. In addition, dense sand curve points out a rapid increase in shear stress reaching a peak value (τ_p), at low shear strains (compared to loose sand) and then show a decrease in shear stress with increasing shear strain (strain softening) ultimately attaining a critical state shear stress.

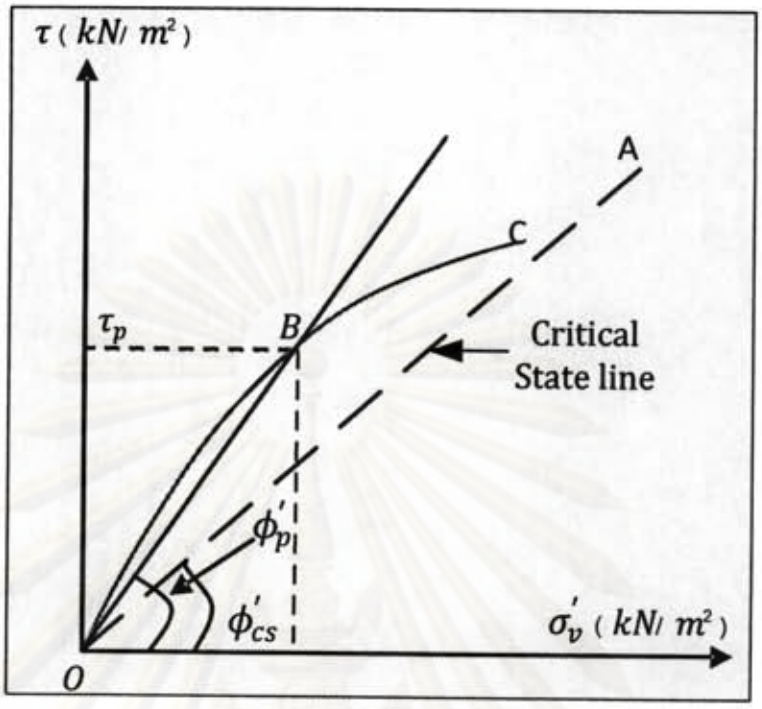

Figure 2-3 Stress path of sand during drained monotonic loading

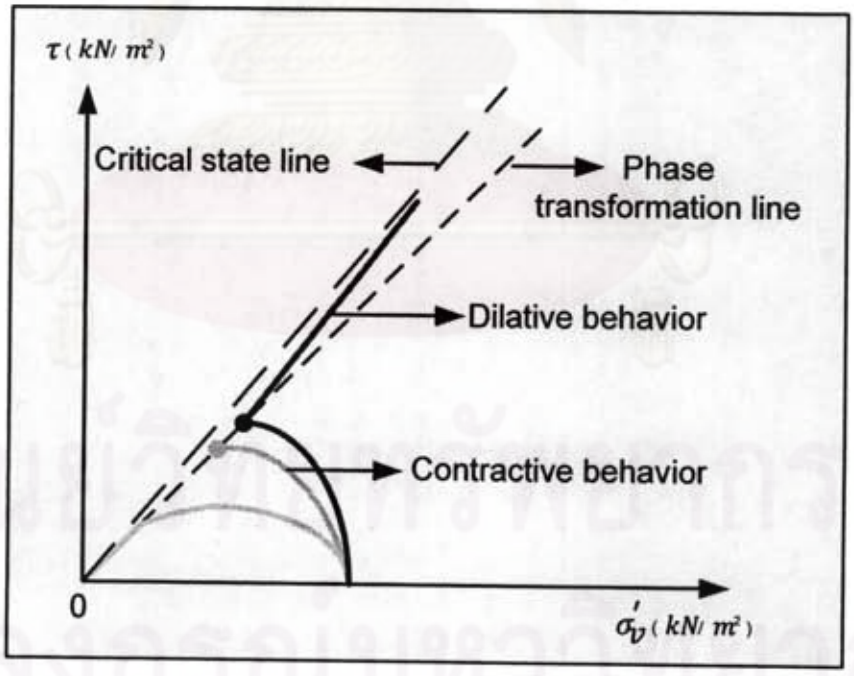

Figure 2-4 Stress path of sand for undrained test

Furthermore, from Figure 2-2, stress path of sand during drained monotonic loading can be drawn as shown in Figure 2-3. Internal friction angle, based on Figure 2-3, can be interpreted by using Coulomb's model:

$$\tau = \sigma_v' tan\emptyset' \quad \textbf{(2-6)}$$

Where τ = shear stress

σ_v' = effective normal stress

$\emptyset'$ = effective friction angle

The straight line is the critical state line (Coulomb failure envelop), and the angle between this line and horizontal line is called effective critical state friction angle ($\emptyset'_{CS}$). Apart from straight line, there is also the curved line of peak shear stress. It is can inferred that peak friction angles ($\emptyset'_p$) are different for different normal effective stress. In addition, peak friction angles are always bigger than critical friction angles.

According to Castro (1977), three types of sand behaviors can be observed under undrained monotonic loading, as shown in Figure 2-4. Dense sand first expresses the contractive behavior (increase of pore water pressure) and then exhibits dilative behavior (decrease of pore water pressure). During the dilation phase, the stress path is straight until touching the critical state line (Castro, 1977; Vanden Berghe, 2001), as depicted in Figure 2-4. Meanwhile, phase transformation line can be drawn from the reference passing the point which the sand response changes from contraction to dilation according to Vaid et al. (1999), and Porcino et al. (2008). Critical and phase transformation state friction angles ($\emptyset'_{CS}$ *and* $\emptyset'_{PT}$) are formed by critical state line and phase transformation line with horizontal line respectively. In accordance with Carter et al. (2000), $\emptyset_{PT}$ is more reliable to design. In case of loose sand, contractive behavior will occur. Besides that, very loose sand points out flow liquefaction behavior resulting in a rapid flow to large strains at low effective normal stress.

2.3.5 Soil Properties under Cyclic Loading

Two main points will be presented in this part. First point describes how dynamic soil properties can be determined. Second point introduces some factors influencing on dynamic properties of soils which will be investigated in this research.

2.3.5.1 Cyclic Soil Properties

When a soil is subjected to symmetric cyclic deformations of amplitude γ_c, the relationship between the shear stress and the shear strain is generally non linear and presents an hysteresis loop as shown on Figure 2-5. This hysteresis loop can be described in two ways: by the actual path of the loop itself, or by parameters describing its shape. The shape of the loop is generally characterized by the slope and the surface. The secant shear modulus (G_s) is defined as the slope between the two extremities of the loop as shown in Equation 2-7. In addition, this modulus (G_s) becomes maximum shear modulus (G_{max}) when shear strain amplitude is very small ($\gamma < 10^{-3}\%$) during monotonic or cyclic tests.

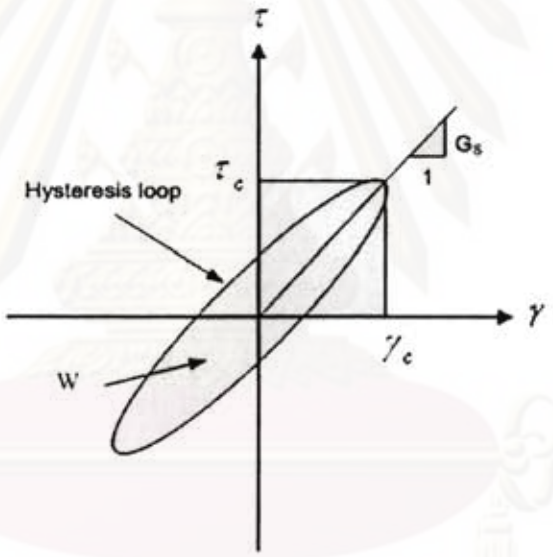

Figure 2-5 Characteristics of hysteresis loops during cyclic shearing

$$G_S = \frac{\tau_c}{\gamma_c} \qquad (2\text{-}7)$$

Where G_S (kPa/m^2) = secant shear modulus
τ_c (kPa/m^2) = maximum shear stress
γ_c (%) = maximum shear strain amplitude

Furthermore, the surface of the loop during the cycle is conveniently described by the damping ratio (λ):

$$\lambda = \frac{1}{4\pi} \times \frac{W}{\frac{1}{2}\gamma_c \tau_c} \quad \text{(2-8)}$$

Where λ (%) = damping ratio

W = area of the hysteresis loop

τ_c (kPa) = maximum shear stress

γ_c (%) = shear strain amplitude

2.3.5.2 Effect of some Parameters on Soil Dynamic Properties

According to previous research carried out by various authors (Silver and Seed, 1971, Iwasaki et al., 1978, Vucetic, 1993, Vucetic et al., 1998, etc.), Severeal parameters can have influence on shear modulus and damping ratio such as shear strain amplitude (γ), vertical stress (σ_v), relative density (D_r), number of cycles (N), frequency (f), plasticity index (PI), etc.

Effect of γ

The shape of the hysteresis loops observed during cyclic loadings is strongly influenced by the shear strain amplitude due to the different induced soil behavior. Secant shear modulus decreases with increasing shear strain amplitude. In contrast, damping ratio increases as shear strain increases, as illustrated in Figure 2-7.

In accordance with Kokusho (1980), and Vucetic (1993), three types of soil behavior can be identified as a function of the strain amplitude:

- Linear elastic behavior
- Elasto-plastic behavior without degradation
- Elasto-plastic behavior with degradation

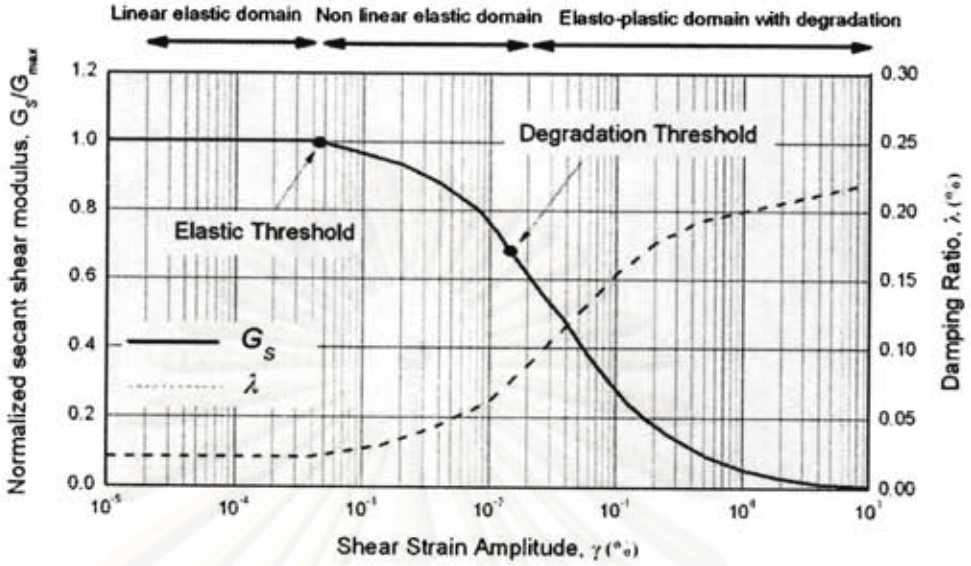

Figure 2-6 Typical relationship between secant shear modulus ratio Gs/G_{max} and damping ratio as a function of the shear strain amplitude (Vucetic, 1993).

The soil behavior during small strain amplitudes cyclic shearing is virtually linear elastic, and the hysteresis loops are reduced to a straight line. This kind of behavior is characterized by a normalized secant shear modulus equal to 1 and a low value of the damping ratio.

When the strain amplitude increases, the soil behavior becomes non linear elastic and hysteresis loops appear. The secant shear modulus (G_S) characterizing the loops decreases when the strain amplitude increases, whereas the damping ratio (λ) increases. The shear strain amplitude corresponding to the transition from the linear elastic behavior to the non linear elastic behavior is called the elastic threshold or threshold of non linearity, as shown in Figure 2-7.

During larger strain amplitude cycles, the grain structure continuously deteriorates, leading to a reduction of the soil resistance during each cycle. It results in a reduction of the secant shear modulus and of the damping ratio as a function of the number of cycles. The shear strain amplitude corresponding to the transition from the non degrading behavior to the degrading behavior is called the degradation threshold or threshold of degradation, as illustrated in Figure 2-7.

Effect of vertical stress, relative density, number of cycles, and frequency

According to Silver and Seed (1971) conducting cyclic drained DSS test on dry silica No. 20 sand, there is a significant increase in shear modulus and some decrease in damping ratio with increasing vertical stress. The relationship between secant shear modulus and vertical stress can be expressed as

$$G_S = k\sigma_v^m$$

Where k = a constant

m = a slope of the line on the log-log plot

In addition, shear modulus was found to slightly increase with increasing relative density. The effect of relative density on damping ratio is likely to be small.

Besides, shear modulus slightly increases with increasing number of cycles. Contrarily, hysteretic damping ratio decreases when number of stress cycles increases. The effect of number of cycles seems to be small after 10 cycles. As to Peacock and Seed (1968), dynamic behavior of soils is largely unaffected by the speed of loading within a range of 0.1 Hz to 4 Hz.

CHAPTER III
EXPERIMENTAL PREPARATION

3.1 Introduction

The main goal of this chapter is to present the experimental preparation of the cyclic direct simple shear (DSS) tests carried out within the framework of this research. First part will describe the plan to conduct the research, which is explained by the flow chart of research framework. Second part of this chapter will present Chiang Mai sand characteristics. Last part will point out the experimental setup with monotonic and cyclic tests.

3.2 Description of Location Investigation

In this study, there are two locations are investigated. First location is Ping River where the typical subsoil section is depicted in Figure B-2. It is Chiang Mai's largest and most important river originating from the mountains of Chiang Dao and flowing southward for 540 km. Sand is collected at the ground surface of the river. Second location is Wat Chedi Luang. It is one of the most important temples in Chiang Mai and used to be suffered from great earthquake in 1545. Sand is taken at approximate depth of 15 m. Soil profile of Wat Chedi Luang subsoil is shown in Table A-1, according to KEC boring log report.

3.3 Flow Chart of Research Framework

Figure 3-1 explains how to conduct the research. First of all, Chiang Mai sands were taken from two different sites (Ping River sand and Wat Chedi Luang sand). After that, direct simple shear (DSS) apparatus was used to conduct the test on these sands. Monotonic and cyclic tests were taken into account. Then, internal friction angles can be determined from monotonic drained and undrained DSS test. In addition, dynamic sand properties can be obtained from cyclic drained test and will be compared with those from previous studies of both field tests (SPT, MASWM, and Downhole Test), and laboratory tests (DSB test, DSS test, and Torsional shear test).

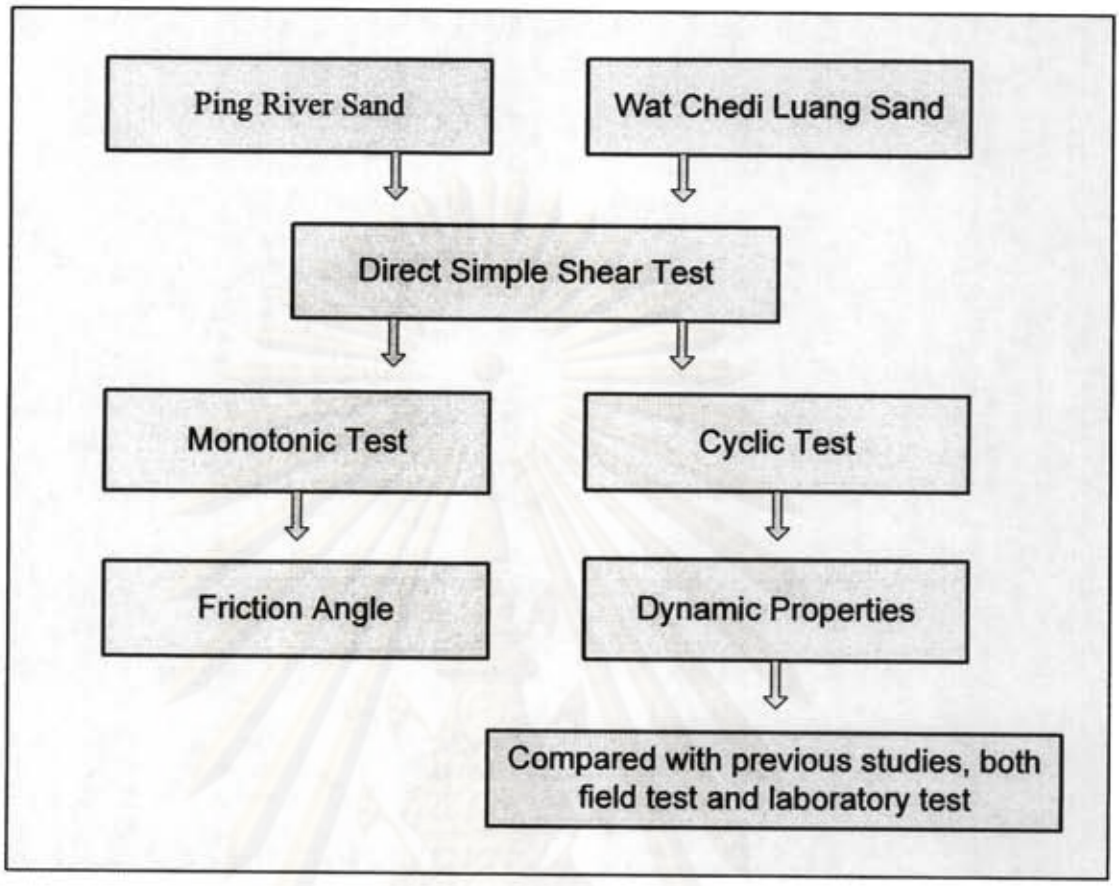

Figure 3-1 Flow chart of research framework

3.4 Index Properties of Chiang Mai Sand

The materials used to conduct the test are sands from Chiang Mai province at two different sites, located in northern part of Thailand, wherein low to medium seismic risk zone can occur. First sand sample is obtained from Chiang Mai River at ground surface and the other from Wat Chedi Luang at the depth of 15 m. Sand particles greater than 4.75 mm were taken out. The physical properties of Chiang Mai River and Wat Chedi Luang sands used in the present study are summarized in Table 3-1 and the grading curves are presented in Figure B-5.

As shown in Table 3-1, sands are classified as SW for RS and SP for WS according to the Unified Soil Classification System (USCS). Meanwhile, RS has value of specific gravity $G_s = 2.62$, maximum void ratio $e_{max} = 0.62$, and minimum void ratio $e_{min} = 0.4$. The specific gravity value of WS is $G_s = 2.61$ with $e_{max} = 0.87$ and $e_{min} = 0.5$.

Table 3-1 Physical properties of tested soils

Sample[1]	D_{50} (mm)[2]	C_u[3]	C_c[4]	%Fines[5]	G_s[6]	e_{max}[7]	e_{min}[8]	USCS Symbol
RS	0.65	8.18	1.03	4.5	2.62	0.62	0.4	SW
WS	0.26	2.5	1.11	6.09	2.61	0.87	0.5	SP

Remarks: 1. RS = River sand, WS = Wat Chidi Luang sand, 2. D_{50} = Median particle size, 3. C_u = Coefficient of uniformity, 4. C_c = Coefficient of curvature, 5. %Fines = % by weight passing No. 200 sieve (0.0075mm), 6. G_s = Specific gravity, 7. e_{max} = Maximum void ratio, 8. e_{min} = Minimum void ratio

Note: Particle size analysis conducted following ASTM D422, G_s determined by ASTM D854, e_{min} determined by ASTM D4253, e_{max} determined by ASTM D4254, and Unified Soil Classification System (USCS) determined by ASTM D2487.

3.5 Experimental Setup

3.5.1 Description of the Direct Simple Shear Apparatus

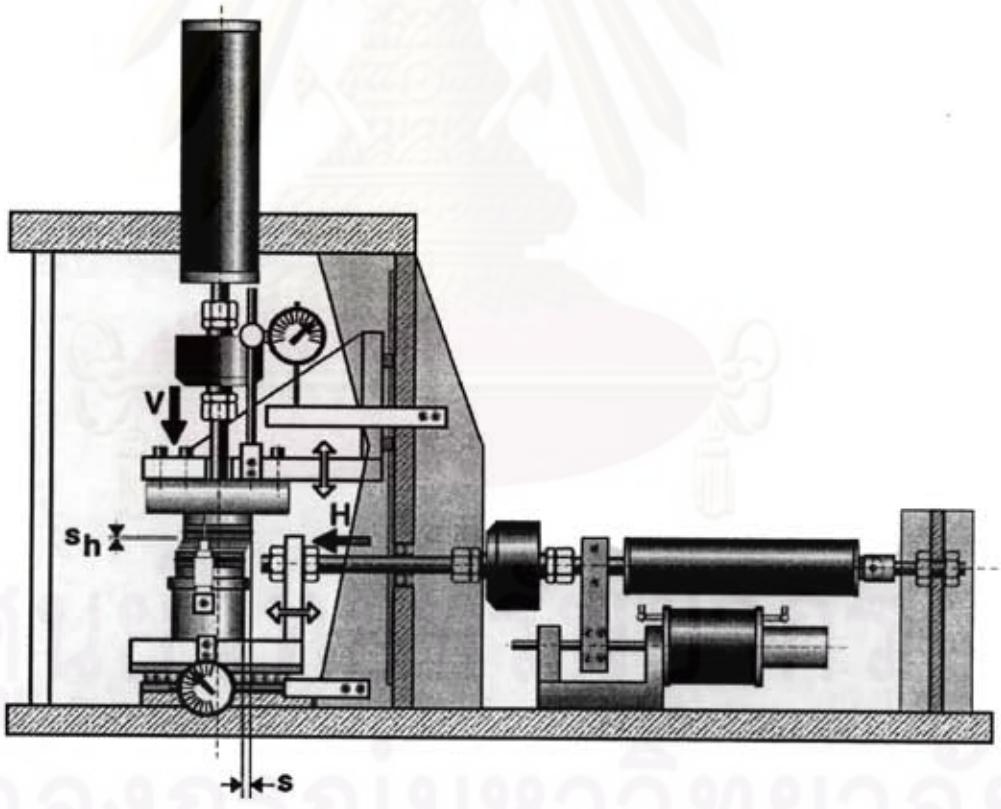

Figure 3-2 New NGI DSS apparatus

There are currently two designs of simple shear apparatus: one developed at Cambridge University and the other at the Norwegian Geotechnical Institute (NGI) in Oslo, as shown in Figure 3-2. In the Cambridge type (Roscoe 1953; Bassett 1967) the sample is rectangular and is completely surrounded by rigid platens. Cambridge DSS apparatus is not convenient owing to complexity in testing installation. However, NGI direct simple shear (DSS) apparatus was developed by Bejerrum & Ladva (1966) and is more convenient. This DSS device has a cylindrical sample with the height and cross-section area of 16 mm and 35 mm^2 respectively, which is contained within a wire-reinforced rubber membrane. This membrane maintains a constant sample circumference, but allows uniform vertical deformation and rotation of the vertical sides of the sample. The whole sample is placed between top and bottom platens. Axial and shear forces are applied via the top platen. Therefore, normal stress and shear stress can be determined. In addition, the vertical and shear strains of a sample can also be measured by observing the vertical and horizontal displacement of the top platen. Detail of key elements of DSS apparatus is demonstrated in Figure B-3 (Appendix B). Besides that, drained and undrained test can be conducted in DSS apparatus. For drained test, the normal stress is kept constant by allowing height of specimen to vary down and up. It is called drained constant normal stress DSS test. The latter is the method to fix the height of specimen by allowing normal stress to change. It is called the undrained constant volume DSS test.

3.5.2 Modification of DSS Apparatus

Figure 3-3 shows monotonic NGI DSS apparatus which is not yet modified to cyclic DSS test. It can only be used in monotonic test. After implementation of a set of cyclic motors, the apparatus is able to perform the cyclic strain-controlled testing, as illustrated in Figure 3-4. The set of cyclic motors, consisting of a motor (3 phases and 3400 rpm), motor gear (speed ratio 1:10), and E-motor, is mounted on a steel plate. E-motor is used to determine the exact frequency during cyclic loading. The main function of cyclic motors set is to driven the horizontal load of NGI DSS apparatus back and forth. Required shear strain amplitude can be obtained by setting up in cyclic motors set.

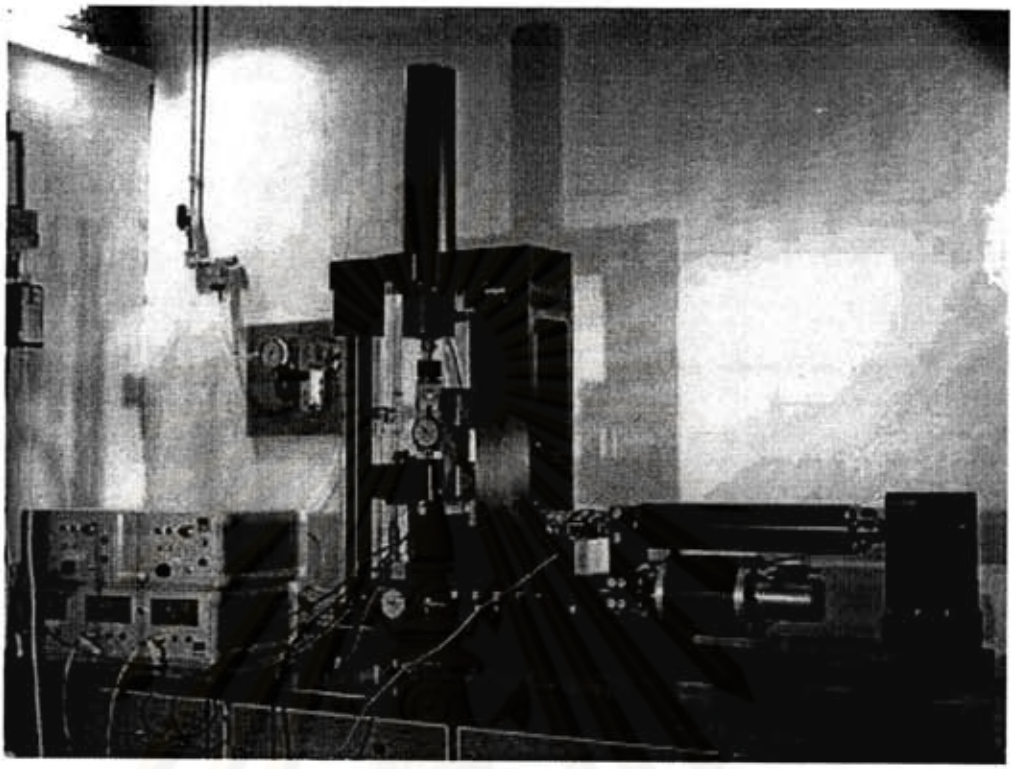

Figure 3-3 Monotonic DSS Apparatus

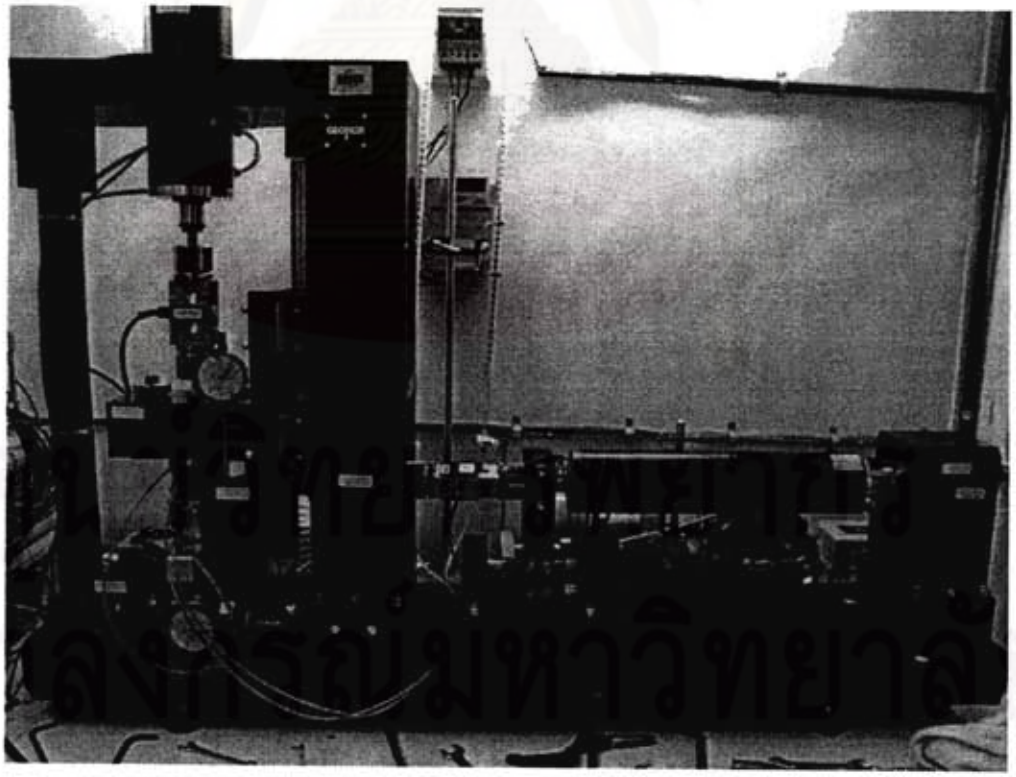

Figure 3-4 NGI DSS apparatus modified to cyclic DSS apparatus

3.5.3 Sample Preparation

The NGI trimming tools, as shown in Figure B-4, are used to reconstitute the sand specimen for all the monotonic and cyclic tests. Two methods are used to reconstitute sand samples. First method is dry tamping technique which is carried out in DSB and drained monotonic DSS tests. Second method names water pluviation technique which is performed in undrained monotonic and drained cyclic DSS tests. The detail of these two techniques will be shown later. Two types of sand will be tested. Firstly, Chiang Mai Ping River sand is reconstituted to relative density $D_r \cong 40\%$ in loose state and to $D_r \cong 80\%$ in dense state. Secondly, Wat Chedi Luang sand taken at depth of 15 m is prepared to natural relative density $D_r \approx 90\%$.

3.5.4 Dry Tamping Method

First of all, index properties of tested sand (G_s, e_{max}, and e_{min}) must be known to get needed relative density as well as the amount of dry sand. The relationship is pointed out in Equation (3-1) and (3-2) as follows:

$$m_s = \frac{G_s \gamma_w}{1 + e_o} V \tag{3-1}$$

$$D_r = \frac{e_{max} - e_0}{e_{max} - e_{min}} \times 100 \tag{3-2}$$

Where m_s (g) = mass of dry sand

G_s = specific gravity

γ_w (g/cm^3) = unit weight of water

$e_0, e_{max}, and\ e_{min}$ = initial, maximum and minimum void ratio

Then, dry sand are poured to the mould covered with rubber membrane. The specimen is tamped directly in a reinforced membrane, as shown in Figure 3-5(a), in two different operations. The first operation, as indicated in Figure 3-5(b), consists of tamping the specimen with a tool that assures the same compaction of the sand near the membrane than in the middle of the specimen. After putting the top cap on the specimen, the second operation, as illustrated in Figure 3-5(c), is begun to compact

the specimen on the entire surface until the height corresponding to the desired relative density is reached. During the second phase of the tamping, the number of hammer blows needed is counted. The same number of blows was usually needed for each specimen having the same density.

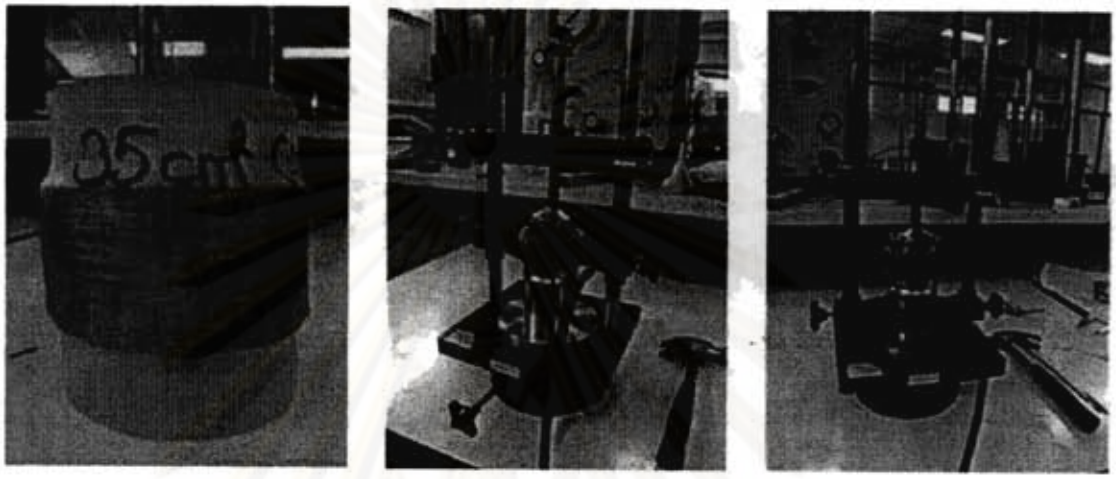

(a) (b) (c)

Figure 3-5 Dry tamping method (a) wire-reinforced rubber membrane; (b) first tamping operation; (c) second tamping operation and height measurement

3.5.5 Water Pluviation Method

In accordance with Vaid et al. (1999) & Porcino et al. (2008), water pluviation technique can closely replicate the in-situ fabric of natural sand deposits of marine origin. In preparing samples, water is filled into the mould until the same height of the specimen (16 mm), as pointed out in Figure 3-6. Sands are then poured from a funnel into water in the mould, layer by layer, regardless of the drop height. The higher densities can be obtained by tapping on the lateral surface or on the base of the mould while maintaining a small seating load on the sample cap and keeping drainage holes open.

3.5.6 Consolidation and Saturation

After sample preparation completes, the specimen is placed in the DSS apparatus and desired normal stress is applied on the specimen, as pointed out in Figure 3-7. In saturated sample case, CO_2 is sent through the specimen from the bottom to the top for 5 minutes. The specimen is then saturated by de-aired water. This will remove air

bubbles in sample. Finally, the drainage of the top of the specimen is connected to a burette. The level of water in the burette is placed in order to maintain a pore pressure at the specimen extremities equal to the atmospheric pressure during the consolidation and the cyclic testing.

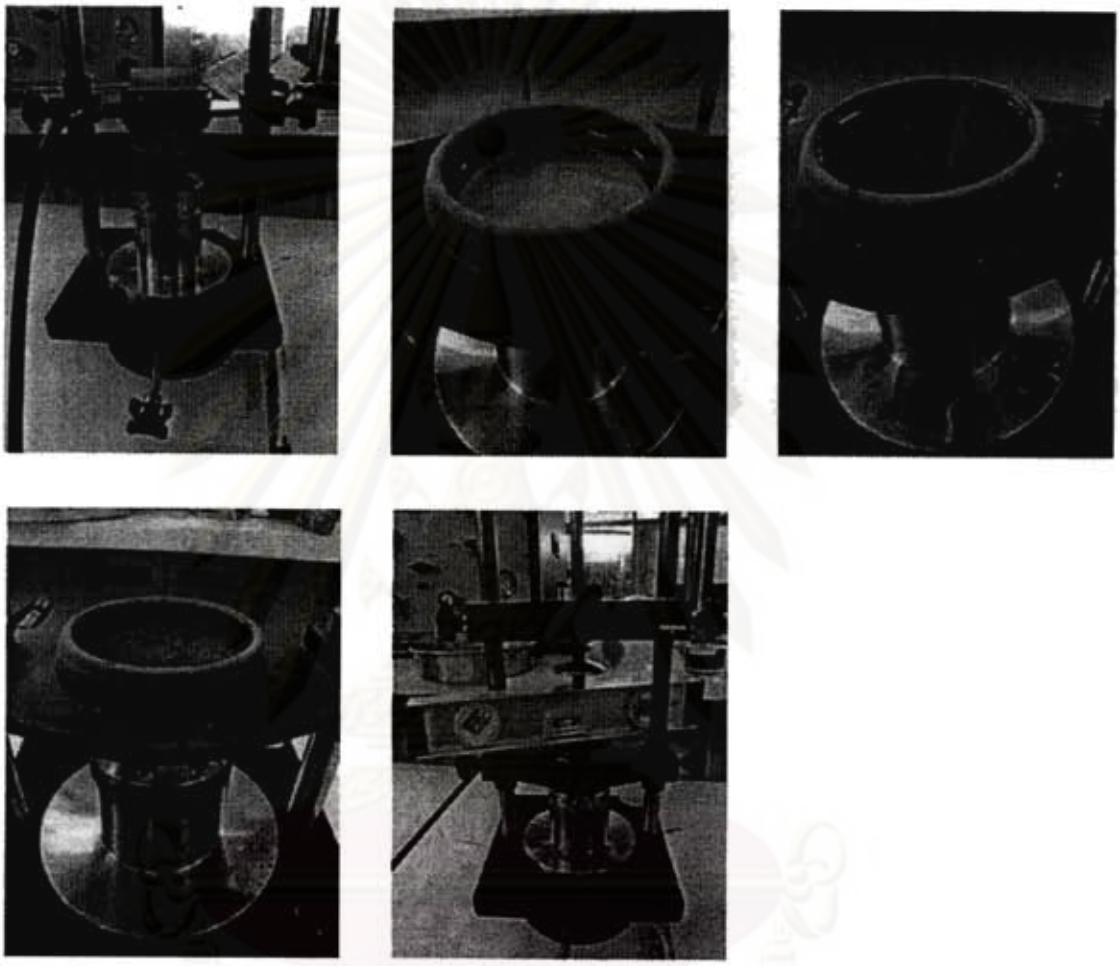

Figure 3-6 Water pluviation methods prepared in NGI trimming tools

The time of the consolidation is approximately 1 hour to reduce the effect of creep of the specimen. An axial deformation is observed to be smaller than 1 μm. The control system of the vertical motor keeps the vertical stress constant in a range of $\pm$ 0.86 kN/m^2. It is vital to notice that in the simple shear test, the consolidation of the specimen is anisotropic. The specimen is consolidated under K_0 conditions (virtually zero lateral strains).

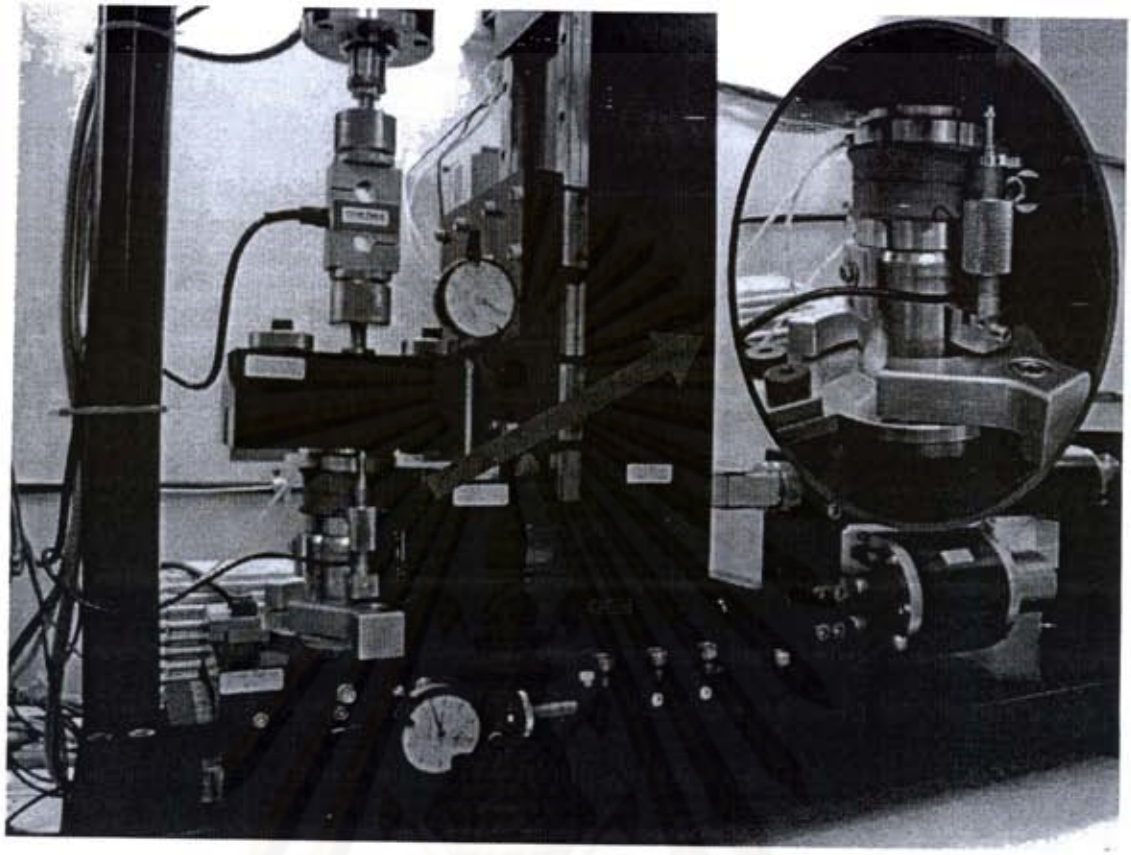

Figure 3-7 Sand sample placed in DSS apparatus

3.5.7 Data Acquisition System and Data Processing

3.5.7.1 Data Acquisition System

For DSS apparatus for static testing, there are control unit with power supply, interface, and data acquisition boards, as shown in Fi ure B-4. A new data acquisition program was developed to expand the capabilities of the NGI simple shear device by allowing cyclic strain controlled testing using the electrically-driven shear motor. This program was written using LabVIEW software. The program acquires the measurements of the vertical and horizontal load cells and of the horizontal and vertical displacement transducers. It converts the measured voltages in physical values and calculates the corresponding strains and stresses. For original cyclic NGI DSS apparatus, the program drives the horizontal load to obtain a cyclic shear strain of the specimen, based on the horizontal shear strain measurement. However, for the modified cyclic NGI DSS apparatus used in this study, a set of cyclic motors is used to move the horizontal load back and forth. An independent system controls the

sample height during the test. The capacity of maximum vertical and horizontal loads is 10 kN and 5 kN respectively.

3.5.7.2 *Data Processing*

A. *Measurement Corrections*

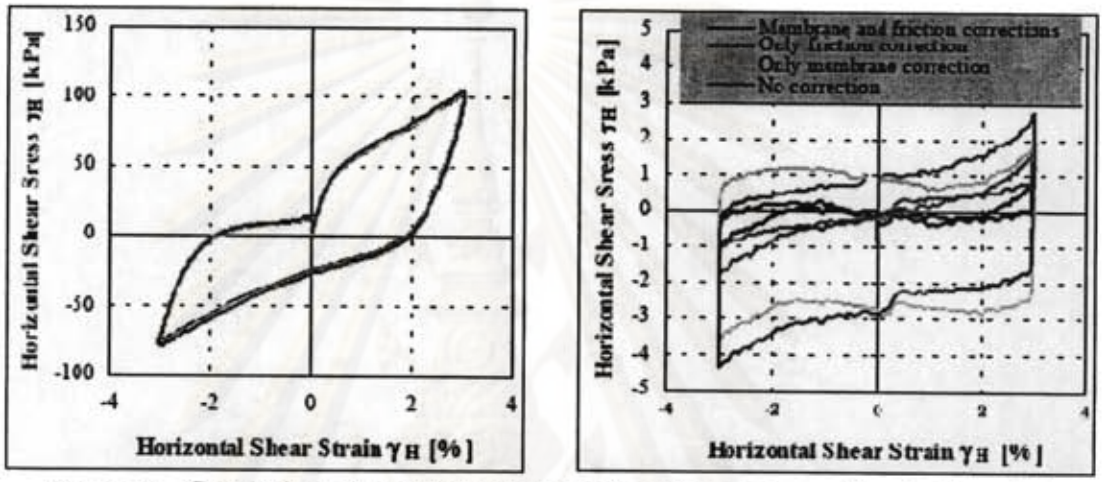

Figure 3-8 Correction on the first and the last cycles during a simple shear test (Vanden Berghe, 2001)

In general, there are some errors occurring during the laboratory testing such as instrument error, and rubber membrane error, etc. Therefore, measurement corrections should be taken into account in data setup. In DSS test, there are usually three kinds of corrections: friction correction, membrane correction, and zero correction.

The friction correction is provoked by DSS apparatus. To calibrate this correction, soil is sheared without any load and shear stress is recorded at first and last cycle of the test. The value of friction correction is found equal to 7 N ($\Delta\tau$ = 2 kPa) according to Vanden Berghe (2001) and is applied to horizontal load, as shown in Figure 3-8. This amplitude can be omitted in the monotonic test because it is very small compared to the shear resistance of the soil.

Another correction which should be considered is membrane correction. This correction includes the resistance of the membrane during shearing. The amplitude of membrane correction is added to shear stress. The calibration curves made by NGI were used, as illustrated in Figure 3-8.

Beside the foregoing friction and membrane corrections, the zero correction ought to be counted for. The zero correction takes into account the weight of top cap, friction in vertical direction, and friction at beginning of the test which is not possible to know that value. This zero correction amplitude is considered to be 0.3 kPa for shear stress and 1.5 kPa for axial stress.

B. Stress and Strain Computation

The stresses and strains presented in the recording file of LabVIEW software are calculated using the following equations:

- Shear consolidation strain $\gamma^{cons}(\%) = \frac{\Delta HD_0}{h_0 - \Delta VD_0} \times 100$ (3-1)
- Axial consolidation strain $\varepsilon_a^{cons}(\%) = \frac{\Delta VD_0}{h_0} \times 100$ (3-2)
- Shear consolidation stress $\tau^{cons}(kPa) = \frac{\Delta HL_0}{A_0}$ (3-4)
- Axial consolidation stress $\sigma_v^{cons}(kPa) = \frac{\Delta VL_0}{A_0}$ (3-3)
- Shear strain $\gamma\ (\%) = \frac{HD}{h_0 - \Delta VD_0} \times 100$ (3-5)
- Axial strain $\varepsilon_a\ (\%) = \frac{VD}{h_0 - \Delta VD_0} \times 100$ (3-6)
- Shear stress $\tau\ (kPa) = \frac{HL + \Delta HL_0 + \Delta HL_{friction} + \Delta HL_{membrane} + \Delta HL_{zero}}{A_0}$ (3-7)
- Axial stress $\sigma_v(kPa) = \frac{VL + \Delta VL_0 + \Delta VL_{zero}}{A_0}$ (3-9)
- Pore pressure $u = -\frac{VL}{A_0}$ (3-8)

Where

HD = the measured horizontal displacement

VD = the measured vertical displacement

HL = the measured horizontal load

VL = the measured vertical load

h_0 = the initial height of the specimen

A_0 = the cross-sectional area of the specimen

ΔHD_0 = the initial horizontal displacement of the specimen

ΔVD_0 = the initial vertical displacement of the specimen

ΔHL_0 = the initial horizontal load applied on the specimen

ΔVL_0 = the initial vertical load applied on the specimen

$\Delta HL_{friction}$ = the friction correction

$\Delta HL_{membrane}$ = the membrane correction

ΔHL_{zero} = the horizontal zero correction

ΔVL_{zero} = the vertical zero correction

CHAPTER 4
MONOTONIC TEST RESULTS

4.1 Introduction

In this chapter, the direct shear box (DSB) test and monotonic direct simple shear (DSS) test will be performed. In order to facilitate the illustration of the data, two main sections are divided. First section is about the results of DSB test on dry sand. Second section presents the results obtained from DSS test on dry sand and saturated sand. The summary of experimental procedures of monotonic test is shown in Table 1. The interpretations of all data from the foregoing laboratory tests will be discussed in Chapter VI.

4.2 Results of DSB Test

This section describes the experimental results of DSB test, which is carried out on dry RS and WS at various effective vertical stress (σ_v'). During testing, the drained (constant normal stress) tests are conducted with dry sand sample reconstituted by dry tamping method, as mentioned in Section 3.4.4. Speed rate of horizontal displacement used to shear specimen is 0.3 mm/s according to ASTM D3080 (2006). Figure 4-1 to Figure 4-3 shows WS at natural relative density $D_r \cong 90\%$ by varying $\sigma_v' = 150\ kPa, 200\ kPa, 250\ kPa, and\ 300\ kP$ to find out internal friction angle. In addition, Figure 4-4 to Figure 4-9 is about RS at $D_r \cong 40\%\ and\ 80\%$ to investigate the difference between loose state and dense state with the range of $\sigma_v' = 50\ kPa, 100\ kPa, 150\ kPa, and\ 200\ kPa$.

Table 4-1Summary of experimental procedures of monotonic test

Test No[1].	Types of Test	Sample Preparation Method	e_0	e_c	e_{cs}	D_r (%)	σ_n'
RS1	Drained DSB	Dry tamping	0.516	NA	NA	47	50
RS2			0.520			45	100
RS3			0.546			34	150
RS4			0.542			36	200
RS5			0.466			70	50
RS6			0.464			71	100
RS7			0.476			66	150
RS8			0.436			84	200
WS9			0.533			91	150
WS10			0.532			91	200
WS11			0.540			89	250
WS12			0.534			91	300
RS13	Constant normal stress (Drained) DSS	Dry tamping	0.532	0.516	0.529	40	50
RS14			0.531	0.515	0.526	41	100
RS15			0.533	0.509	0.517	40	150
RS16			0.533	0.510	0.520	40	200
RS17			0.456	0.449	0.463	75	50
RS18			0.449	0.436	0.436	78	100
RS19			0.450	0.442	0.454	77	150
RS20			0.453	0.430	0.445	76	200
WS21			0.522	0.504	0.520	94	150
WS22			0.523	0.504	0.515	94	200
WS23			0.525	0.500	0.509	93	250
WS24			0.519	0.493	0.504	95	300
RS25	Constant volume (Undrained) DSS	Water pluviation	0.535	NA	NA	38.54	50
RS26			0.527			42.10	100
RS27			0.529			41.45	150
RS28			0.525			42.97	200
RS29			0.460			72.51	50
RS30			0.450			77.30	100
RS31			0.450			77.36	150
RS32			0.449			77.82	200
WS3			0.548			86.99	150
WS4			0.535			90.46	200
WS5			0.525			93.32	250
WS6			0.543			88.40	300

Note: e_0 = initial void ratio
e_c = void ratio presheared
e_{cs} = critical void ratio

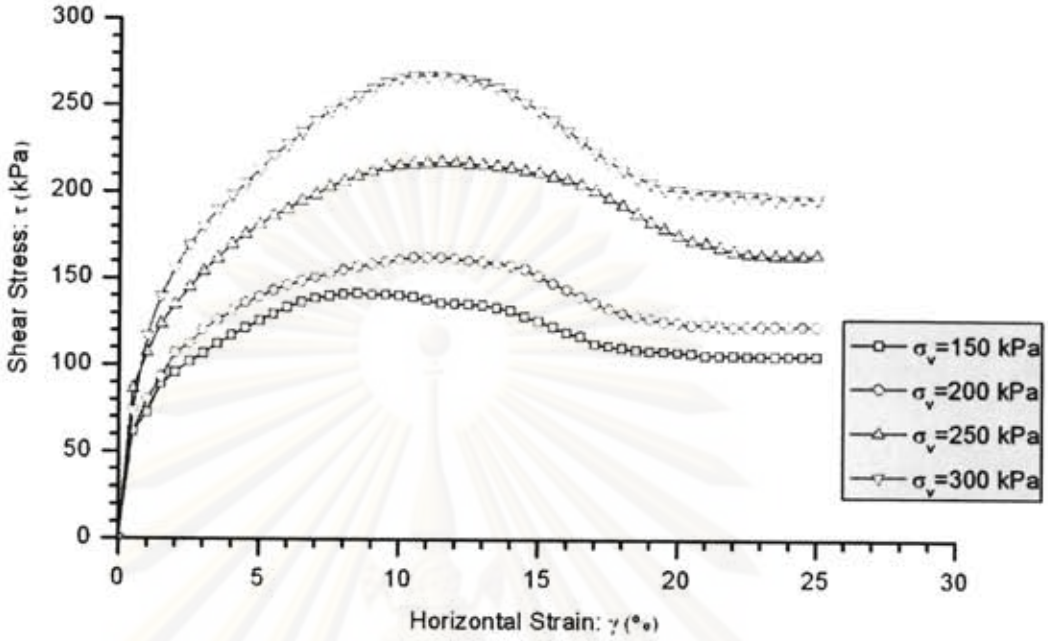

(a)

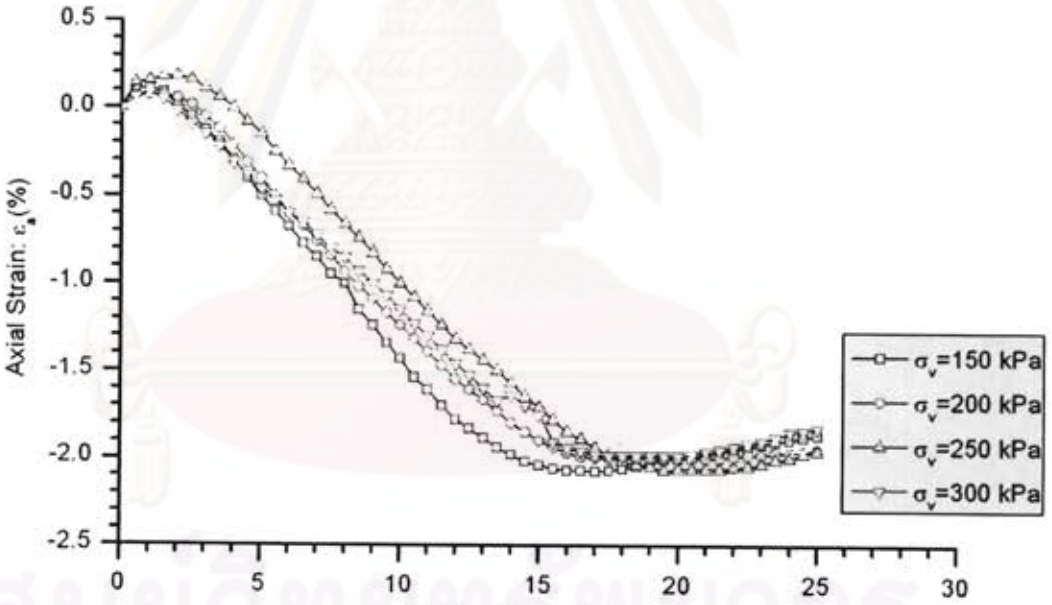

(b)

Figure 4-1 DSB test on dry WS at $D_r \cong 90\%$ ($e_0 = 0.54$); (a) Stress-strain behavior; (b) Axial strain-horizontal strain relationship

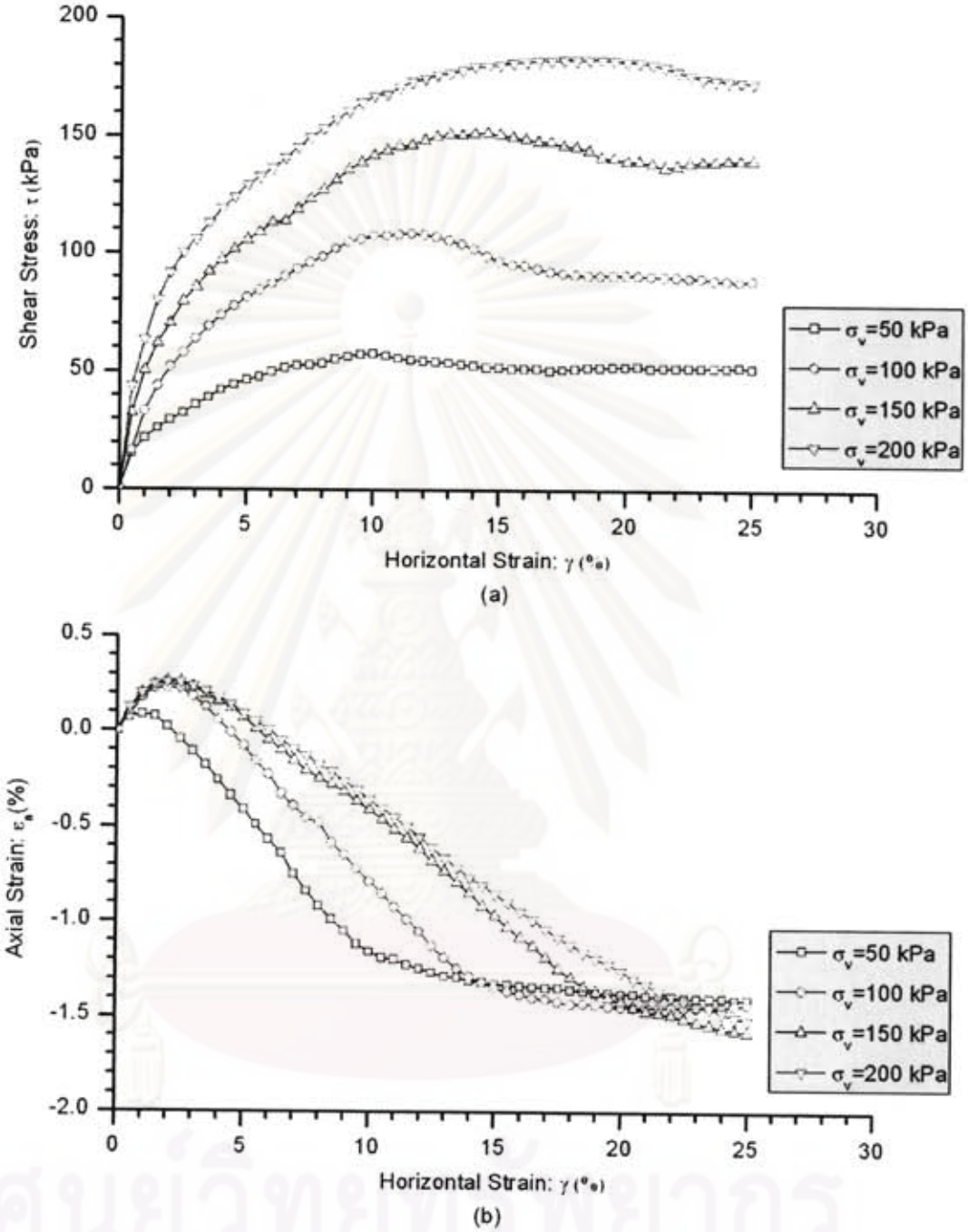

Figure 4-2 DSB test on dry RS at $D_r \cong 40\%$ ($e_0 = 0.53$); (a) Stress-strain behavior; (b) Axial strain-horizontal strain relationship

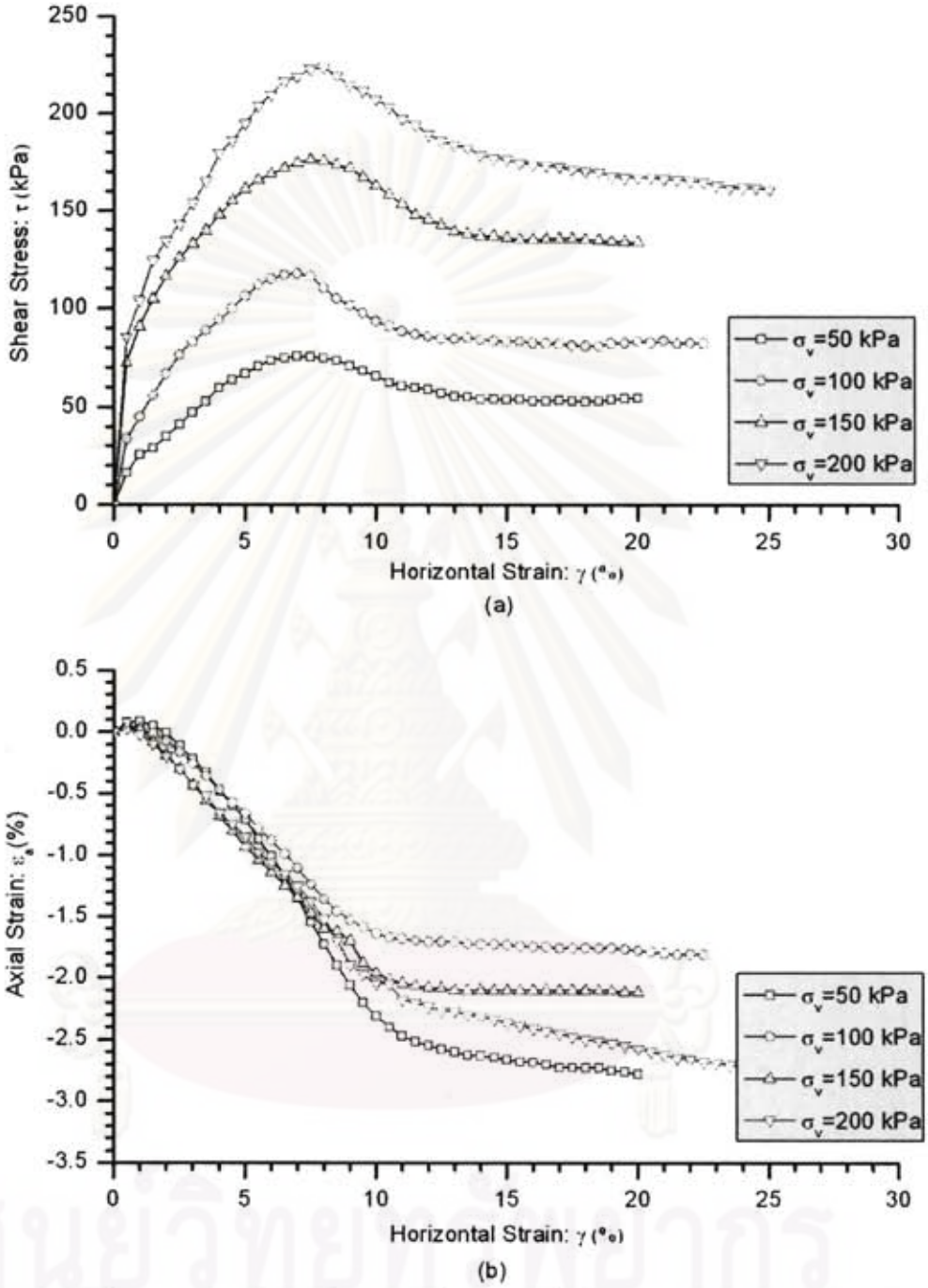

Figure 4-3 DSB test on dry RS at $D_r \cong 80\%$ ($e_0 = 0.44$); (a) Stress-strain behavior; (b) Axial strain-horizontal strain relationship

4.3 Results of DSS Test

In this section, the testing results of monotonic DSS test are separated into two parts. First part exhibits the dry sand results from drained test, and second part presents the saturated sand results from undrained (constant volume) test. Analysis and comparison of these two conditions will be discussed later.

4.3.1 Drained Monotonic DSS Test

Laboratory results of drained DSS test conducted on dry RS and WS will be shown in this part. Tested sands are prepared by dry tamping method, as detailed in Section 3.4.4. Speed rate to shear the specimen is approximately equal to 15% per hour, according to ASTM D6528 (2006). Figure 4-10 to Figure 4-12 illustrates results of WS at $D_r \cong 90\%$ with $\sigma_v' = 150\ kPa, 200\ kPa, 250\ kPa, and\ 300\ kPa$. In addition, results of RS are pointed out in Figure 4-13 to Figure 4-18 at $D_r \cong 40\%\ and\ 80\%$ with $\sigma_v' = 50\ kPa, 100\ kPa, 150\ kPa, and\ 200\ kPa$.

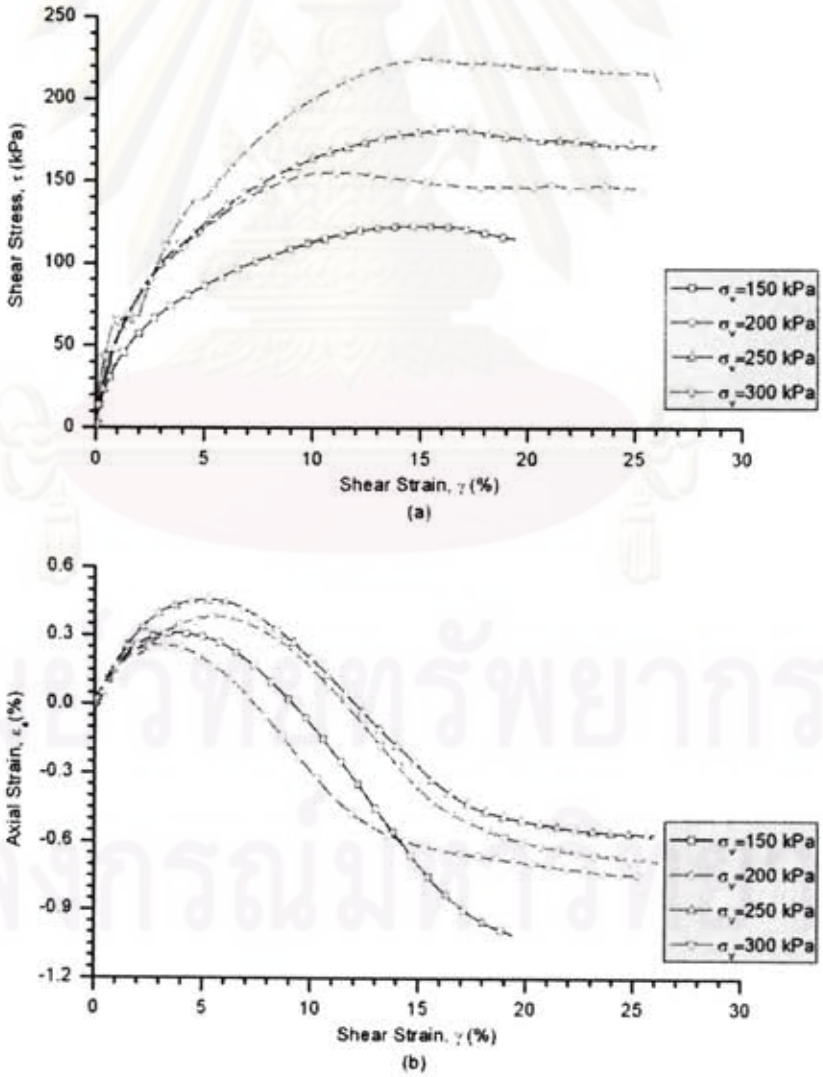

Figure 4-4 Drained DSS test on dry WS at $D_r \cong 90\%$ ($e_0 = 0.54$); (a) Stress-strain behavior; (b) Axial strain-horizontal strain relation

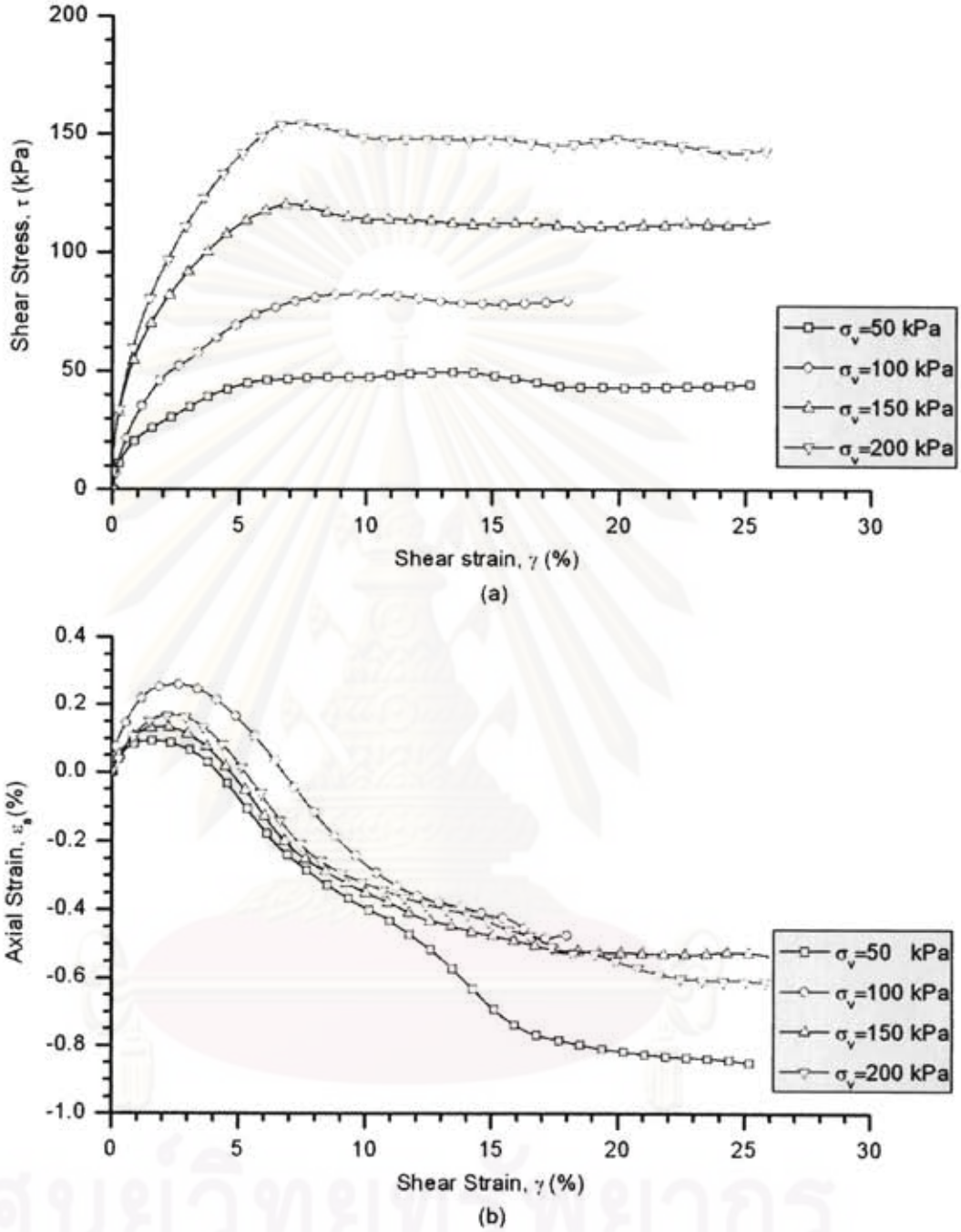

Figure 4-5 Drained DSS test on dry RS at $D_r \cong 40\%$ ($e_0 = 0.53$); (a) Stress-strain behavior; (b) Axial strain-horizontal strain relation

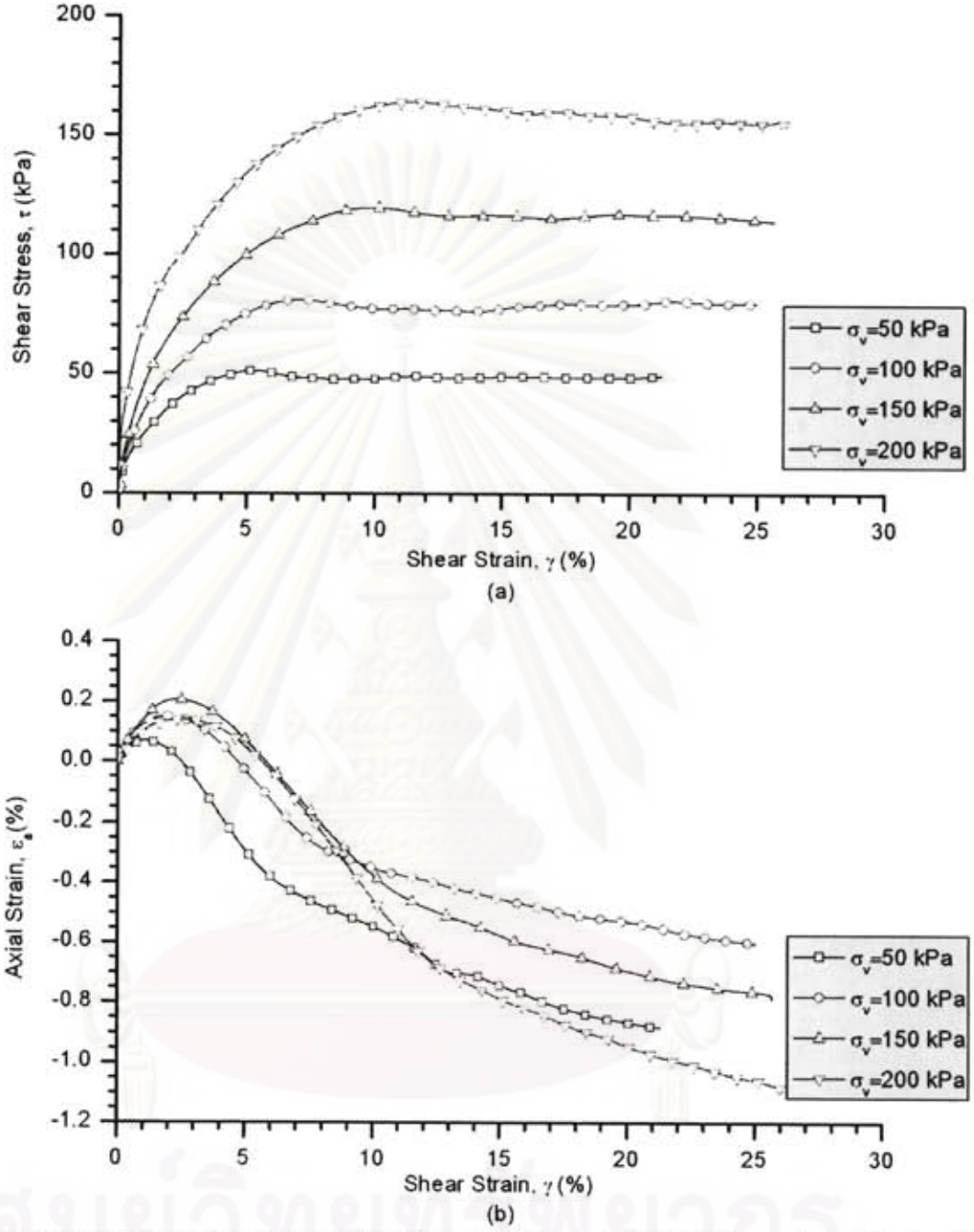

Figure 4-6 Drained DSS test on dry RS at $D_r \cong 80\%$ ($e_0 = 0.44$); (a) Stress-strain behavior; (b) Axial strain-horizontal strain relation

4.3.2 Undrained Monotonic DSS Test

Interesting experimental results of undrained or constant volume DSS test on saturated RS and WS will be depicted in this part. Tested sands are reconstituted by water pluviation method, as clearly indicated in Section 3.4.5. Speed rate to shear specimen is the same as drained monotonic DSS test, 15% per hour. Figure 4-19 to Figure 4-24 indicate the WS results at $D_r \cong 90\%$ with $\sigma_v' = 150\ kPa, 200\ kPa, 250\ kPa, and\ 300\ kPa$. Furthermore, the results of RS are shown in Figure 4-25 to Figure 4-36 at $D_r \cong 40\%\ and\ 80\%$ with $\sigma_v' = 50\ kPa, 100\ kPa, 150\ kPa, and\ 200\ kPa$.

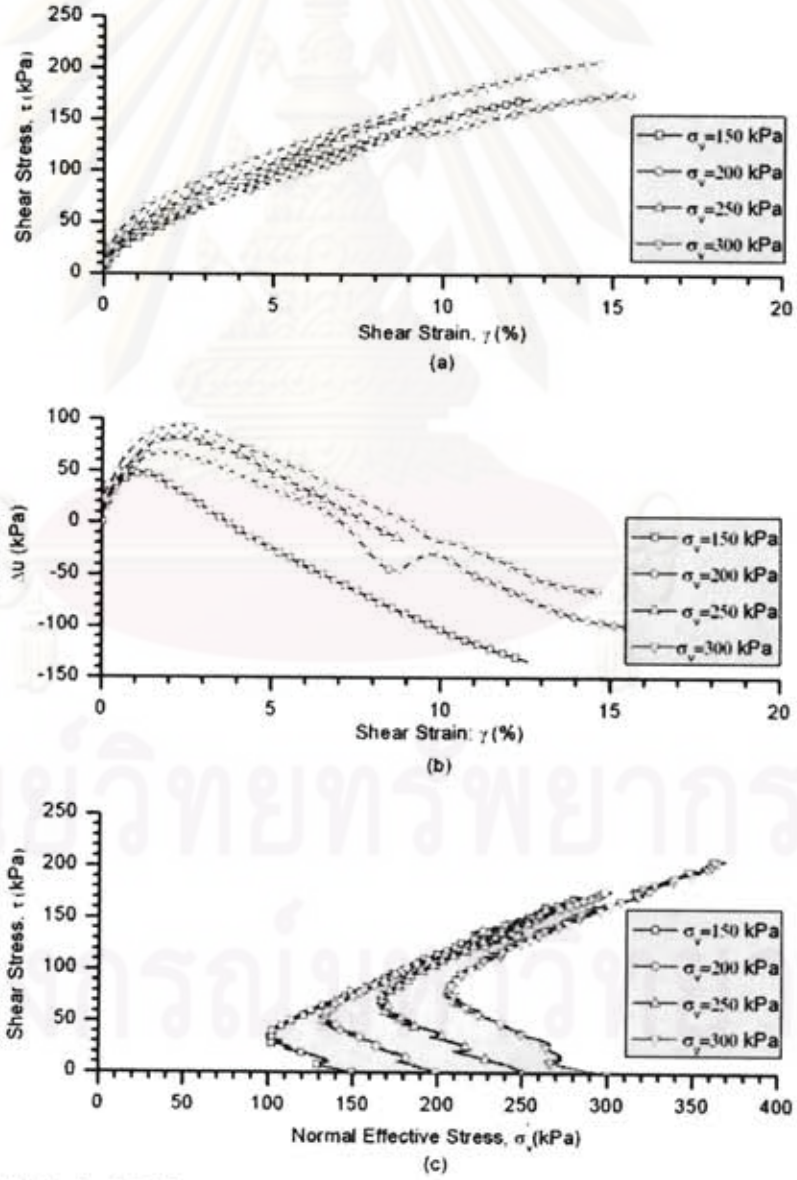

Figure 4-7 Undrained DSS test on saturated WS at $D_r \cong 90\%$ ($e_0 = 0.54$); (a) Stress-strain behavior; (b) Excess pore water pressure-shear strain relationship; (c) Stress path

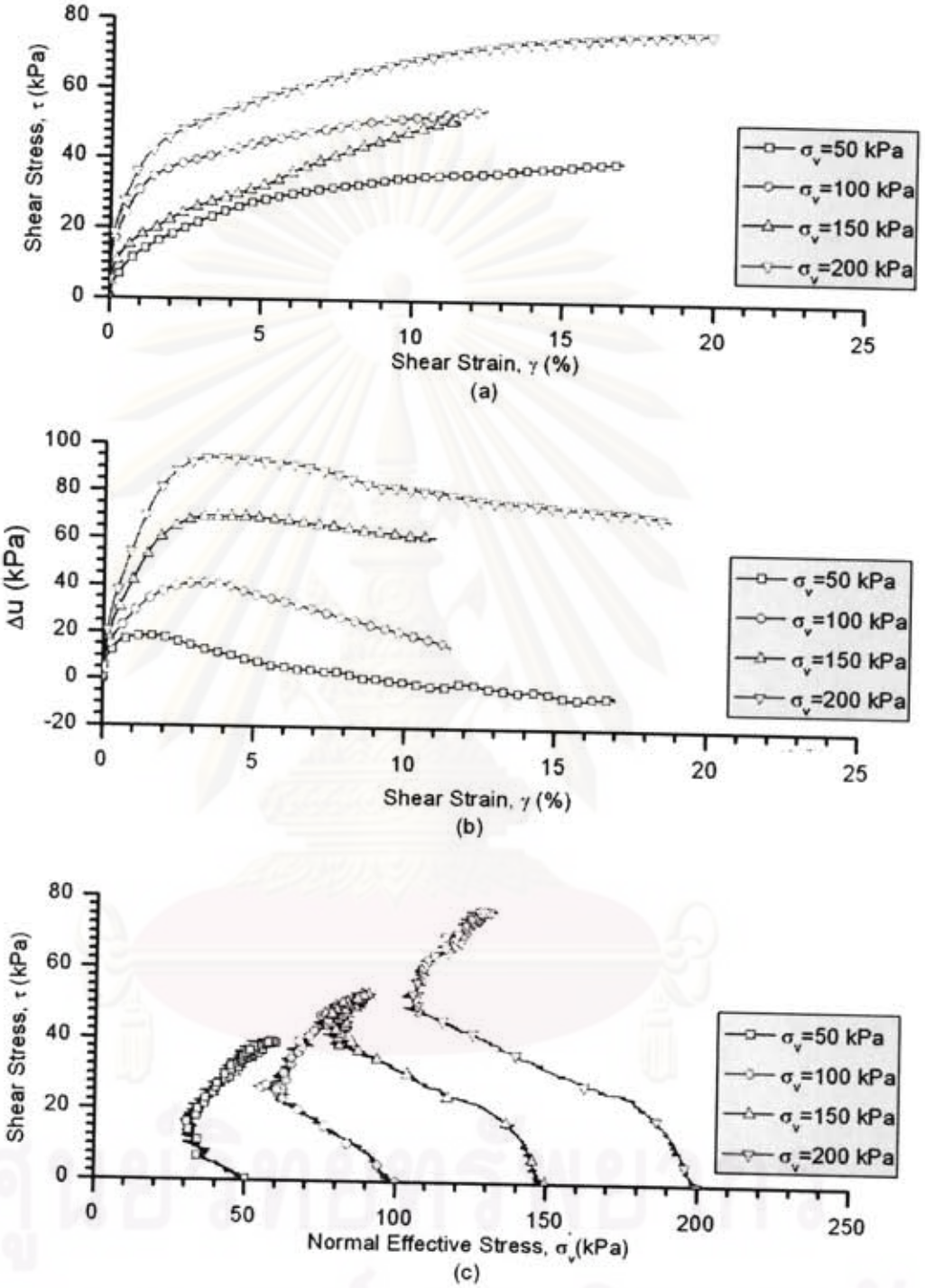

Figure 4-8 Undrained DSS test on saturated RS at $D_r \cong 40\%$ ($e_0 = 0.53$); (a) Stress-strain behavior; (b) Excess pore water pressure-shear strain relationship; (c) Stress path

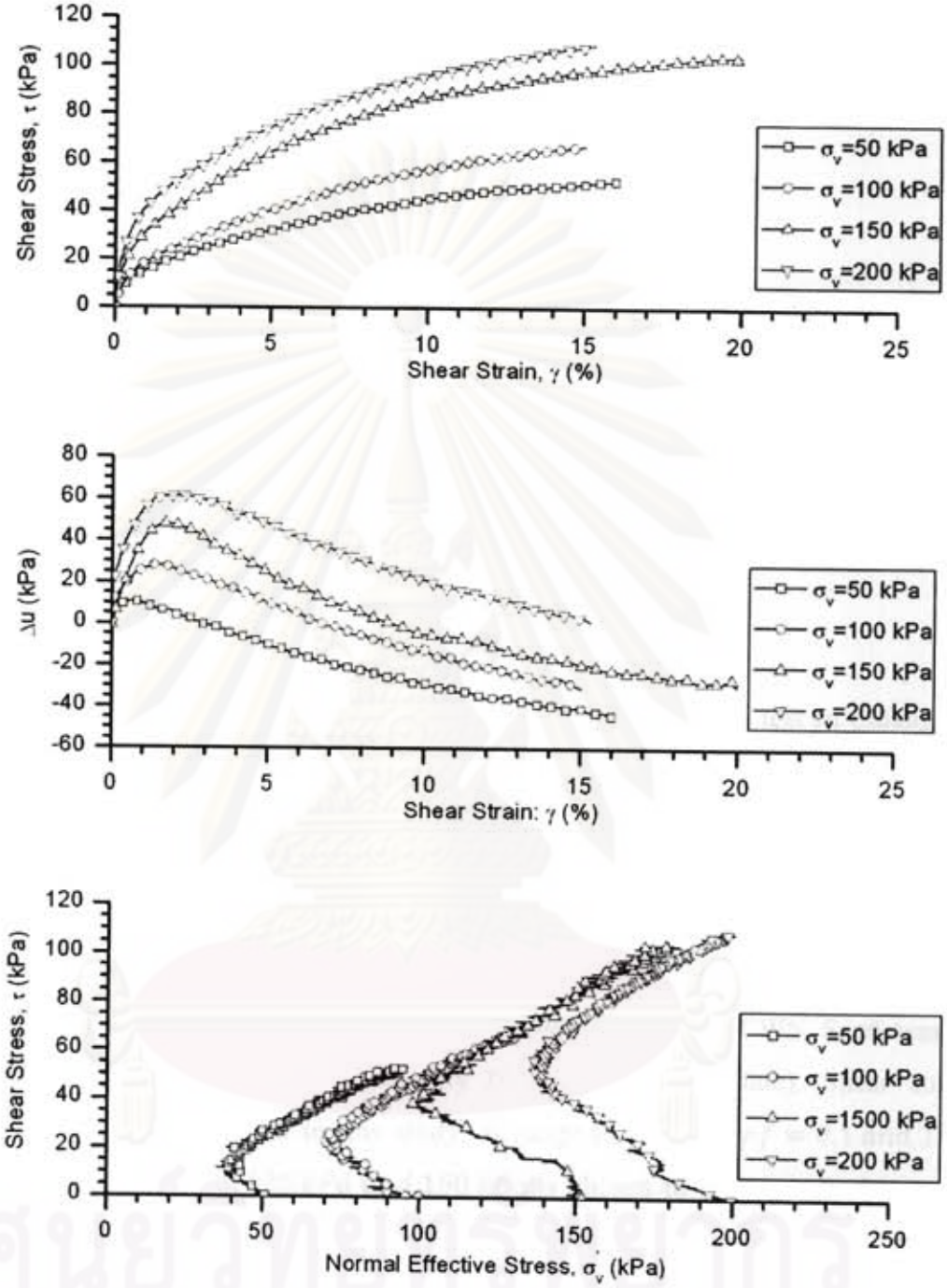

Figure 4-9 undrained DSS test on saturated RS at $D_r \cong 80\%$ ($e_0 = 0.44$); (a) Stress-strain behavior; (b) Excess pore water pressure-shear strain relationship; (c) Stress path

CHAPTER 5
CYCLIC TEST RESULTS

5.1 Introduction

In this chapter, cyclic direct simple shear (DSS) test will be carried out in drained or constant normal stress condition to determine dynamic properties of Chiang Mai sand (G_S *and* λ). Several parameters, such as relative density (D_r), shear strain amplitude (γ), vertical stress (σ_v), and frequency (f), are varied so as to investigate the effect on cyclic response of studied sand. In order to facilitate the demonstration of the data, two major sections are separated:

- The results of DSS test on Wat Chedi Luang sand (WS)
- The results of DSS test on River sand (RS)

The summary of experimental procedure and results of cyclic DSS test on Chiang Mai sand is given in Table 5-1.

5.2 Results of Cyclic DSS test on Wat Chedi Luang Sand

This section presents the results of drained cyclic DSS test on Wat Chedi Luang sand. The experiment is conducted to simulate the in-situ condition of WS. Sand samples are prepared to natural relative density $D_r \cong 90\%$ (dense state). Shear strains amplitude $\gamma = 0.5\%$ is used in this study. A range of frequency $f = 0.1$ *and* $1\ Hz$, and vertical stress $\sigma_v = 125\ kPa$ *and* $150\ kPa$ is chosen to observe whether or not such variation of f, and σ_v can greatly affect the dynamic properties of WS. In addition, the number of stress cycles (N) is expected to reach 1000 cycles in each sample during cyclic testing in order to figure out the influence on sand dynamic properties. However, some samples cannot get N = 1000 cycles owing to the error of DSS apparatus data acquisition system. This issue can be handled by extending the fitting curves and will be pointed out in Chapter VI.

Figure 5-1 shows a typical set of cyclic shear response of Test WS1 at $\sigma_v = 125\ kPa$ *and* $f = 0.1\ Hz$. As shown in Figure 5-1(a), hysteresis loop

(*shear stress against shear strain*) is plotted on the top of left hand side. Figure 5-1(b) and (c) illustrate shear stress (τ) plotted against number of cycle (N) on the top of right hand side, and N against γ on the bottom of left hand side, respectively. Figure 5-1(d) on the bottom of right hand side expresses the stress path (τ *versus* σ_v) with critical state line ($\emptyset'_{CS} = 30^0$), which is determined from monotonic DSS test in preceding chapter. The interpretation and discussion of these results will be shown in next chapter. In addition, Figure 5-2 depicts the detail of hysteresis loop of Test WS1 at $\sigma_v = 125\ kPa$ *and* $f = 0.1\ Hz$ for various N. Similarly, Figure 5-3 to 5-8 shows the cyclic response and detail of hysteresis loop of WS at different σ_v *and* f.

Table 5-1 Summary list of test procedures and dynamic properties results at N = 10th cycle

Test No.	e_0	D_r	γ	σ_v	f	G_S	λ_d
		(%)	(%)	*(kPa)*	*(Hz)*	*(MPa)*	(%)
WS1	0.55	87.48	0.5	125	0.1	6.92	12.21
WS2	0.54	88.09	0.5	125	1	7.28	12.20
WS3	0.54	89.50	0.5	150	0.1	7.03	12.08
WS4	0.55	86.50	0.5	150	1	6.87	11.57
RS-LS1	0.53	39.93	0.5	100	0.1	6.78	18.33
RS-LS2	0.54	37.22	0.5	200	0.1	11.98	14.89
RS-LS3	0.53	41.88	0.5	300	0.1	13.67	12.25
RS-LS4	0.54	38.47	1	100	0.1	4.11	17.27
RS-LS5	0.53	39.78	1	200	0.1	6.48	12.01
RS-LS6	0.53	39.27	1	300	0.1	8.61	11.74
RS-LS7	0.53	40	2	100	0.1	2.82	17.29
RS-LS8	0.53	40.87	2	200	0.1	6.38	19.03
RS-LS9	0.53	41.16	2	300	0.1	7.31	17.10
RS-DS1	0.44	81.31	0.5	100	0.1	5.24	17.17
RS-DS2	0.46	74.29	0.5	200	0.1	10.15	12.67
RS-DS3	0.44	81.44	0.5	300	0.1	14.42	13.87
RS-DS4	0.44	81.44	1	100	0.1	4.18	14.61
RS-DS5	0.44	82.15	1	200	0.1	7.01	15.70
RS-DS6	0.44	81.50	1	300	0.1	9.57	12.38
RS-DS7	0.45	78.27	2	100	0.1	3.80	20.57
RS-DS8	0.44	80	2	200	0.1	5.27	18.52
RS-DS9	0.44	79.70	2	300	0.1	7.76	18.71

Note: LS = loose state
DS = dense state

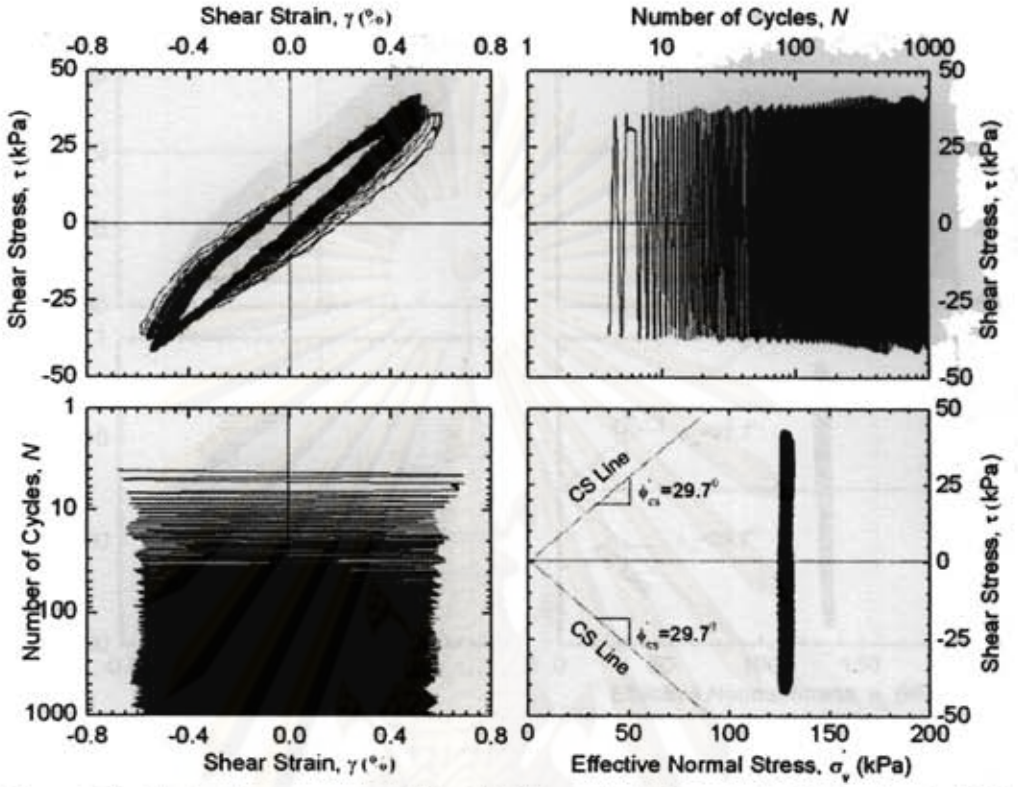

Figure 5-1 Cyclic shear response of Test WS1 ($\gamma = 0.5\%$; $\sigma_v = 125\ kPa$; $f = 0.1\ Hz$)

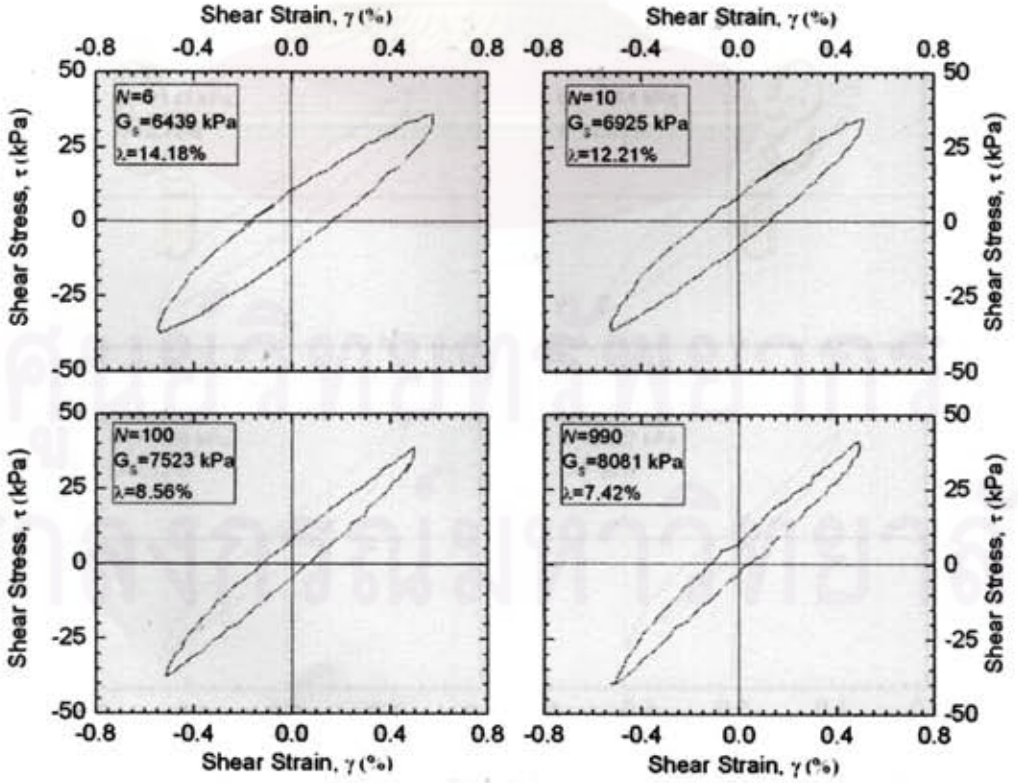

Figure 5-2 Detail of hysteresis loop of Test WS1 ($\gamma = 0.5\%$; $\sigma_v = 125\ kPa$; $f = 0.1\ Hz$)

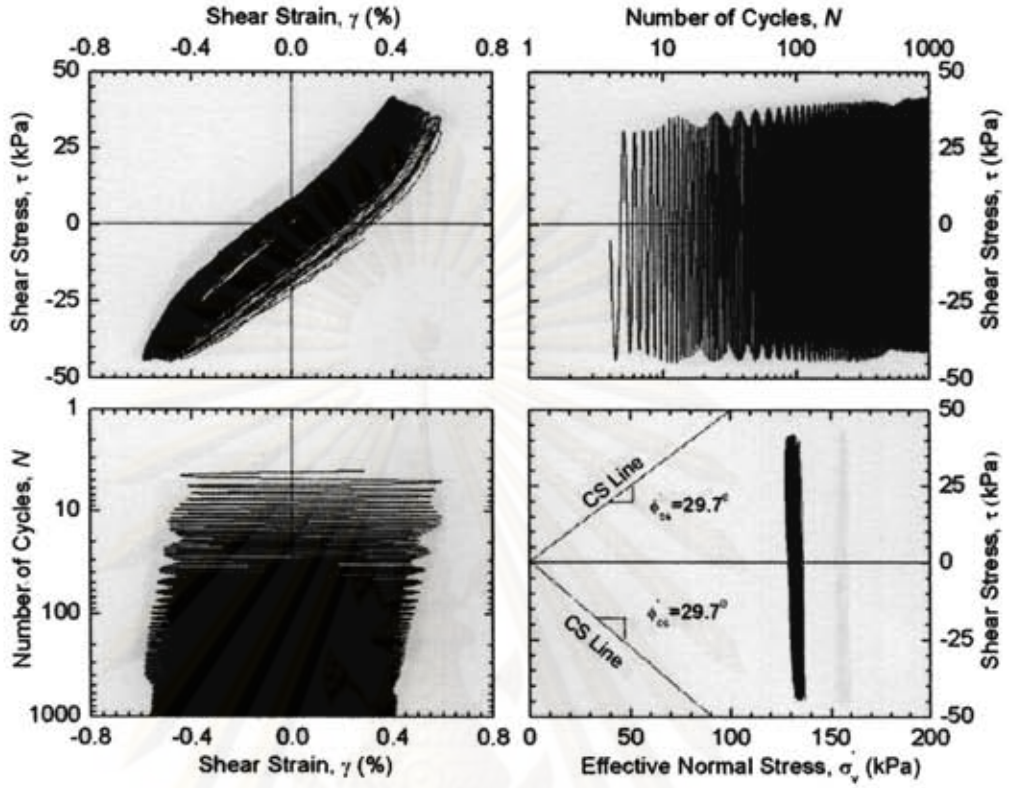

Figure 5-3 Cyclic shear response of Test WS2 ($\gamma = 0.5\%$; $\sigma_v = 125\ kPa$; $f = 1\ Hz$)

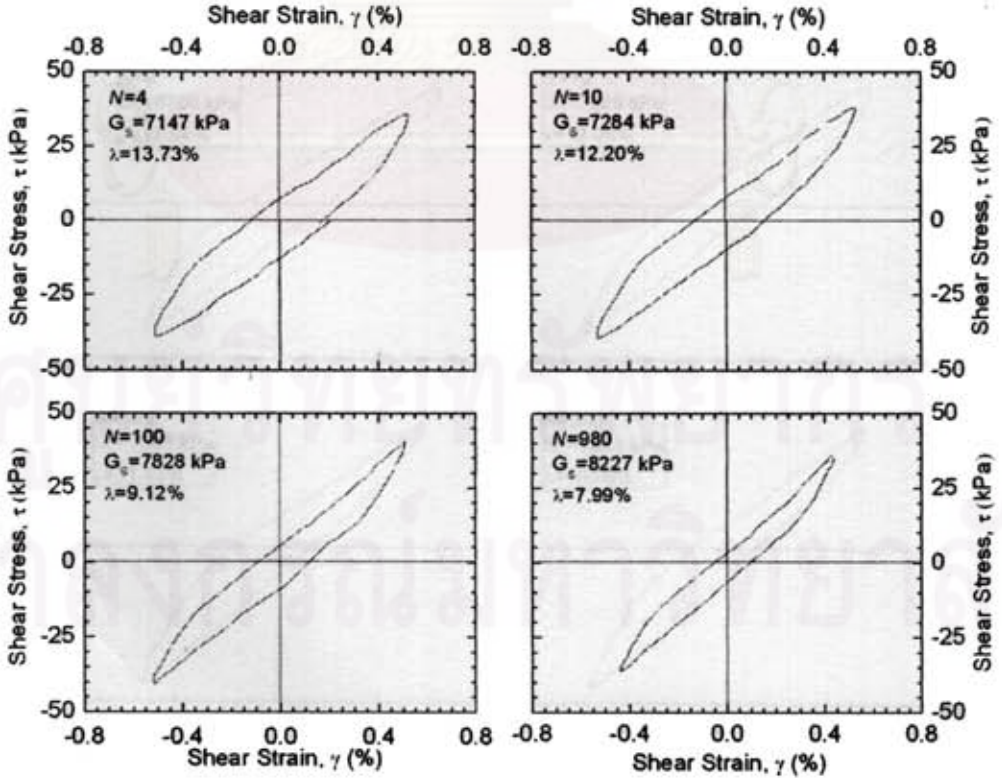

Figure 5-4 Detail of hysteresis loop of Test WS2 ($\gamma = 0.5\%$; $\sigma_v = 125\ kPa$; $f = 0.1\ Hz$)

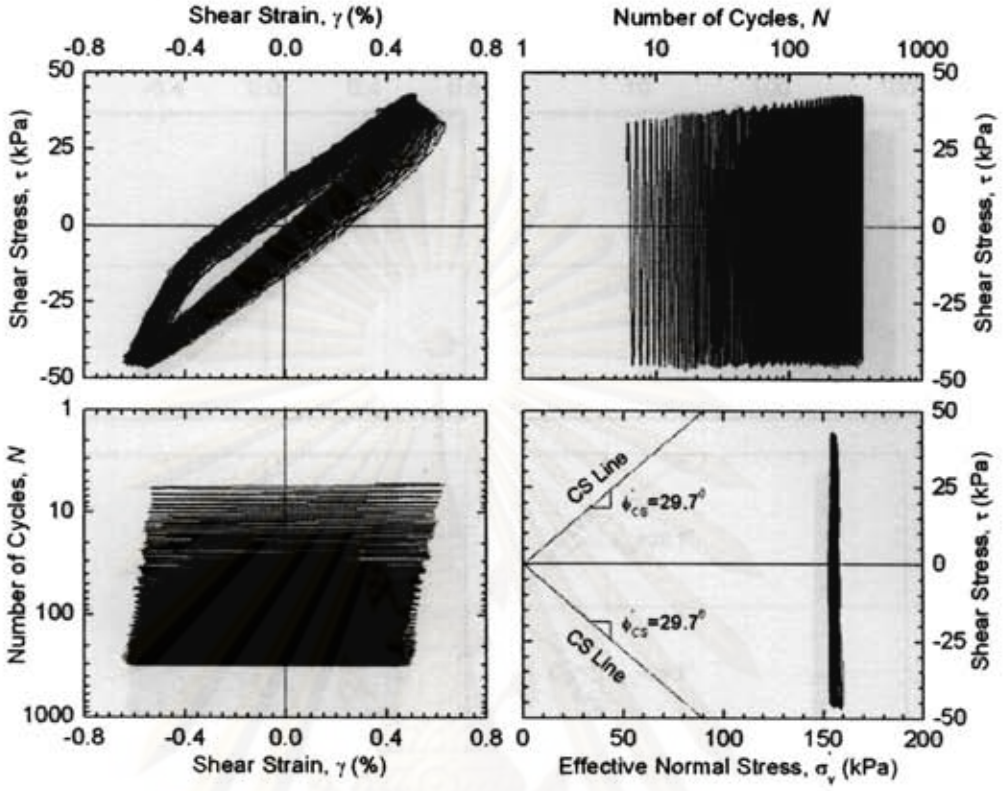

Figure 5-5 Cyclic shear response of Test WS3 ($\gamma = 0.5\%$; $\sigma_v = 150\ kPa$; $f = 0.1\ Hz$)

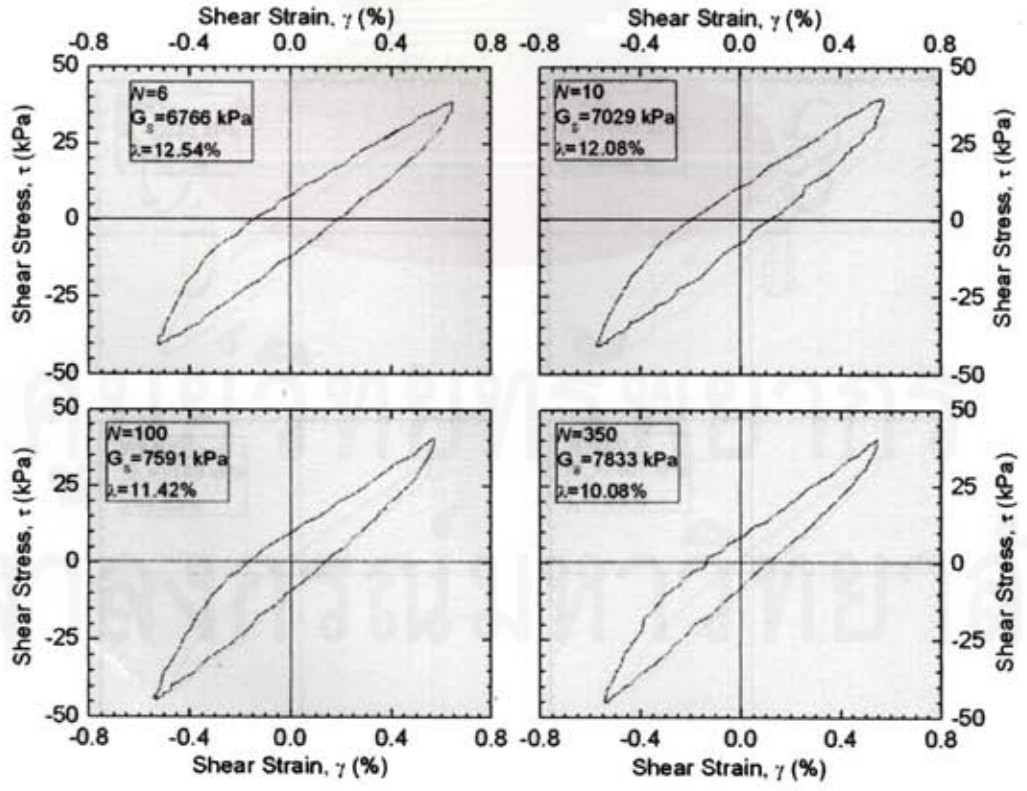

Figure 5-6 Detail of hysteresis loop of Test WS3 ($\gamma = 0.5\%$; $\sigma_v = 150\ kPa$; $f = 0.1\ Hz$)

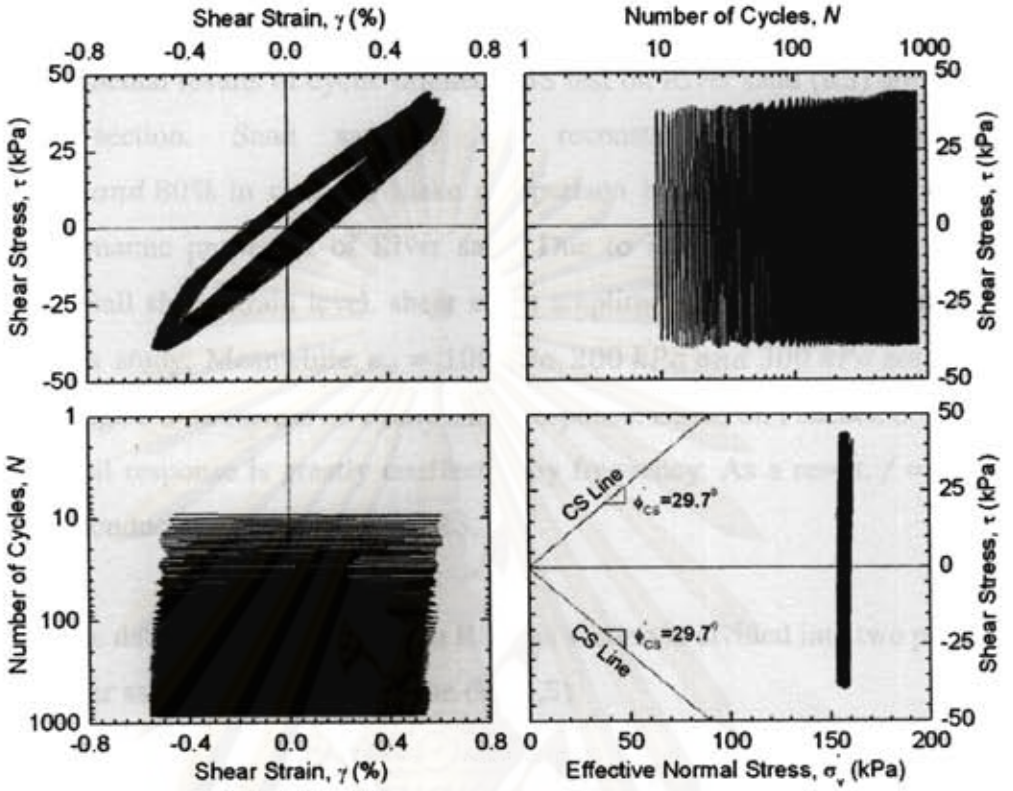

Figure 5-7 Cyclic shear response of Test WS4 ($\gamma = 0.5\%$; $\sigma_v = 150\ kPa$; $f = 1\ Hz$)

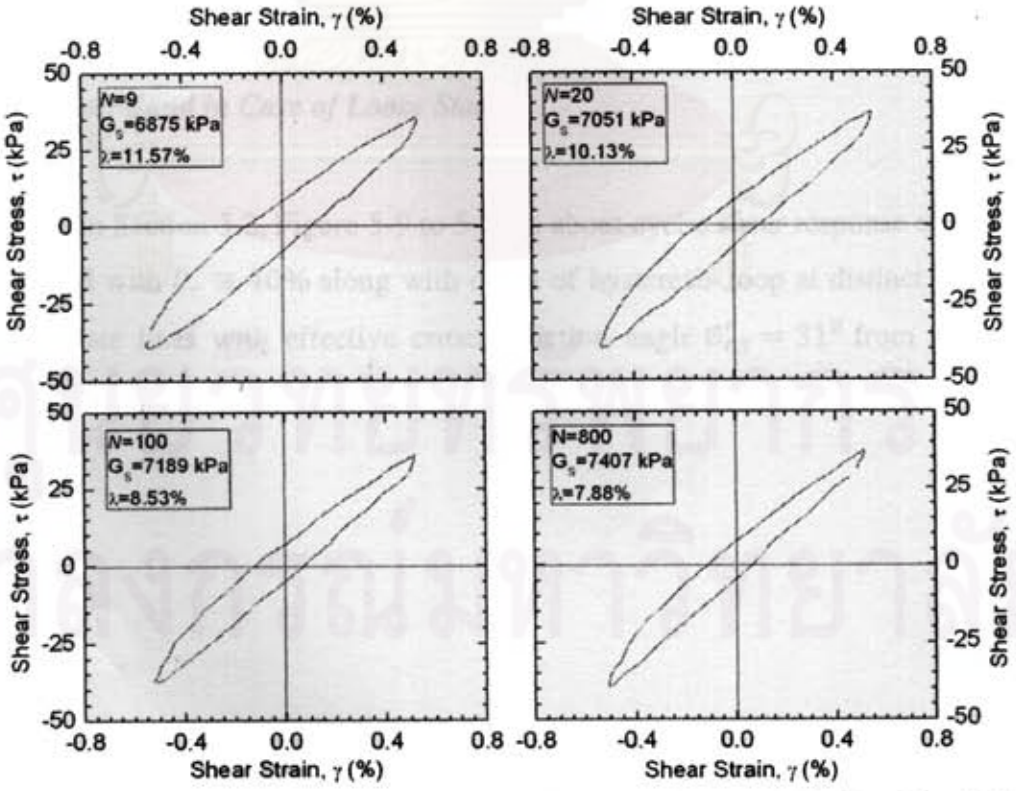

Figure 5-8 Detail of hysteresis loop of Test WS4 ($\gamma = 0.5\%$; $\sigma_v = 150\ kPa$; $f = 1\ Hz$)

5.3 Results of Cyclic DSS Test on River Sand

The experimental results of cyclic drained DSS test on River sand (RS) are illustrated in this section. Sand samples are reconstituted to relative density $D_r \cong 40\%\ and\ 80\%$ in order to make comparison between loose state and dense state on dynamic properties of River sand. Due to inability of the DSS apparatus tested at small shear strain level, shear strain amplitudes $\gamma = 0.5\%, 1\%, and\ 2\%$ are used in this study. Meanwhile, $\sigma_v = 100\ kPa, 200\ kPa\ and\ 300\ kPa$ are varied so as to investigate their effects on cyclic shear response. Based on Peacock et al. (1968), dynamic soil response is greatly unaffected by frequency. As a result, $f = 0.1$ Hz is chosen to conduct the experiment for RS.

Due to large data of cyclic DSS test on RS, this section is divided into two parts:

- River sand in case of loose state (RS-LS)
- River sand in case of dense state (RS-DS)

The interpretation and discussion of these results will be taken into account in later chapter.

5.3.1 River Sand in Case of Loose State

Likewise in Section 5.2, Figure 5-9 to 5-26 is about cyclic shear response of saturated River sand with $D_r \cong 40\%$ along with detail of hysteresis loop at distinct $\gamma\ and\ \sigma_v$. Critical state lines with effective critical friction angle $\emptyset'_{CS} = 31^0$ from monotonic DSS test are plotted in stress path schematic diagrams as shown in the foregoing figure.

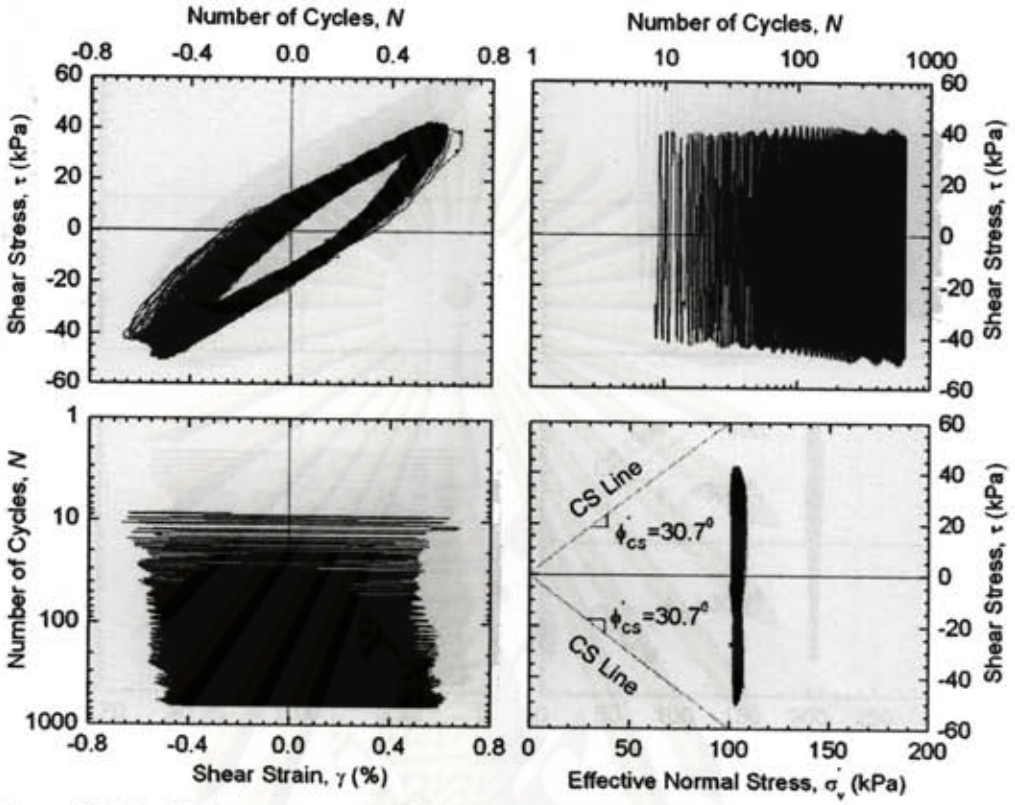

Figure 5-9 Cyclic shear response of Test RS-LS1 ($\gamma = 0.5\%$; $\sigma_v = 100\ kPa$; $f = 0.1\ Hz$)

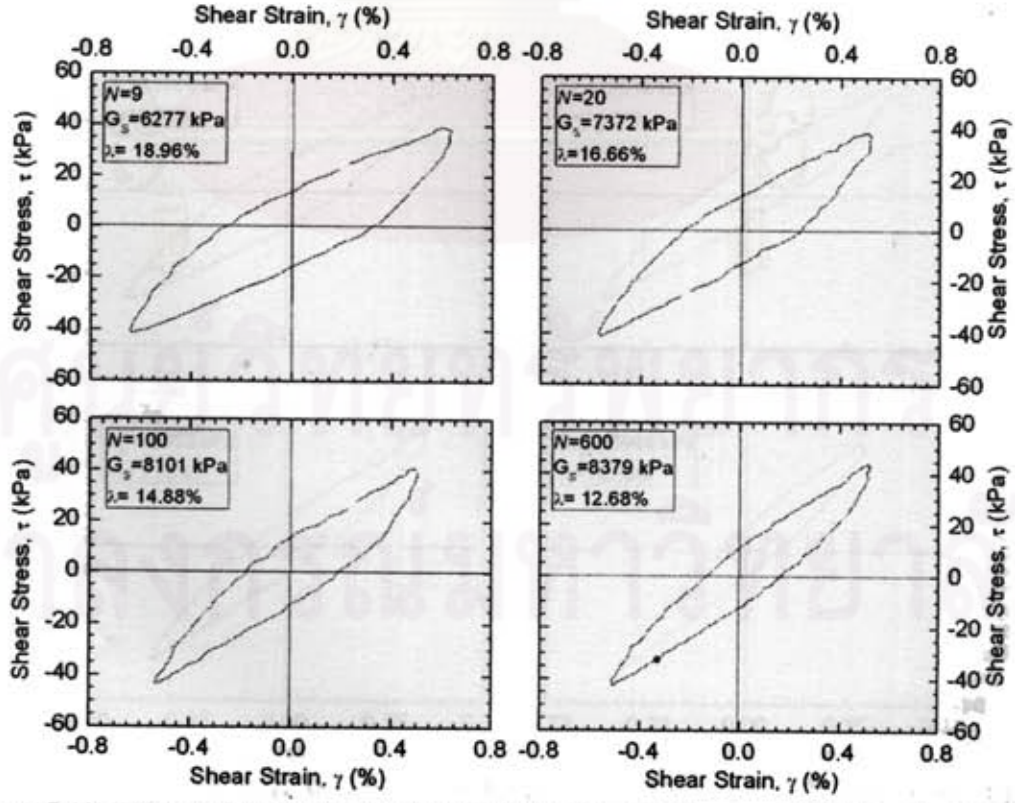

Figure 5-10 Detail of hysteresis loop of Test RS-LS1 ($\gamma = 0.5\%$; $\sigma_v = 100\ kPa$; $f = 0.1\ Hz$)

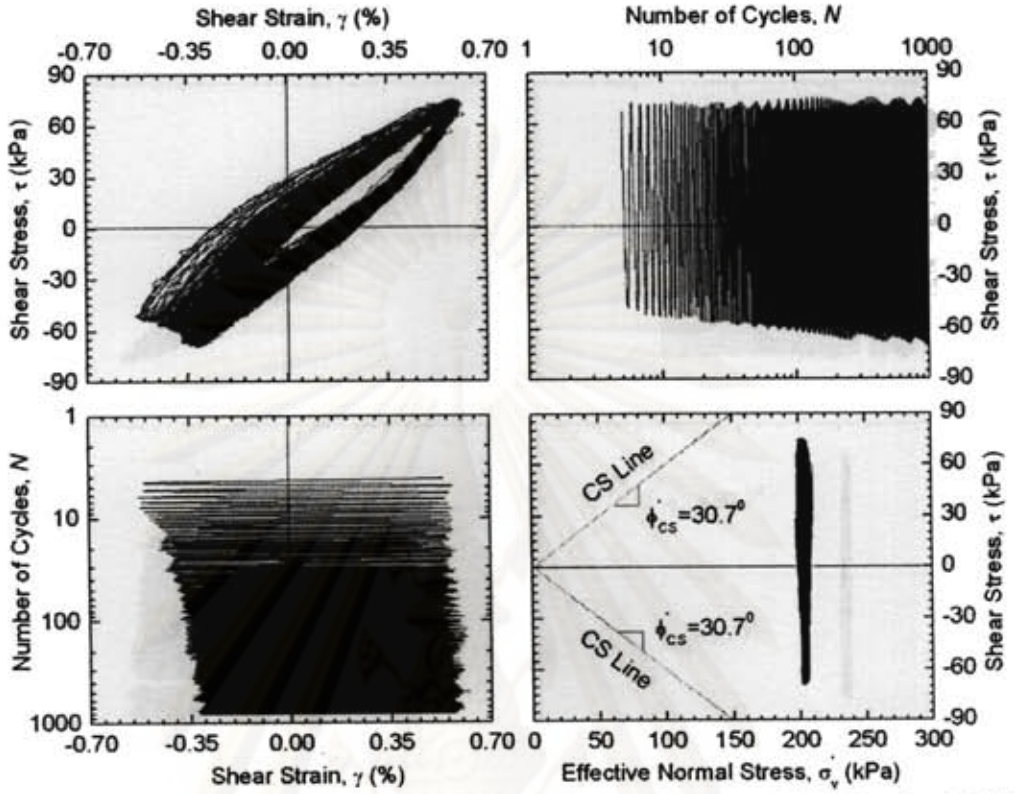

Figure 5-11 Cyclic shear response of Test RS-LS2 ($\gamma = 0.5\%$; $\sigma_v = 200\ kPa$; $f = 0.1\ Hz$)

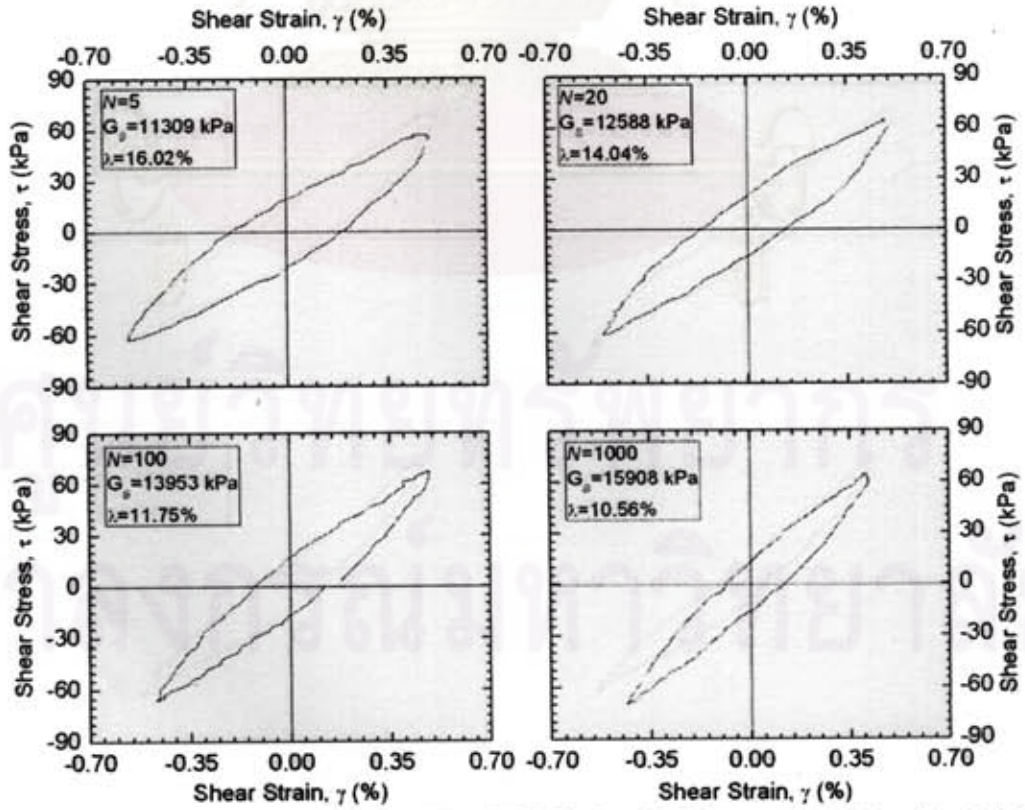

Figure 5-12 Detail of hysteresis loop of Test RS-LS2 ($\gamma = 0.5\%$; $\sigma_v = 200\ kPa$; $f = 0.1\ Hz$)

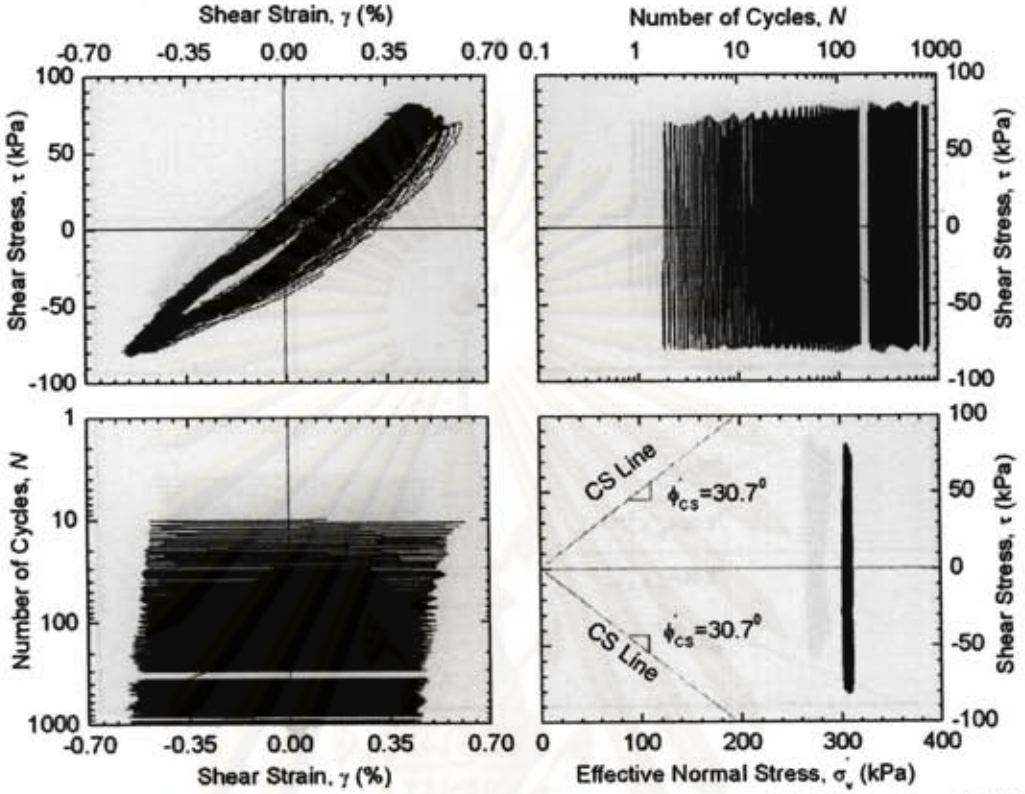

Figure 5-13 Cyclic shear response of Test RS-LS3 ($\gamma = 0.5\%$; $\sigma_v = 300\ kPa$; $f = 0.1\ Hz$)

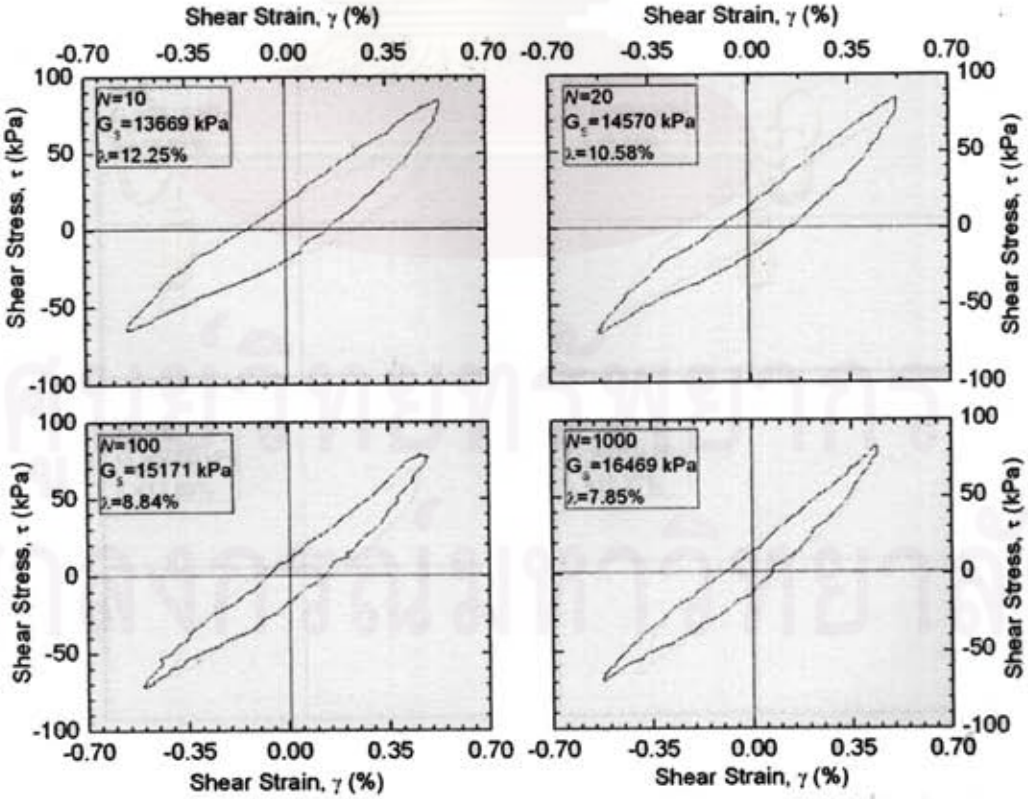

Figure 5-14 Detail of hysteresis loop of Test RS-LS3 ($\gamma = 0.5\%$; $\sigma_v = 300\ kPa$; $f = 0.1\ Hz$)

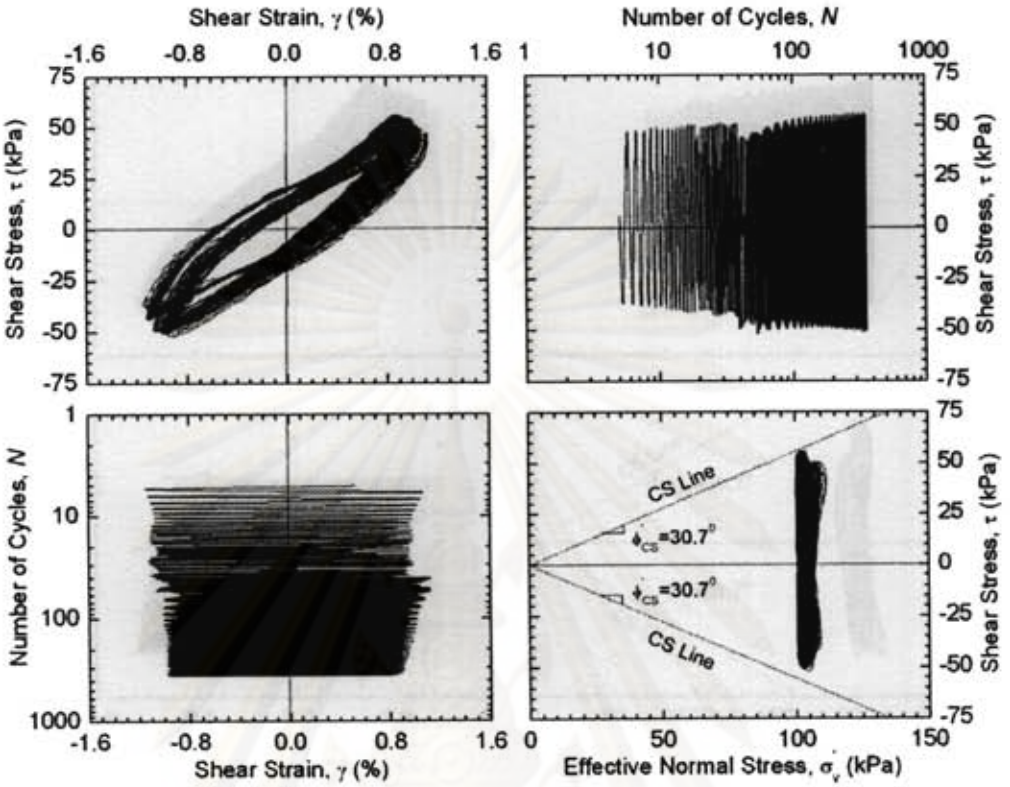

Figure 5-15 Cyclic shear response of Test RS-LS4 ($\gamma = 1\%$; $\sigma_v = 100\ kPa$; $f = 0.1\ Hz$)

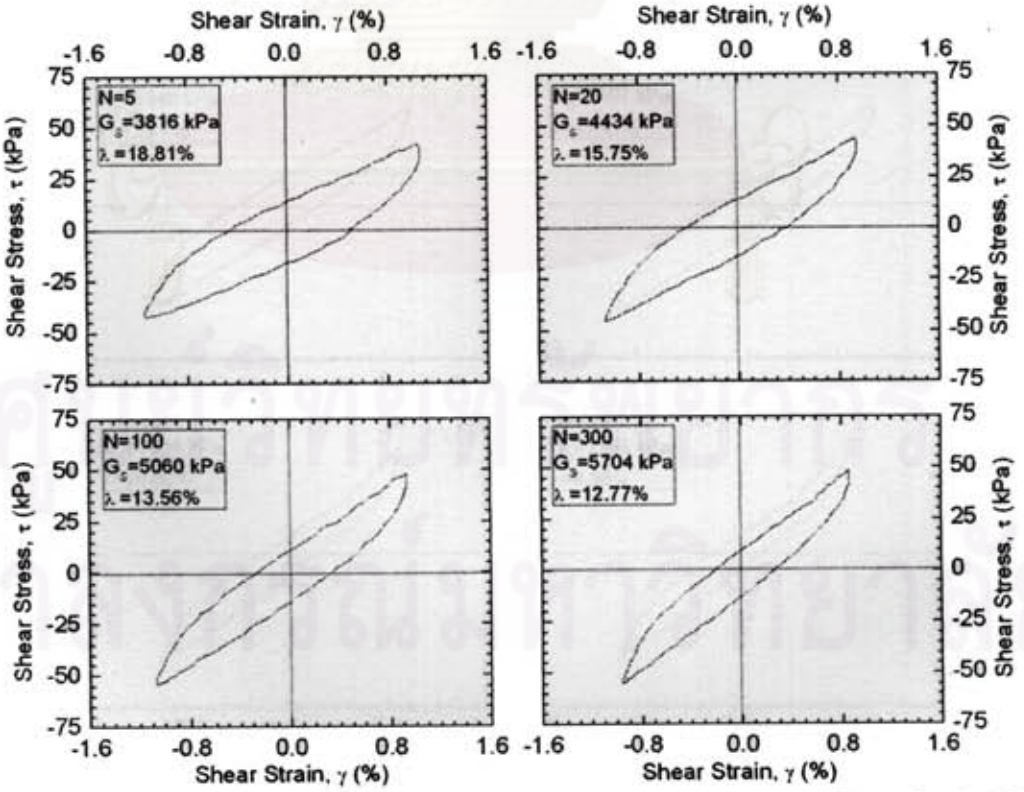

Figure 5-16 Detail of hysteresis loop of Test RS-LS4 ($\gamma = 1\%$; $\sigma_v = 100\ kPa$; $f = 0.1\ Hz$)

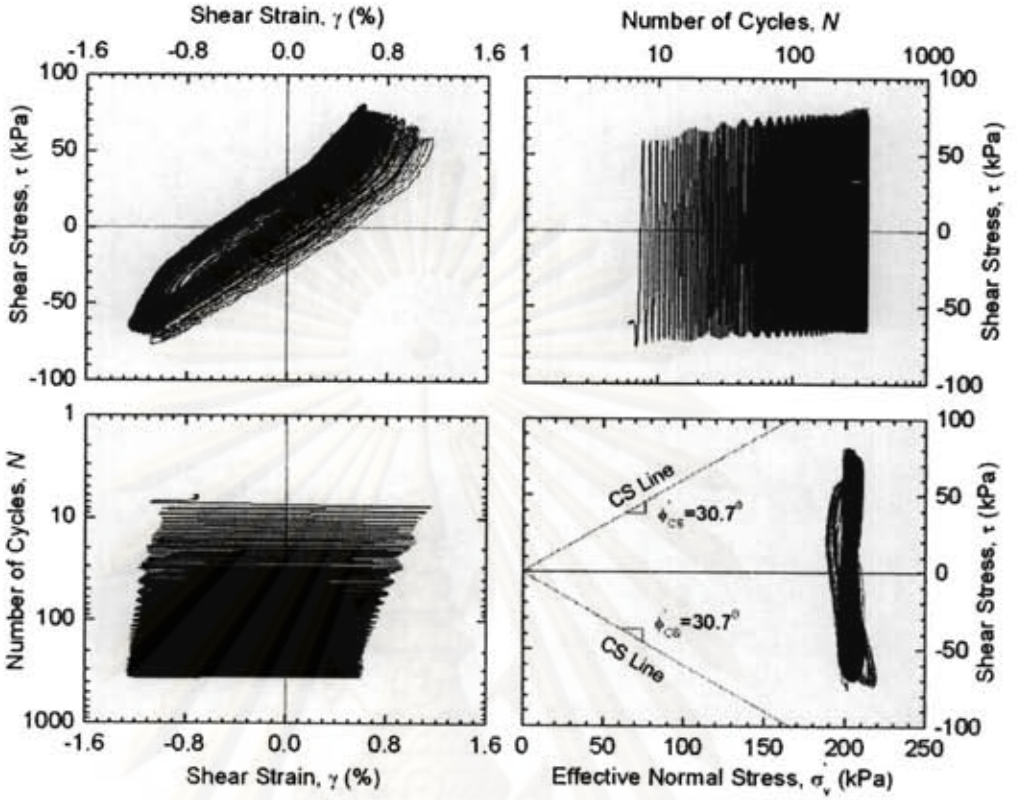

Figure 5-17 Cyclic shear response of Test RS-LS5 ($\gamma = 1\%$; $\sigma_v = 200\ kPa$; $f = 0.1\ Hz$)

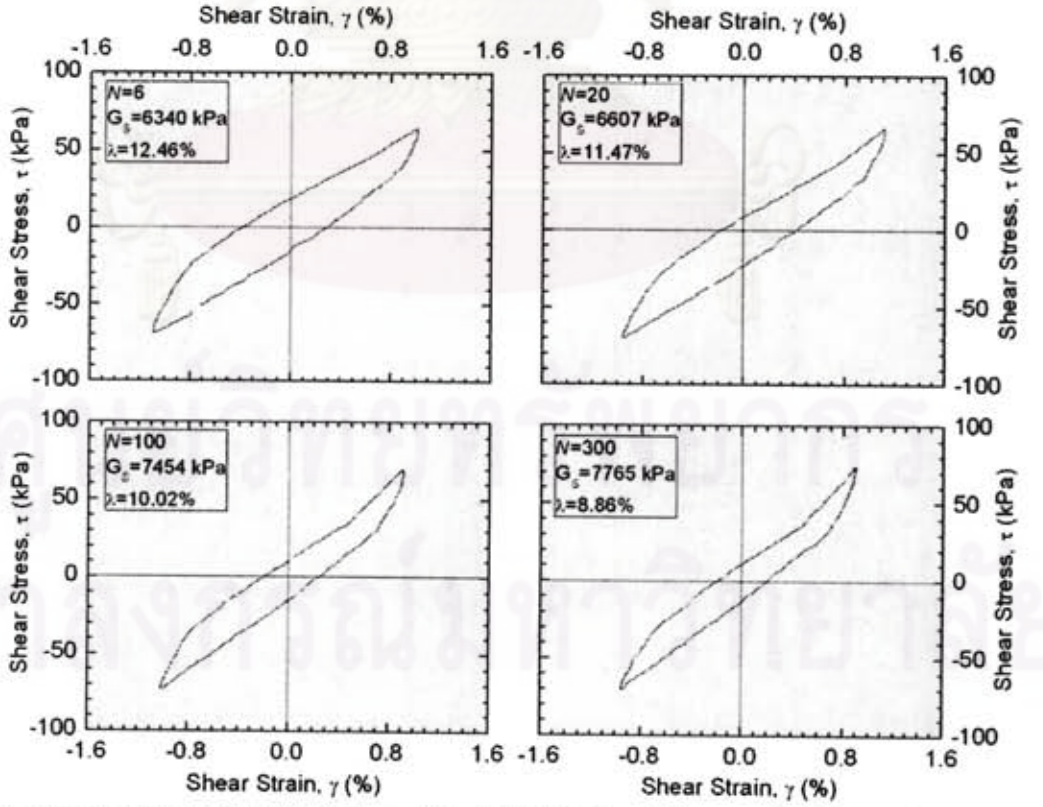

Figure 5-18 Detail of hysteresis loop of Test RS-LS5 ($\gamma = 1\%$; $\sigma_v = 200\ kPa$; $f = 0.1\ Hz$)

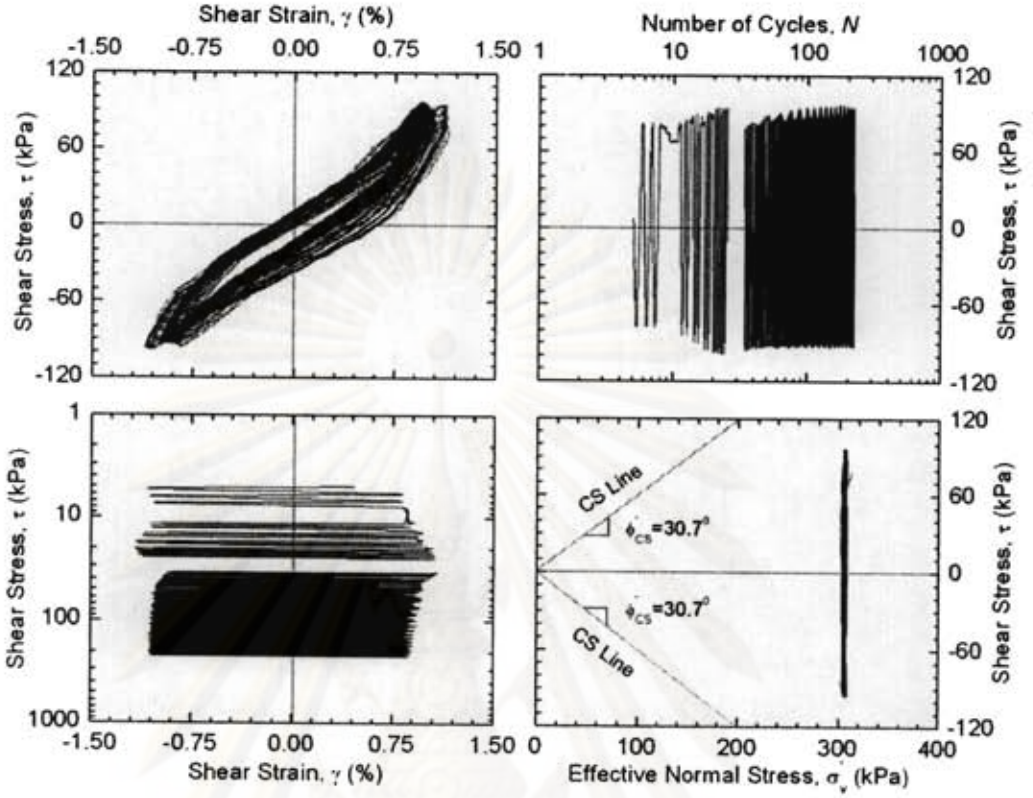

Figure 5-19 Cyclic shear response of Test RS-LS6 ($\gamma = 1\%$; $\sigma_v = 300\ kPa$; $f = 0.1\ Hz$)

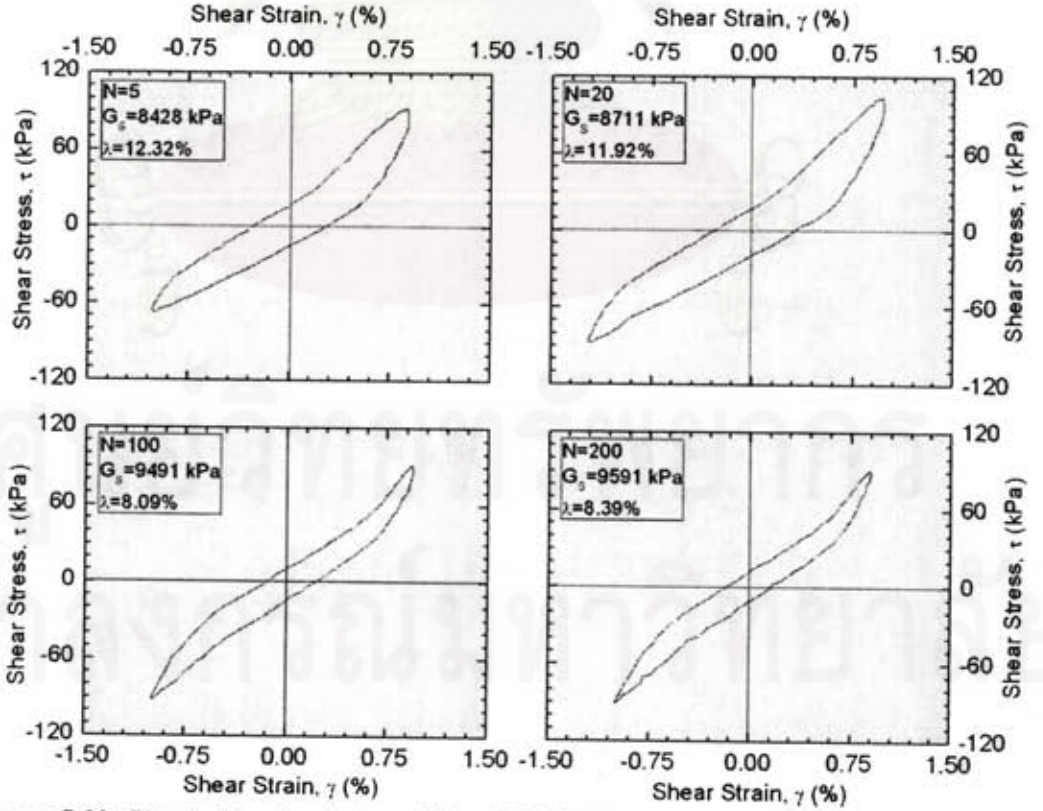

Figure 5-20 Detail of hysteresis loop of Test RS-LS6 ($\gamma = 1\%$; $\sigma_v = 300\ kPa$; $f = 0.1\ Hz$)

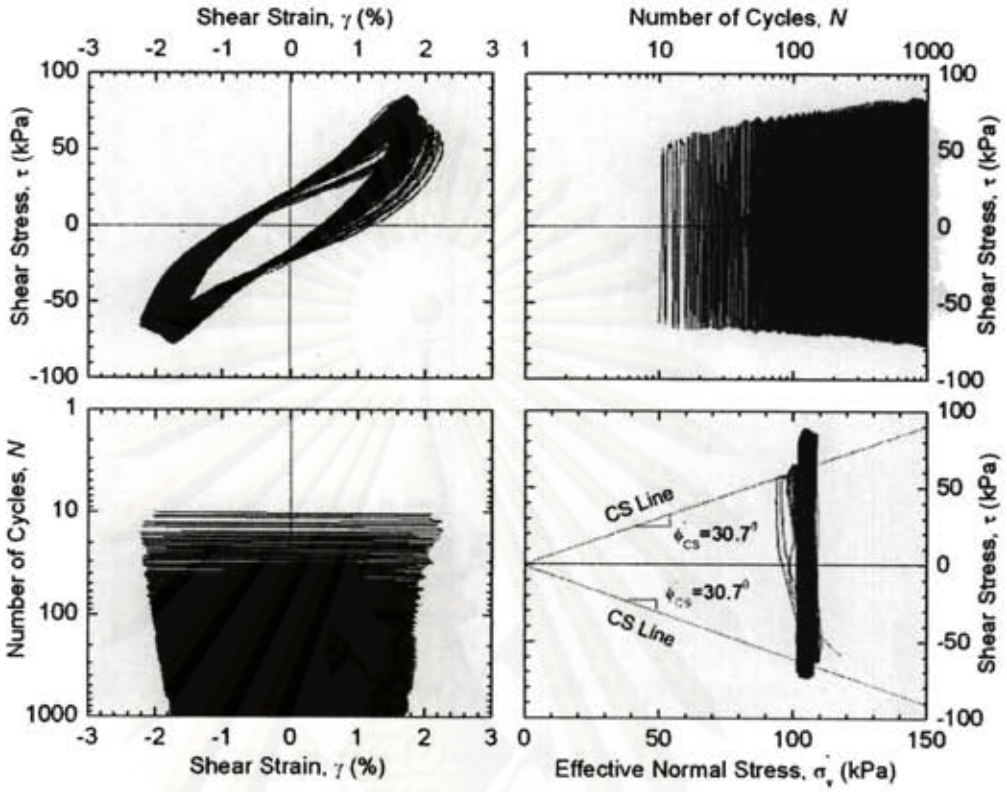

Figure 5-21 Cyclic shear response of Test RS-LS7 ($\gamma = 2\%$; $\sigma_v = 100\ kPa$; $f = 0.1\ Hz$)

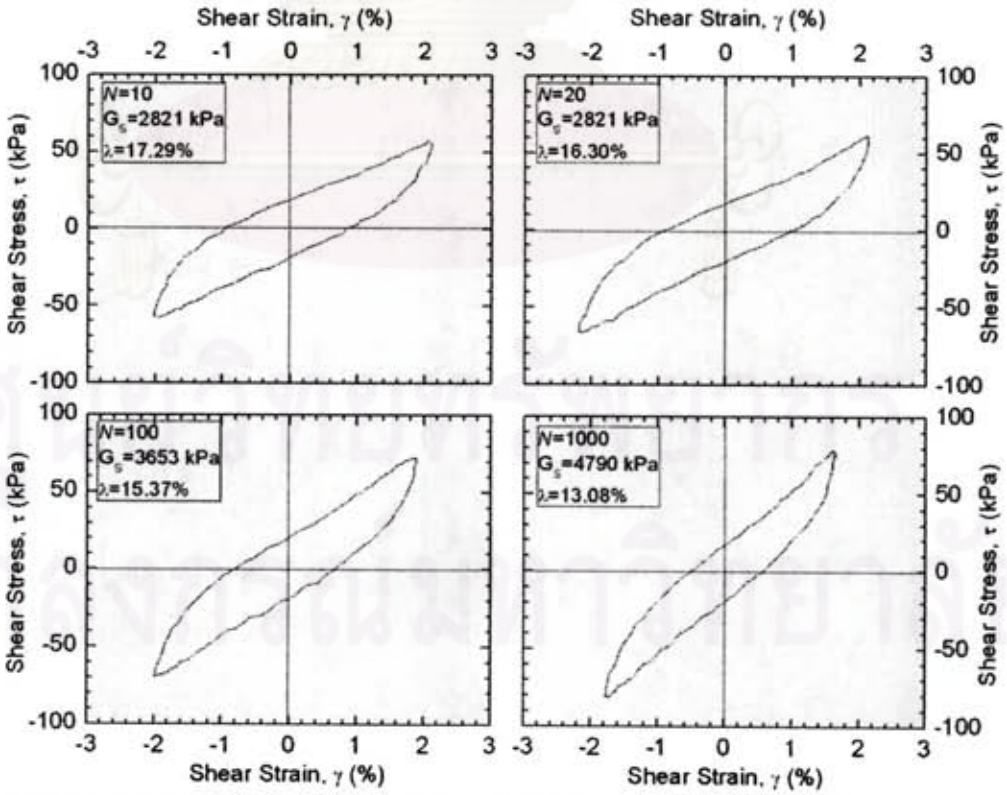

Figure 5-22 Detail of hysteresis loop of Test RS-LS7 ($\gamma = 2\%$; $\sigma_v = 100\ kPa$; $f = 0.1\ Hz$)

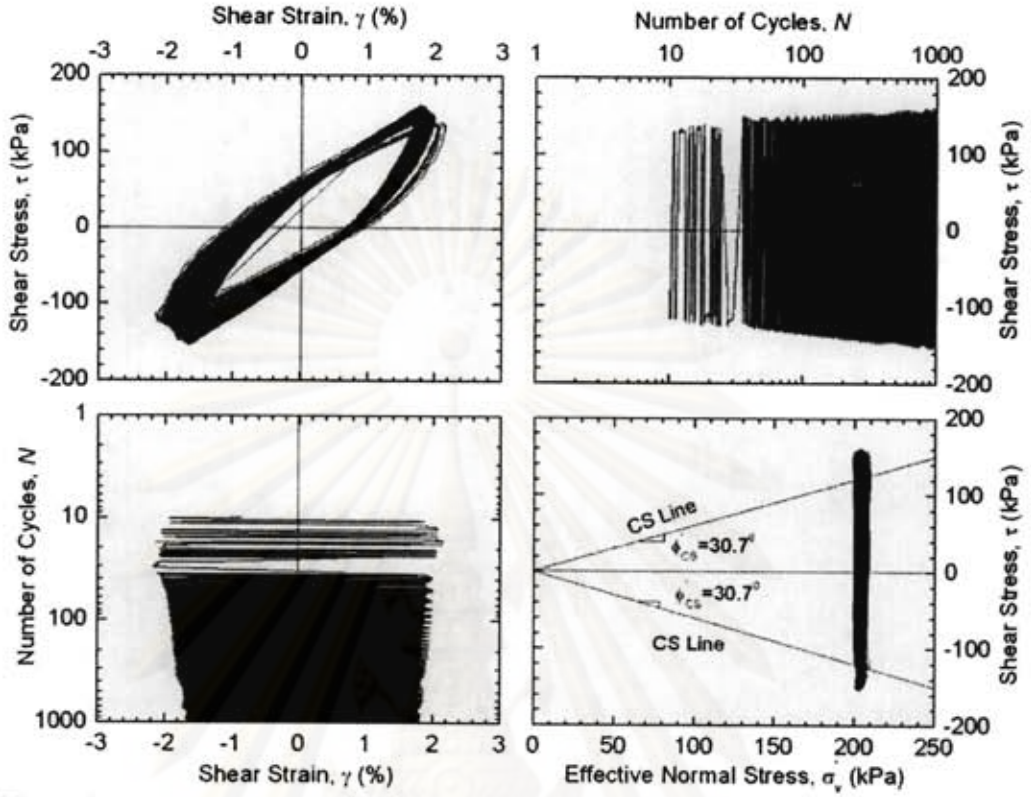

Figure 5-23 Cyclic shear response of Test RS-LS8 ($\gamma = 2\%$; $\sigma_v = 200\ kPa$; $f = 0.1\ Hz$)

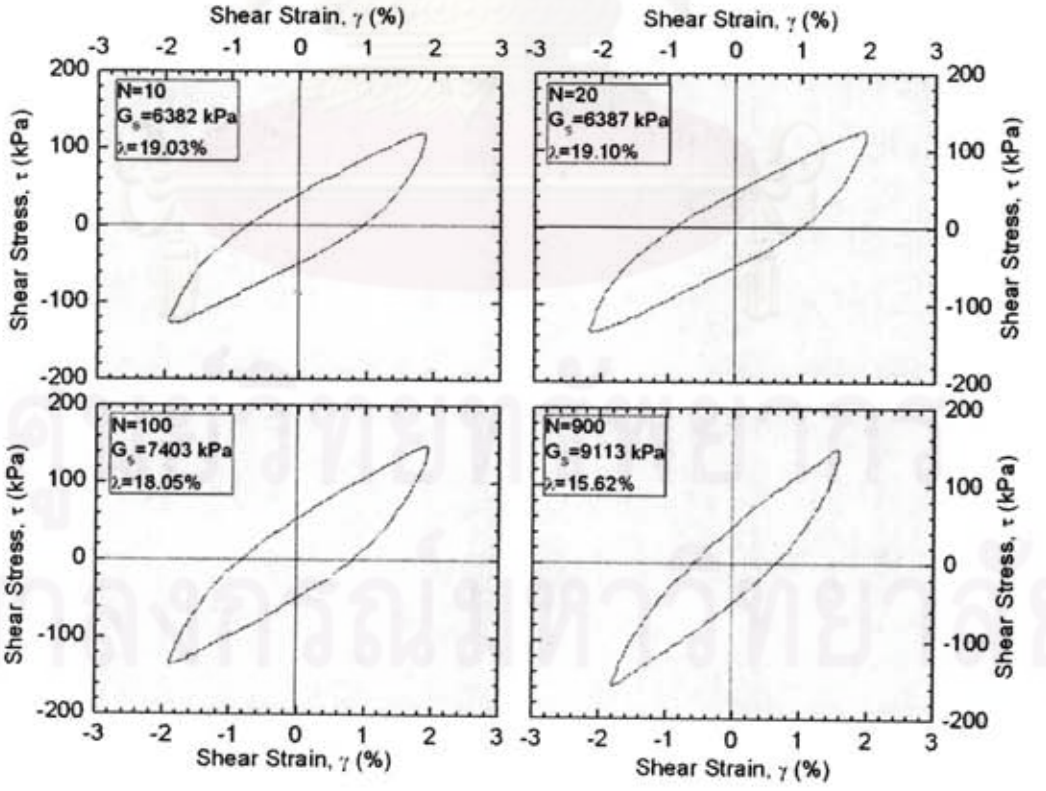

Figure 5-24 Detail of hysteresis loop of Test RS-LS8 ($\gamma = 2\%$; $\sigma_v = 200\ kPa$; $f = 0.1\ Hz$)

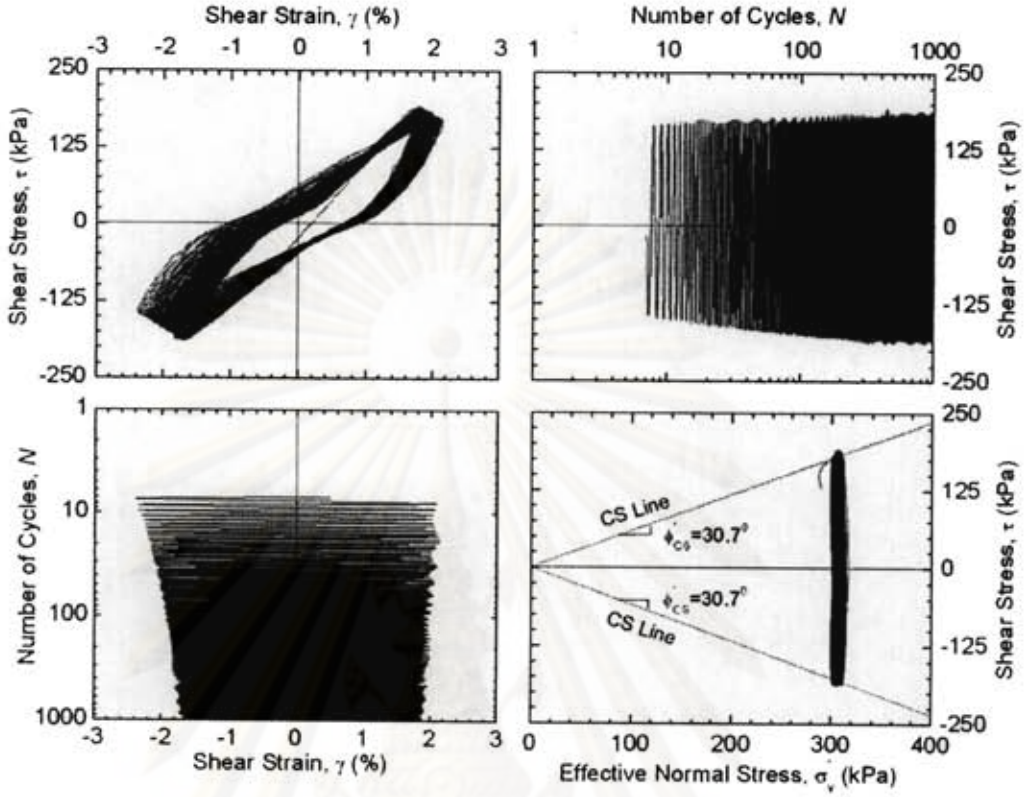

Figure 5-25 Cyclic shear response of Test RS-LS9 ($\gamma = 2\%$; $\sigma_v = 300\ kPa$; $f = 0.1\ Hz$)

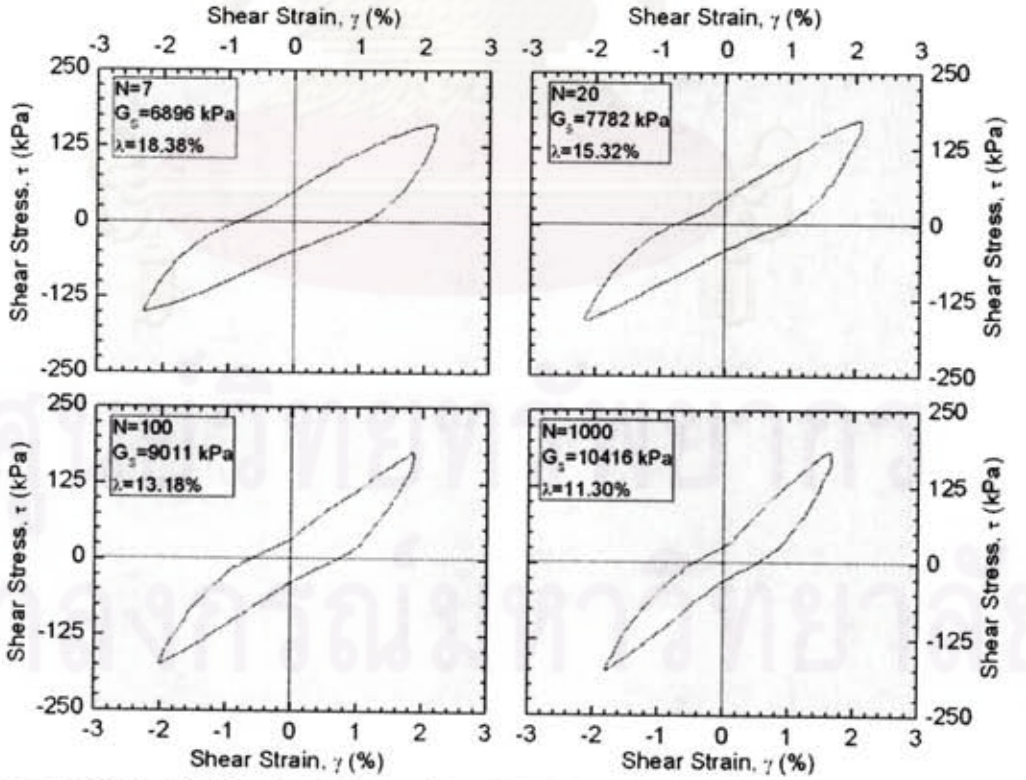

Figure 5-26 Detail of hysteresis loop of Test RS-LS9 ($\gamma = 2\%$; $\sigma_v = 300\ kPa$; $f = 0.1\ Hz$)

5.3.2 *River Sand in Case of Dense State*

In this part, cyclic shear response of saturated River sand with $D_r \cong 80\%$ along with detail of hysteresis loop at discrete γ *and* σ_v is pointed out in Figure 5-27 to 5-44. Critical state lines with effective critical friction angle $\emptyset'_{CS} = 31^0$ from monotonic DSS test are plotted in stress path schematic diagrams as depicted in foregoing figures.

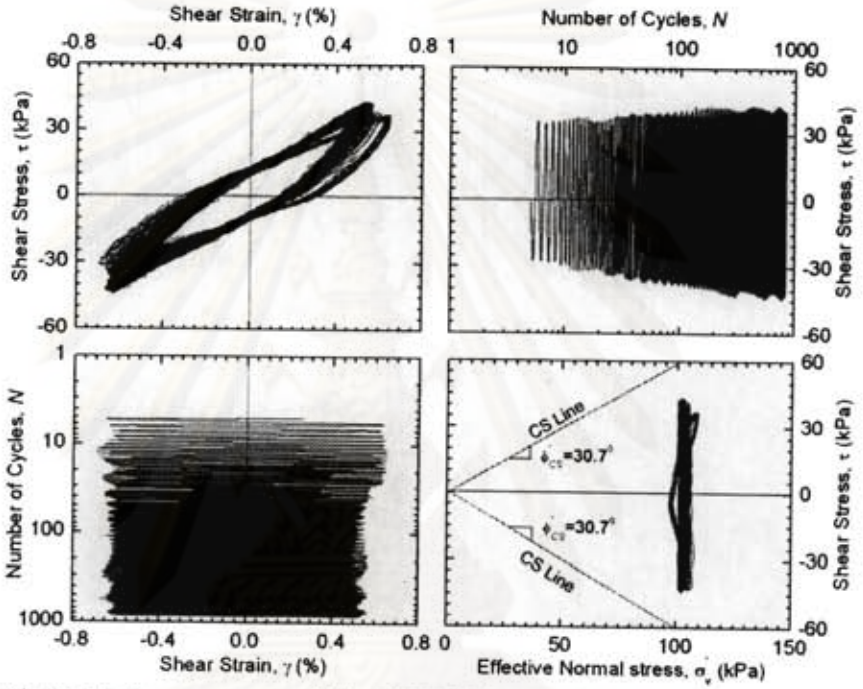

Figure 5-27 Cyclic shear response of Test RS-DS1 ($\gamma = 0.5\%$; $\sigma_v = 100\ kPa$; $f = 0.1\ Hz$)

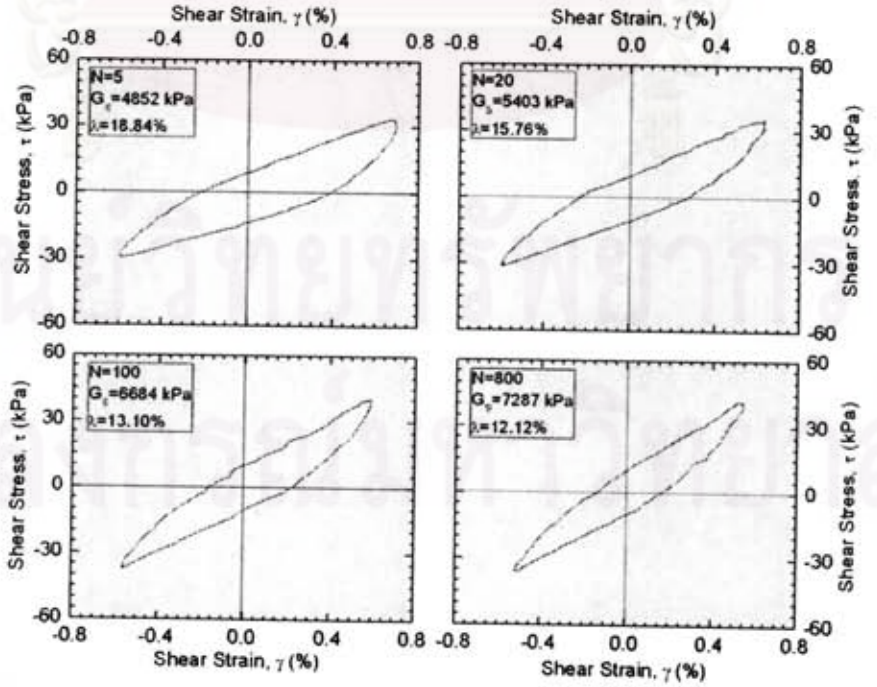

Figure 5-28 Detail of hysteresis loop of Test RS-DS1 ($\gamma = 0.5\%$; $\sigma_v = 100\ kPa$; $f = 0.1\ Hz$)

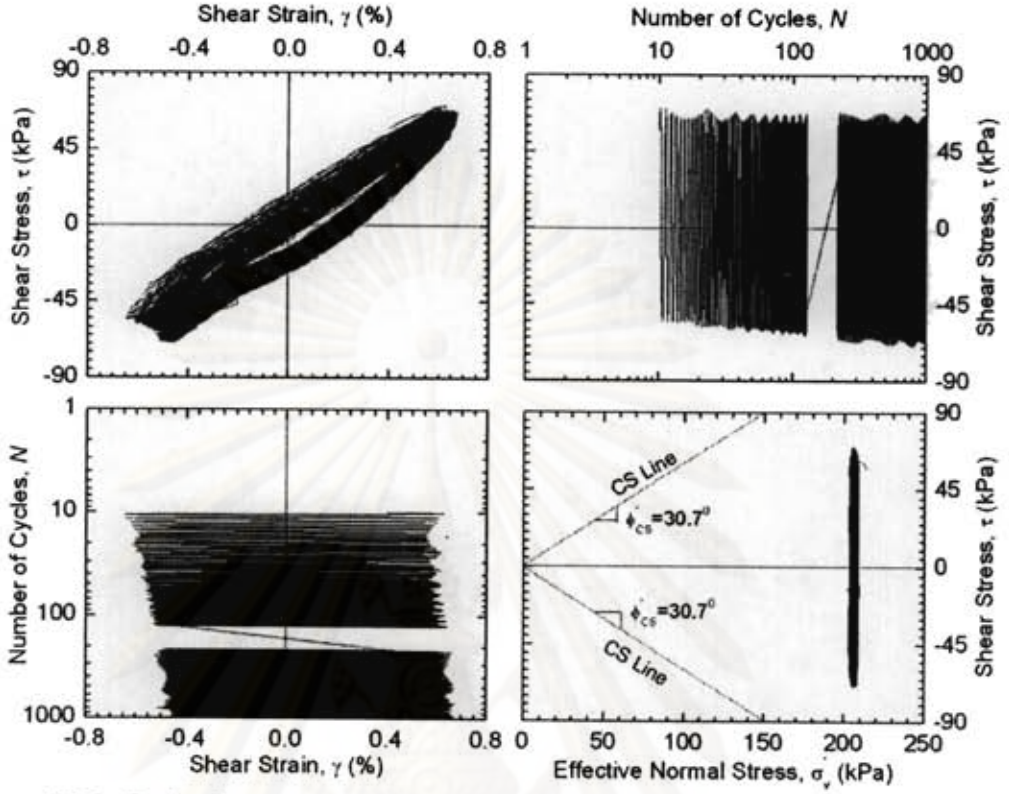

Figure 5-29 Cyclic shear response of Test RS-DS2 ($\gamma = 0.5\%$; $\sigma_v = 200\ kPa$; $f = 0.1\ Hz$)

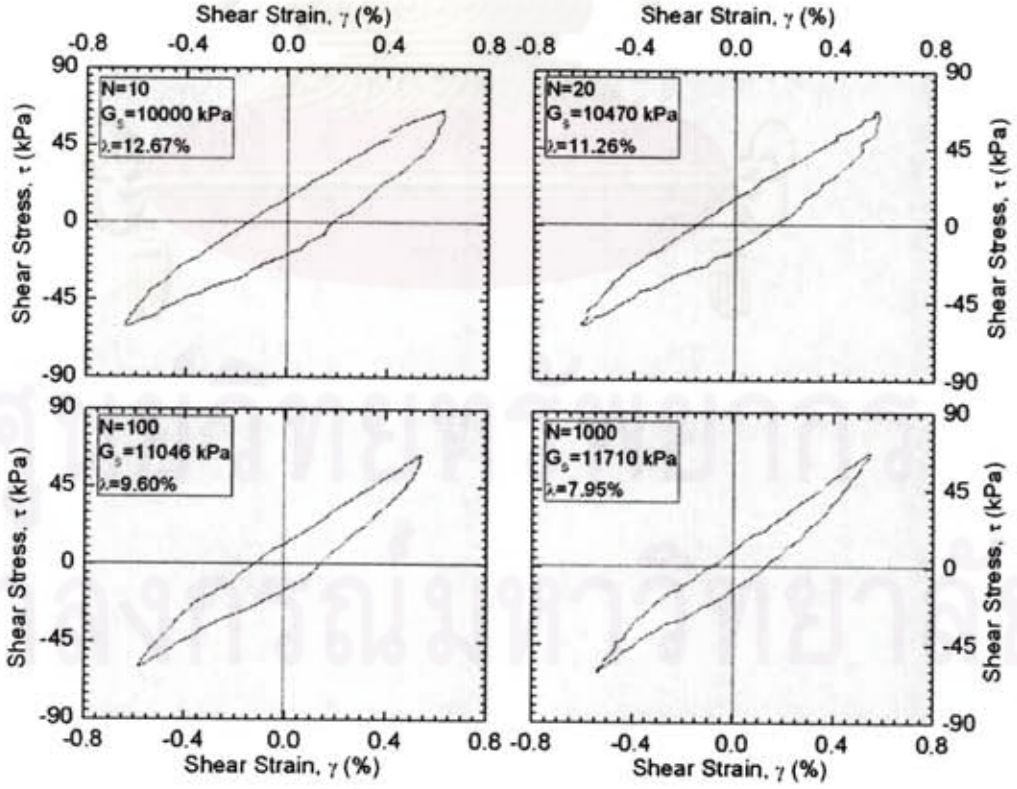

Figure 5-30 Detail of hysteresis loop of Test RS-DS2 ($\gamma = 0.5\%$; $\sigma_v = 200\ kPa$; $f = 0.1\ Hz$)

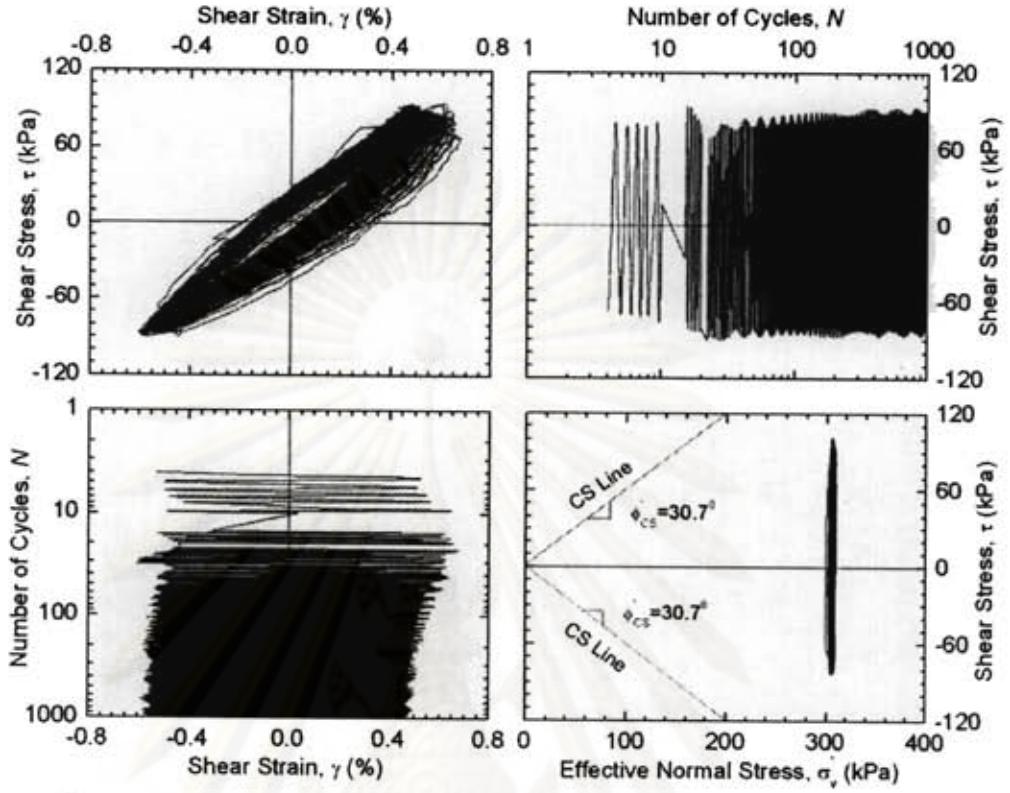

Figure 5-31 Cyclic shear response of Test RS-DS3 ($\gamma = 0.5\%$; $\sigma_v = 300\ kPa$; $f = 0.1\ Hz$)

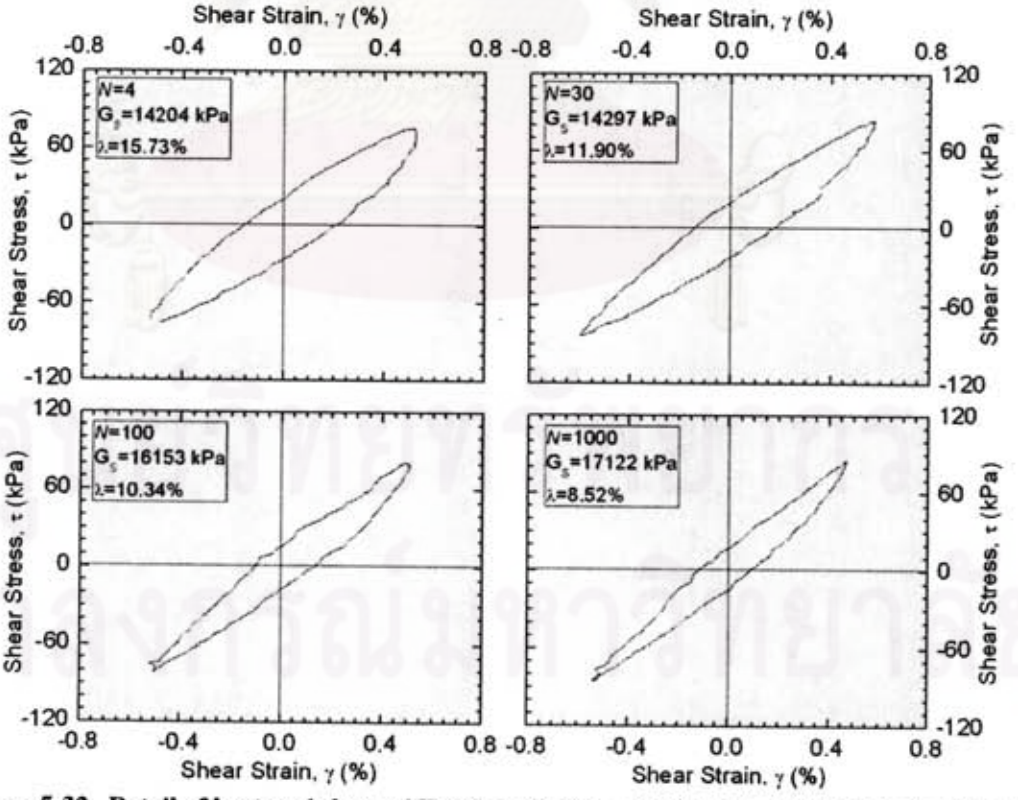

Figure 5-32 Detail of hysteresis loop of Test RS-DS3 ($\gamma = 0.5\%$; $\sigma_v = 300\ kPa$; $f = 0.1\ Hz$)

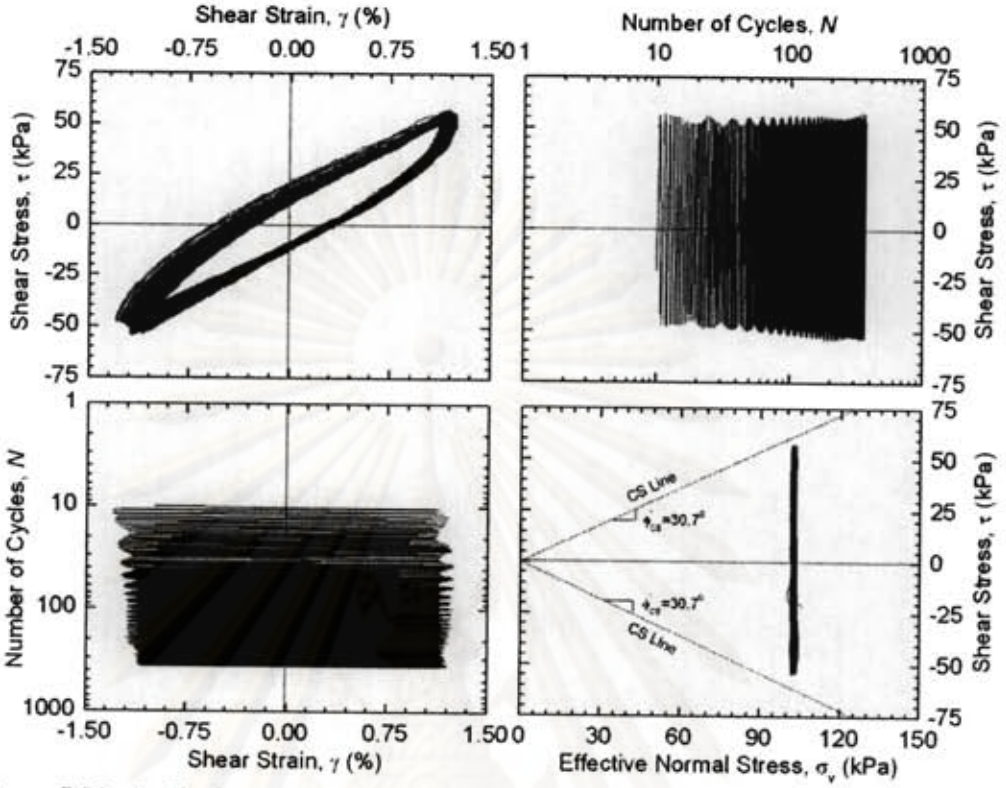

Figure 5-33 Cyclic shear response of Test RS-DS4 ($\gamma = 1\%$; $\sigma_v = 100\ kPa$; $f = 0.1\ Hz$)

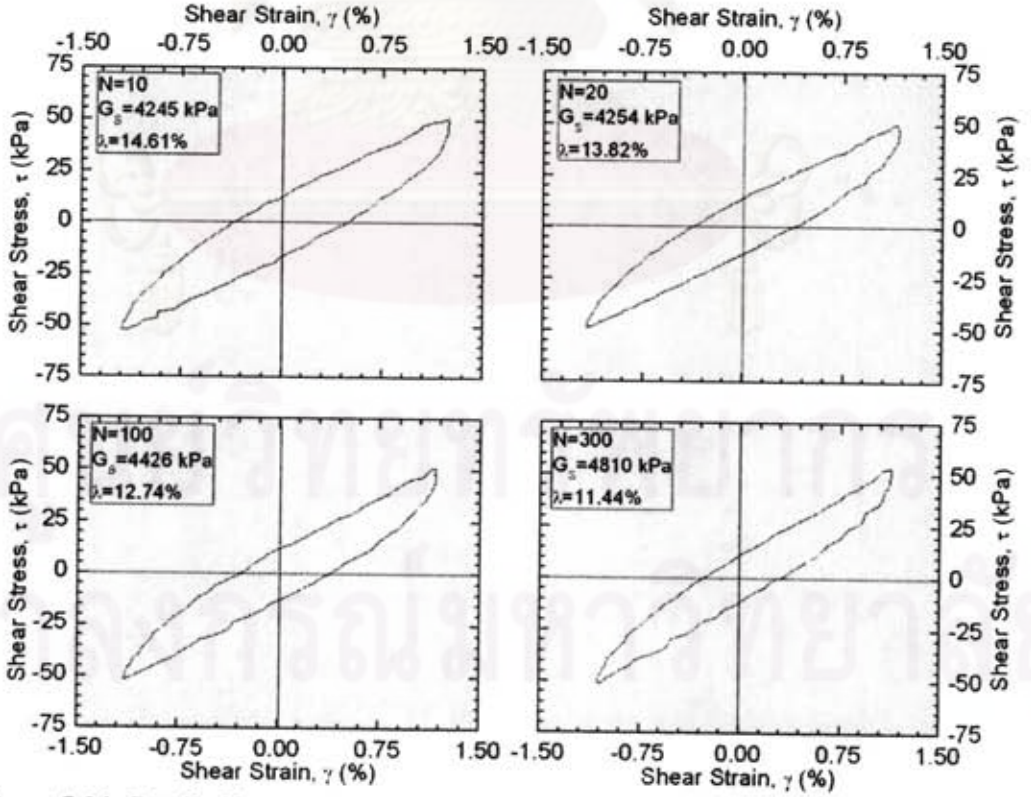

Figure 5-34 Detail of hysteresis loop of Test RS-DS4 ($\gamma = 1\%$; $\sigma_v = 100\ kPa$; $f = 0.1\ Hz$)

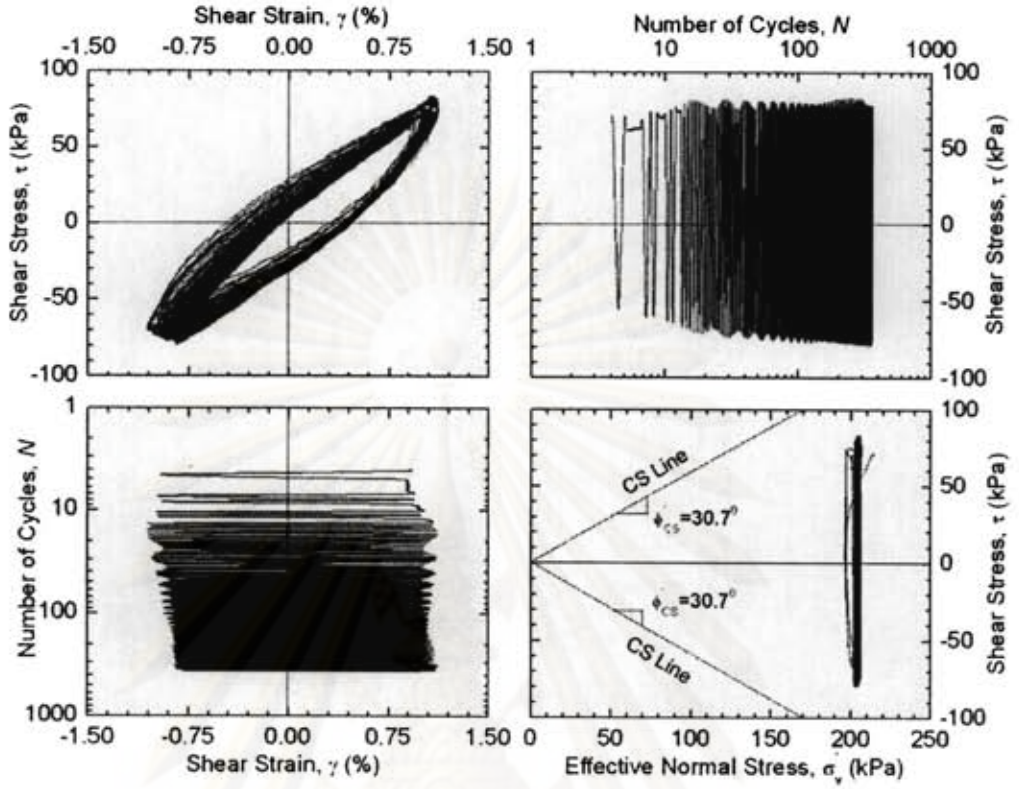

Figure 5-35 Cyclic shear response of Test RS-DS5 ($\gamma = 1\%$; $\sigma_v = 200\ kPa$; $f = 0.1\ Hz$)

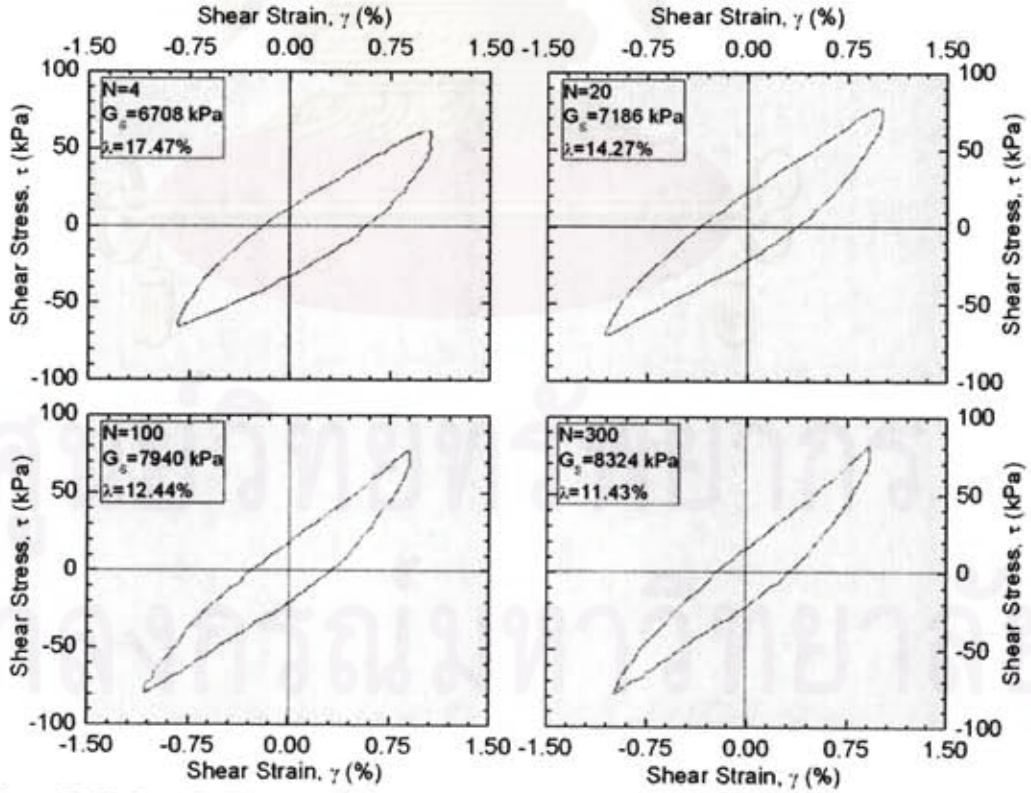

Figure 5-36 Detail of hysteresis loop of Test RS-DS5 ($\gamma = 1\%$; $\sigma_v = 200\ kPa$; $f = 0.1\ Hz$)

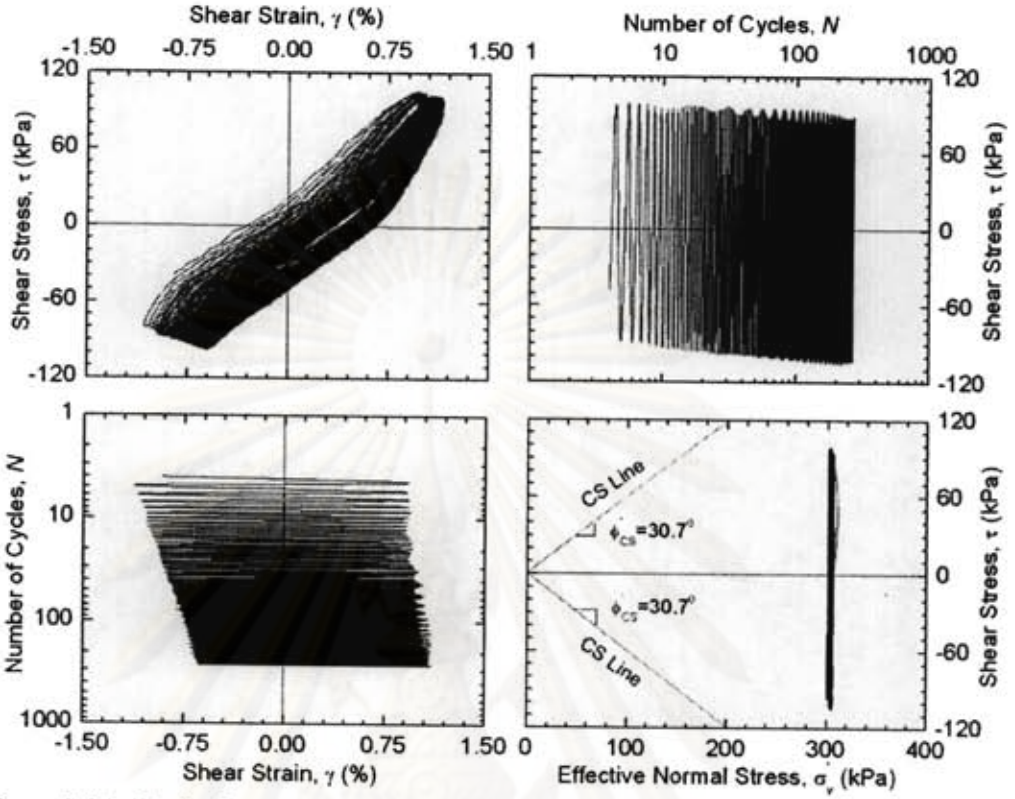

Figure 5-37 Cyclic shear response of Test RS-DS6 ($\gamma = 1\%$; $\sigma_v = 300\ kPa$; $f = 0.1\ Hz$)

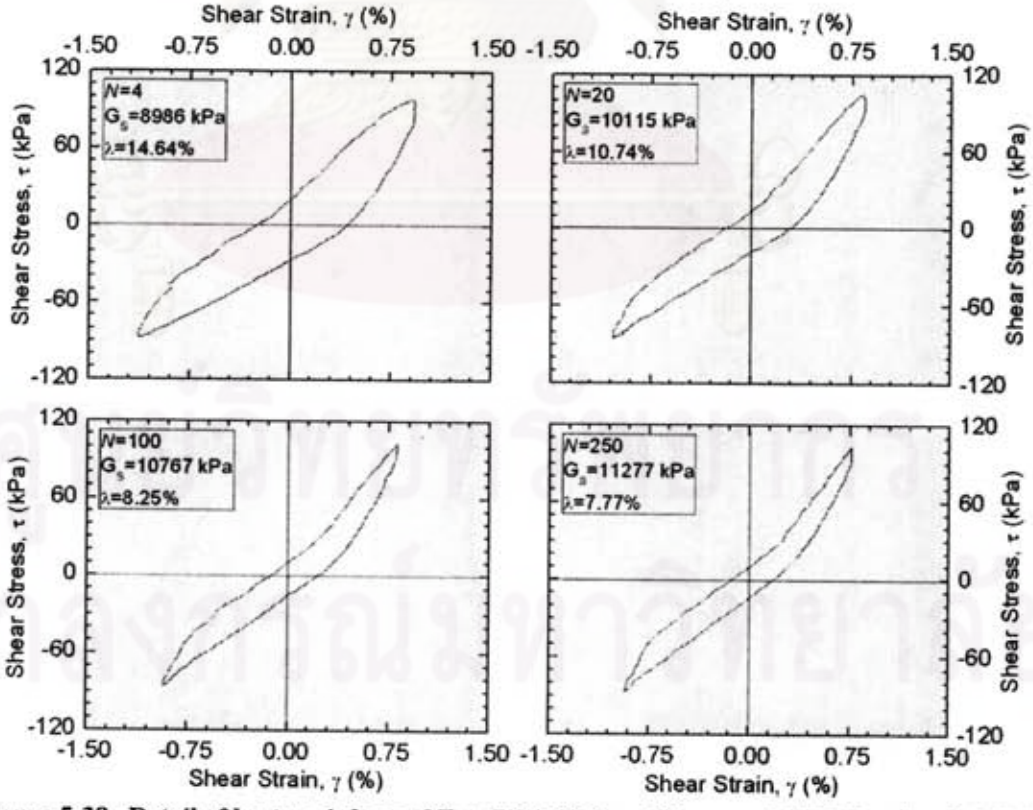

Figure 5-38 Detail of hysteresis loop of Test RS-DS6 ($\gamma = 1\%$; $\sigma_v = 300\ kPa$; $f = 0.1\ Hz$)

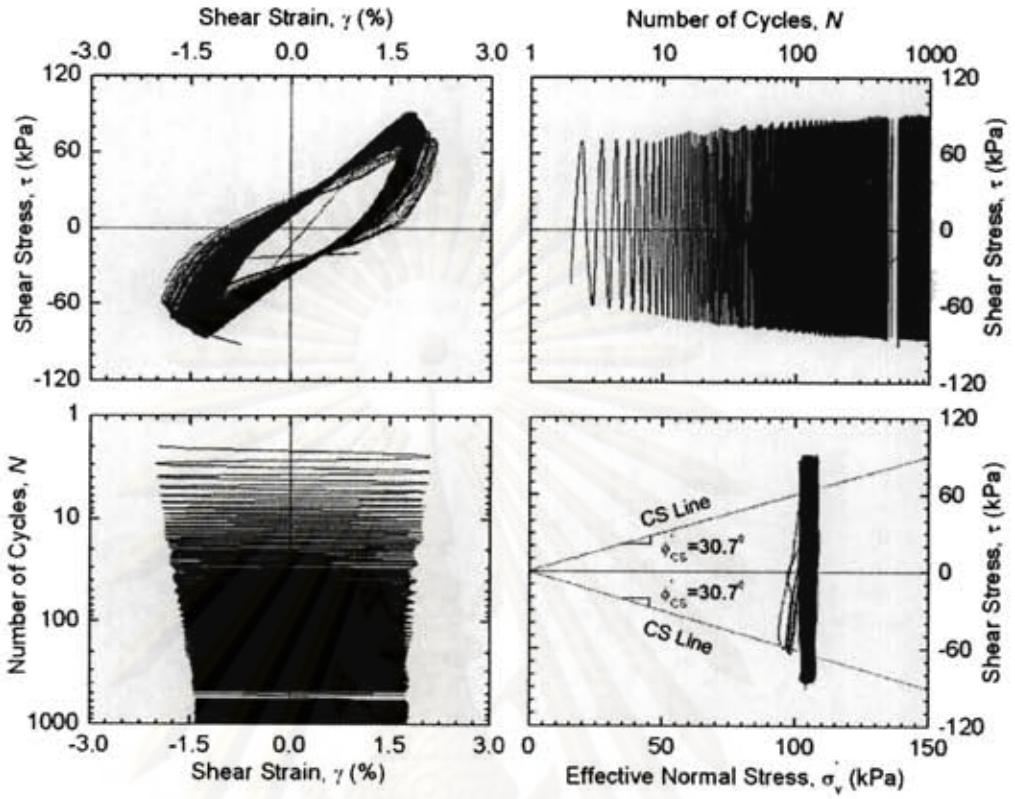

Figure 5-39 Cyclic shear response of Test RS-DS7 ($\gamma = 2\%$; $\sigma_v = 100\ kPa$; $f = 0.1\ Hz$)

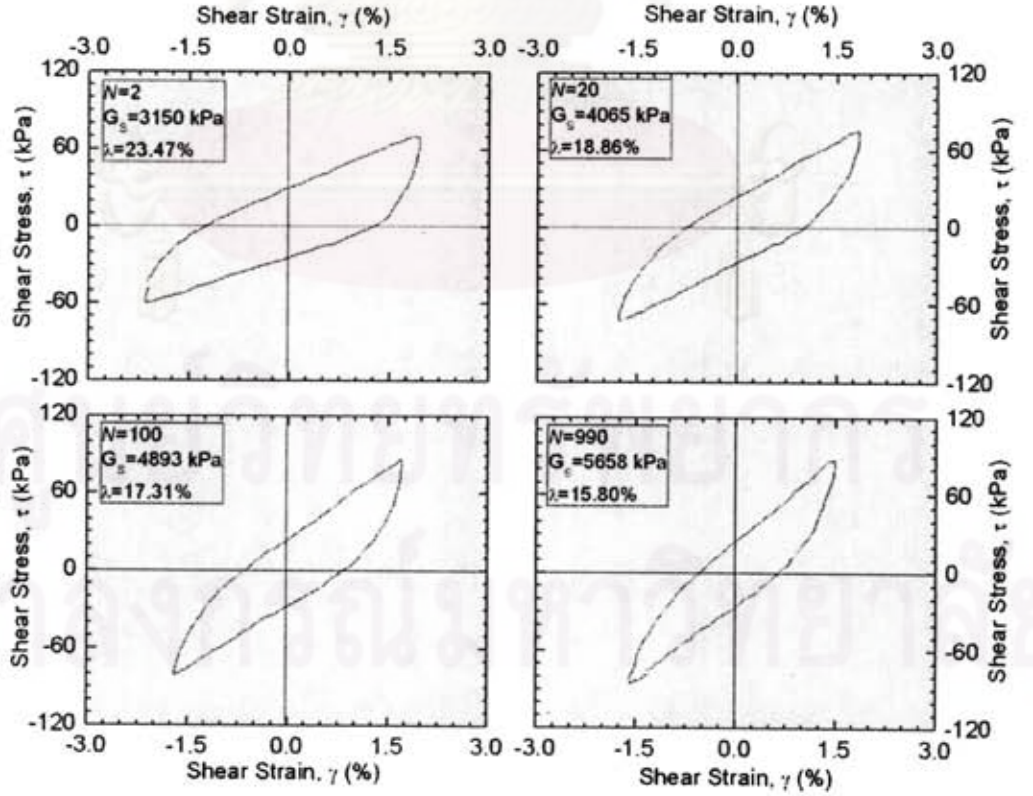

Figure 5-40 Detail of hysteresis loop of Test RS-DS7 ($\gamma = 2\%$; $\sigma_v = 100\ kPa$; $f = 0.1\ Hz$)

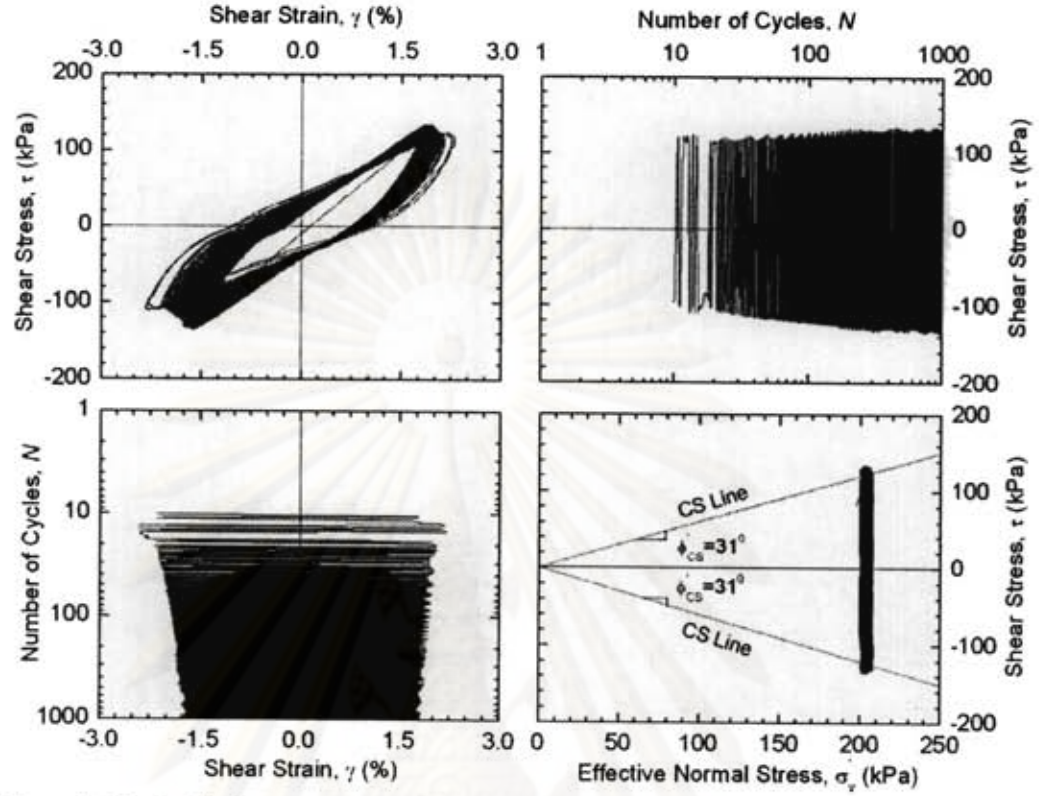

Figure 5-41 Cyclic shear response of Test RS-DS8 ($\gamma = 2\%$; $\sigma_v = 200\ kPa$; $f = 0.1\ Hz$)

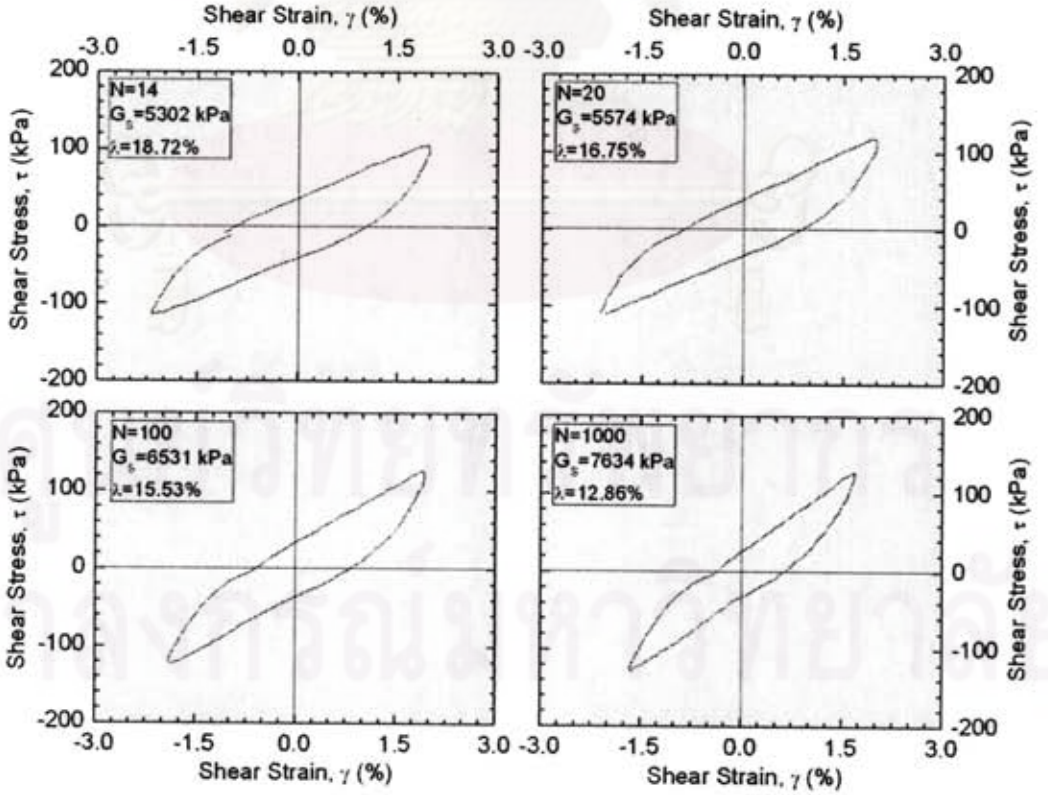

Figure 5-42 Detail of hysteresis loop of Test RS-DS8 ($\gamma = 2\%$; $\sigma_v = 200\ kPa$; $f = 0.1\ Hz$)

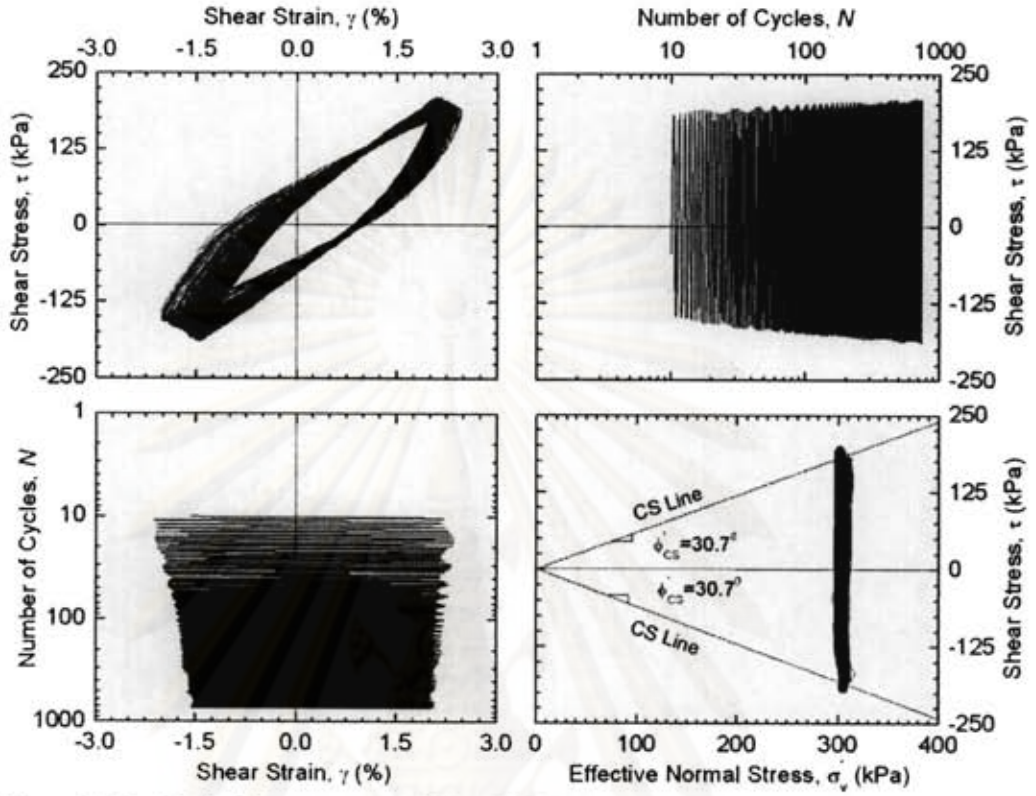

Figure 5-43 Cyclic shear response of Test RS-DS9 ($\gamma = 2\%$; $\sigma_v = 300\ kPa$; $f = 0.1\ Hz$)

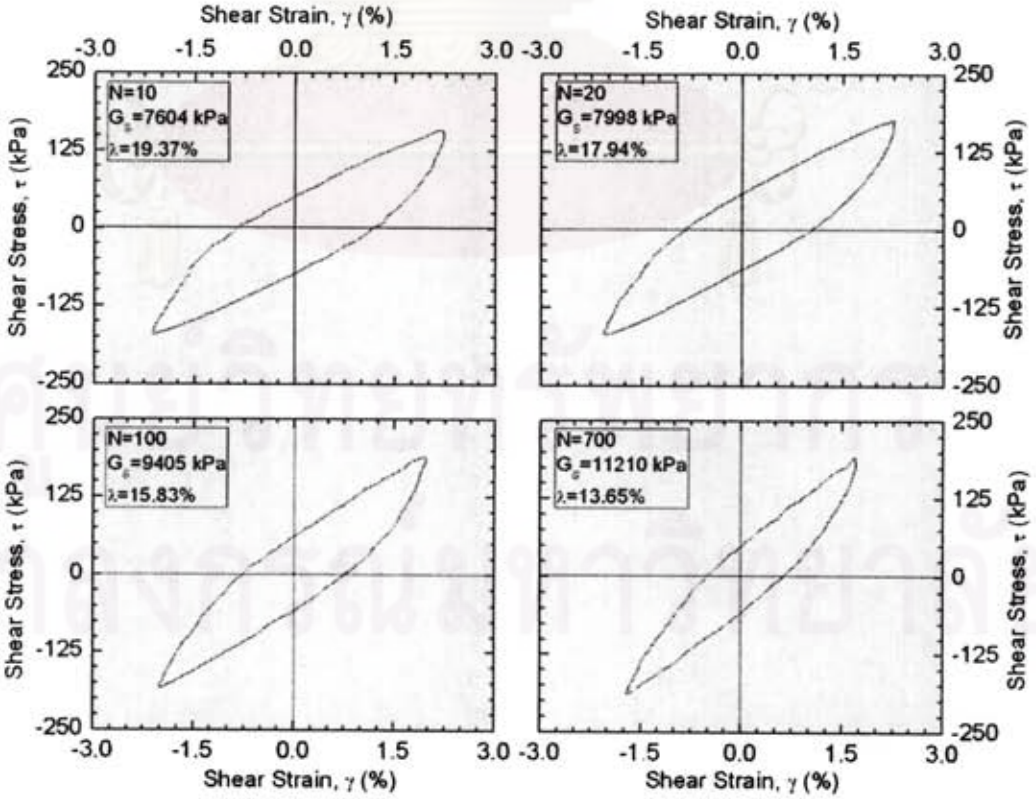

Figure 5-44 Detail of hysteresis loop of Test RS-DS9 ($\gamma = 2\%$; $\sigma_v = 300\ kPa$; $f = 0.1\ Hz$)

CHAPTER VI
INTERPRETATION OF RESULTS

6.1 Introduction

All experimental results from static test (36 samples) and cyclic test (22 samples) will be analyzed and interpreted in this chapter. The interpretation of dynamic properties of Chiang Mai sand using cyclic DSS test will be performed in detail, based on previous studies by various researchers (Silver & Seed, 1971, Iwasaki et al., 1978 & Vucetic et al., 1998, etc.). In addition, due to main objective of this research focused on determining cyclic sand response induced by dynamic loading, the results from monotonic test will be discussed briefly.

6.2 Monotonic Test

In monotonic loading test, DSB, drained, and undrained DSS tests are used to find out effective internal friction angle ($\emptyset'$) of Chiang Mai sands. DSB test are performed on dry sand by using dry tamping method, as mentioned in Section 3.4.4. Furthermore, DSS test are carried out on both dry sand and saturated sand by using dry tamping method and water pluviation method, respectively, as shown in Section 3.4.5. The interpretation of $\emptyset'$ from three foregoing tests is based on the assumption proposed by Roscoe (1970) that horizontal plane is the plane of maximum shear stress.

6.2.1 Interpretation of DSB and Drained DSS Tests

As shown in Figure 4-1 to 4-6, shear stress (τ) starts to increase gradually until the peak stress (τ_p) before decreasing to critical state stress (τ_{CS}) which is constant stress without changing the volume during large consecutive shearing. Shear stress (τ) increases with increasing vertical stress (σ_v). In addition, sand behavior is dilative, regardless of loose sand and dense sand after being compressive at the beginning of shearing. It is contrary to normal belief that loose sand is subjected to compressive

behavior. The reason of this case is due to vertical stress (σ_v) used, based on Vaid and Sivathayalan (1996).

Figure 6-1 and 6-2 present stress path of DSB and drained DSS test on WS and RS at different vertical stress (σ_v). The critical state effective internal friction angle ($\emptyset'_{CS}$) can be interpreted by using Coulomb's model in Equation (2-7). It is evident from Figure 6-1 that effective friction angle of WS ($\emptyset'_{CS}$ (WS)) is equal to 33.3^0 and that of RS in loose state $\emptyset'_{CS}\ (RS-LS)$ and dense state $\emptyset'_{CS}\ (RS-DS)$ is approximately 41.8^0 and 40.2^0, respectively. The value of $\emptyset'_{CS}\ (RS-LS) and\ \emptyset'_{CS}\ (RS-DS)$ has a small difference. This implies that $\emptyset'_{CS}$ is independent of void ratio, which is in agreement with Schofield and Wroth (1968). Thus, the average value of $\emptyset'_{CS}\ (RS)$ is 41^0. Similarly, the effective friction angle, as shown in Figure 6-2 from drained DSS test, are $\emptyset'_{CS}$ (WS) = 35.6^0, $\emptyset'_{CS}\ (RS-LS) = 36.4^0$, $\emptyset'_{CS}\ (RS-DS) = 38^0$, and average value of $\emptyset'_{CS}\ (RS) = 37.2^0$. It is noted that $\emptyset'_{CS}$ obtained from DSB and drained DSS test for the same sand are not too different.

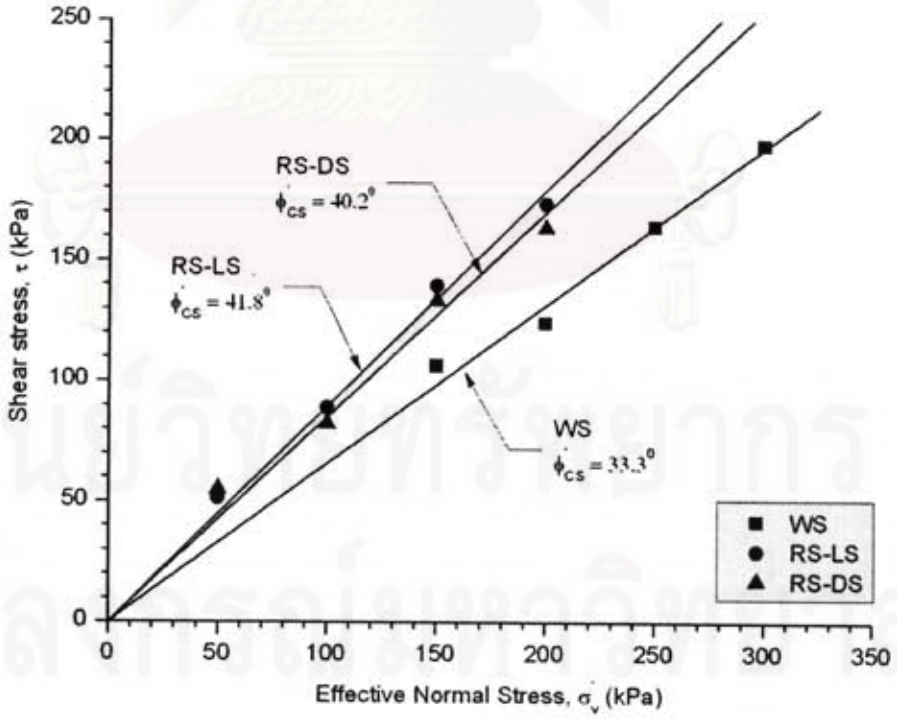

Figure 6-1 Stress path of DSB test

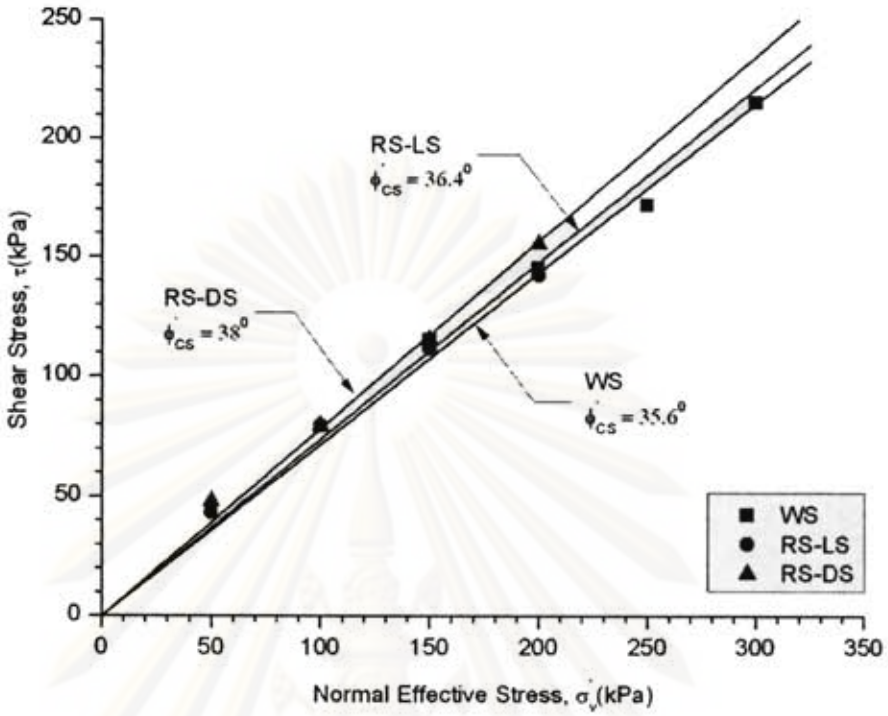

Figure 6-2 Stress path of drained DSS test

6.2.2 Interpretation of Undrained DSS Test

Figure 4-7 to 4-9 shows monotonic behavior of WS and RS obtained from undrained DSS test at discrete vertical stress (σ_v'). It can be seen that shear stress and pore water pressure increase as vertical stress increase for a given shear strain. In addition, the tested sand exhibits contractive behavior until reaching phase transformation state (PT) (Vaid et al. (1999), and Porcino et al. (2008)) at a very early stage of the test. The excess pore water pressure increases and vertical effective stress decreases. Shear stress, then, continues to develop strain hardening response, which shows dilative behavior of sand. During the dilation phase, the stress path is straight until touching the critical state line (Castro, 1977; Vanden Berghe, 2001), and change in water pressure starts decreasing.

According to Figure 6-3 to 6-6 illustrating stress path of undrained DSS test for WS and RS, critical state effective internal friction angle ($\emptyset'_{CS}$) and phase transformation friction angle ($\emptyset'_{PT}$) can be figured out. It is obvious from Figure 6-3 to 6-5 that $\emptyset'_{CS}$ (WS) = 29.7^0, $\emptyset'_{CS}$ (RS-LS) = 31.9^0, $\emptyset'_{CS}$ (RS-DS) = 29.4^0, and average value of $\emptyset'_{CS}$ (RS) = 30.65. In addition, $\emptyset'_{PT}(WS)$ is equal to 20.9^0. It can be noticed that all PT

points fall into two straight lines (PT lines) for loose and dense sand with the value of $\emptyset'_{PT}(RS-LS) = 23.8^0, and\ \emptyset'_{PT}(RS-DS) = 19.6^0$. The value of $\emptyset'_{PT}$ is approximately 29% smaller than that of $\emptyset'_{CS}$. It is believed that effective friction angle at phase transformation is often more realistic to design. Furthermore, $\emptyset'_{CS}$ from drained DSS test is larger than that from undrained DSS test in accordance with Table 6-1.

Table 6-1 Summary of all critical friction angles from monotonic testing results

Test	DSB Test			Drained DSS Test			Undrained DSS Test		
Soil	WS	RS-LS	RS-DS	WS	RS-LS	RS-DS	WS	RS-LS	RS-DS
$\emptyset'_{CS}$	33.3^0	41.8^0	40.2^0	35.6^0	36.4^0	38^0	29.7^0	31.9^0	29.4^0
Av. $\emptyset'_{CS}$	33.3^0	41^0		35.6^0	37.2^0		29.7^0	30.7^0	

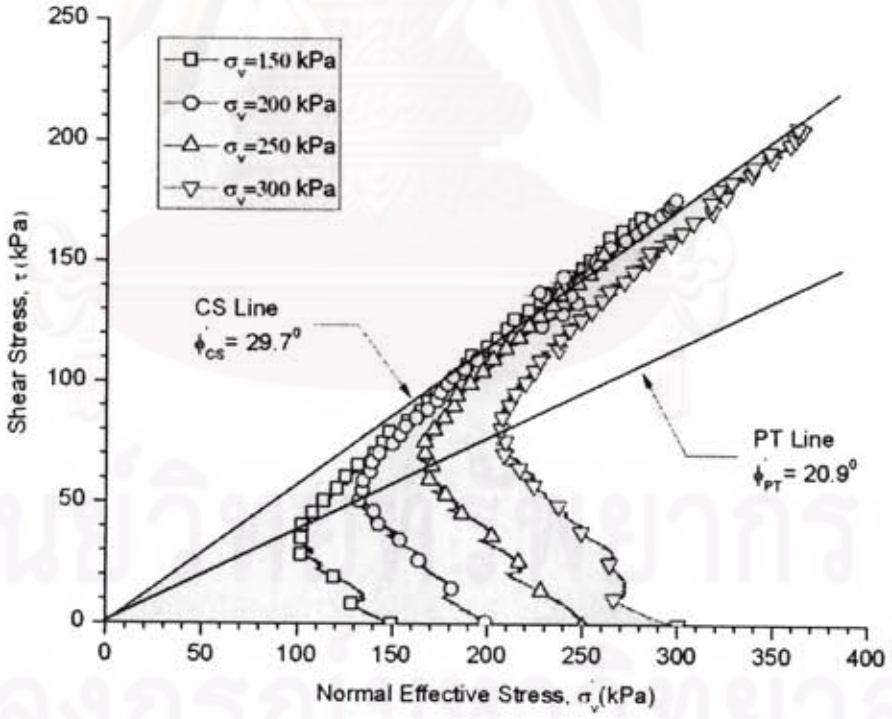

Figure 6-3 Stress path of undrained DSS test for WS

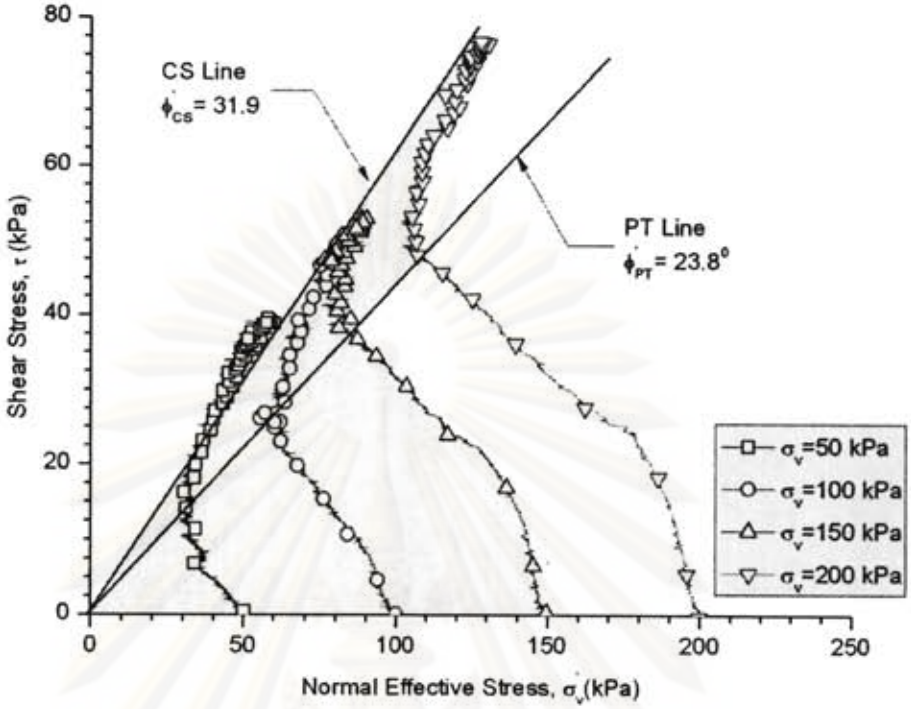

Figure 6-4 Stress path of undrained DSS test for RS-LS

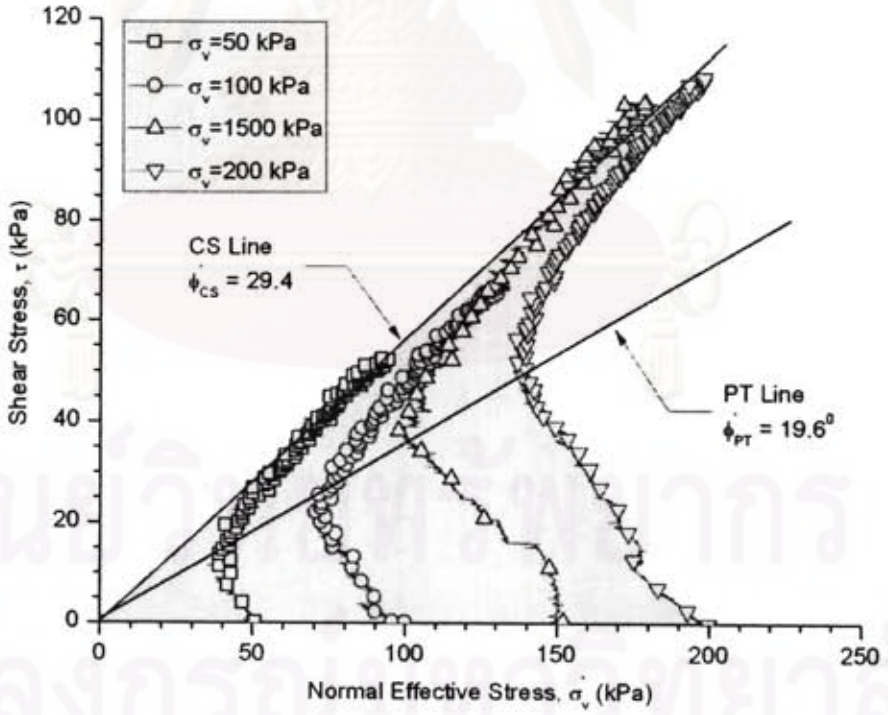

Figure 6-5 Stress path of undrained DSS test for RS-DS

6.3 Cyclic Drained DSS Test

In this study, cyclic direct simple shear (DSS) test is conducted in drained or constant normal stress condition to figure out cyclic response of Chiang Mai sand as well as secant shear modulus G_S and damping ratio λ. Several parameters, such as relative density (D_r), shear strain amplitude (γ), vertical stress (σ_v), and frequency (f), are varied so as to observe the effect on dynamic sand properties.

6.4 Cyclic Drained DSS Test on Wat Chedi Luang Sand

The main objective to conduct the cyclic drained DSS test on Wat Chedi Luang sand (WS) is to simulate the in-situ condition. Experimental inputs used to achieve the goal acquire natural relative density $D_r \cong 90\%$ (dense state), shear strains amplitude $\gamma = 0.5\%$, a range of frequency $f = 0.1\ and\ 1\ Hz$, and of vertical stress $\sigma_v = 125\ kPa\ and\ 150\ kPa$.

6.4.1 Secant Shear Modulus on Wat Chedi Luang Sand

Figure 6-6 is plotted as secant shear modulus (G_S) against number of cycles (N) at $\gamma = 0.5\ \%$. A range of frequency $f = 0.1\ and\ 1\ Hz$, and of vertical stress $\sigma_v = 125\ kPa\ and\ 150\ kPa$ is chosen to observe whether or not such variation of f, and σ_v can greatly affect the dynamic properties of WS. Fitted curves are used to fit the data points. It can be seen from the same figure that secant shear modulus (G_S) increase when number of cycles (N) increase.

According to Figure 6-6(a) and (b), the effect of f = 0.1 Hz and 1 Hz at the same $D_r\ and\ \sigma_v$ have minor effect to G_S. This is in good agreement with Peacock et al. (1968). Similarly, Figure 6-6(c) and (d) also exhibits the small effect of f on G_S. In addition, the effect of σ_v can be noticed from Figure 6-6(a) and (c) and from Figure 6-6(b) and (d). The small changes of σ_v at the same D_r and f does not have great influence on G_S. Therefore, a global curve of is drawn to fit all data points of G_S of Ws, as illustrated in Figure 6-7. This graph may be used to find out shear modulus in

real application with ground shaking deformation around 0.5% for Wat Chedi Luang sand at depth of approximately 15m.

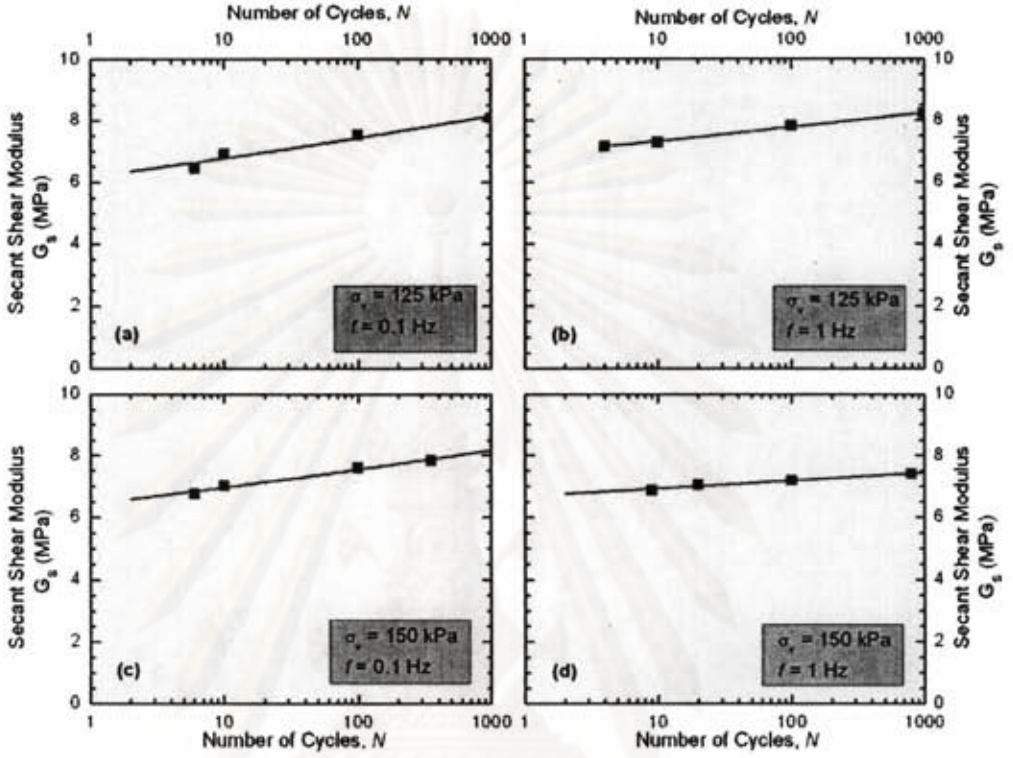

Figure 6-6 Secant shear modulus of WS at $\gamma = 0.5\%$ for different σ_v and f

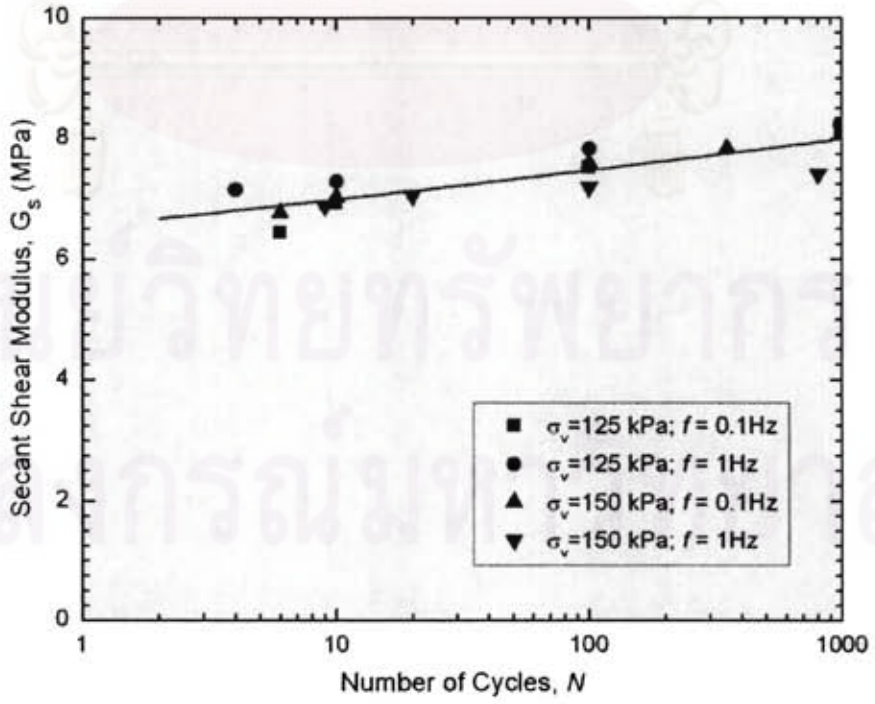

Figure 6-7 Global secant shear modulus of WS at $\gamma = 0.5\%$

6.4.2 Damping Ratio on Wat Chedi Luang Sand

Figure 6-8 depicts damping ratio (λ) plotted against number of cycles (N) at $\gamma =$ 0.5 %. Fitted curves are used to fit the data points. It is clear that λ decreases with increasing N. In accordance with Figure 6-8(a) and (b), the effect of $f = 0.1$ Hz and 1 Hz at the same D_r *and* σ_v have minor effect to G_S. This is in good consistency with Peacock et al. (1968). Similarly, Figure 6-8(c) and (d) also points out the small effect of f on G_S. Furthermore, the effect of σ_v can be noted from Figure 6-6(a) and (c) and from Figure 6-6(b) and (d). The small changes of $\sigma_v = 125\ kPa$ *and* $150\ kPa$ at the same D_r and f does not have great influence on G_S. As consequence, a global curve of is drawn to fit all data points of G_S of Ws, as shown in Figure 6-9. This graph may be used to find out damping ratio in real application with ground shaking deformation around 0.5% for Wat Chedi Luang sand at depth of approximately 15m.

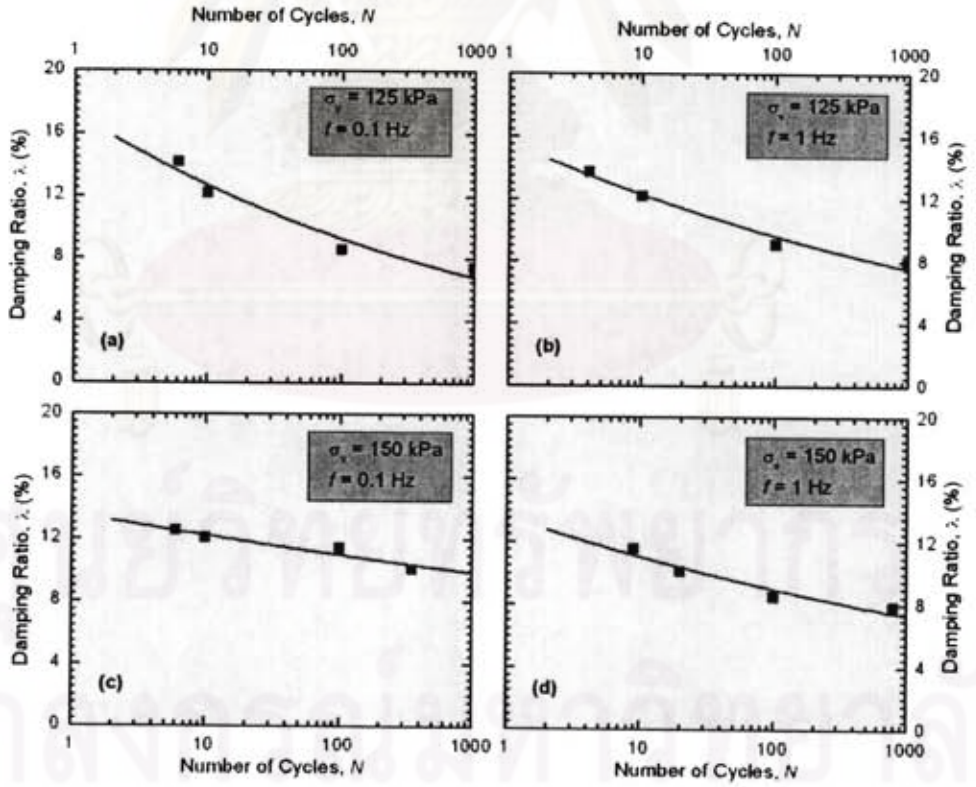

Figure 6-8 Damping Ratio of WS at $\gamma = 0.5\%$ for different σ_v *and* f

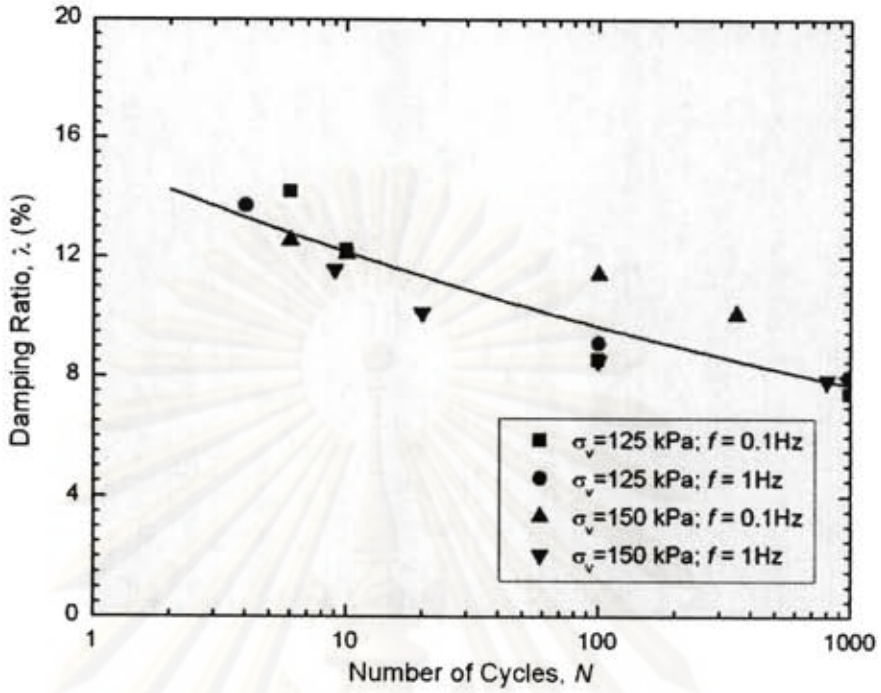

Figure 6-9 Global damping ratio of WS at $\gamma = 0.5\%$

6.5 Cyclic Drained DSS Test on River Sand

The main purpose to carry out the cyclic drained DSS test on River sand (RS) is to investigate the effects of shear strain amplitude (γ), vertical stress (σ_v), and relative density (D_r) on secant shear modulus (G_S) and damping ratio (λ). Experimental inputs used to achieve the goal comprise $D_r \cong 40\%\ and\ 80\%$, $\gamma = 0.5\%, 1\%\ and\ 2\%$, $\sigma_v = 100\ kPa, 200\ kPa\ and\ 300\ kPa$, and $f = 0.1\ Hz$.

6.5.1 Secant Shear Modulus of River Sand

In order to be easy to understand, interpretation of the experimental results of secant shear modulus of River sand are divided into two cases:

- Secant shear modulus of River sand in case of loose state ($D_r \cong 40\%$)
- Secant shear modulus of River sand in case of dense state ($D_r \cong 80\%$)

6.5.1.1 River Sand in Case of Loose State

Figure 6-10 shows secant shear modulus (G_S) - number of cycles (N) relationship of River sand in loose state (RS-LS) for relative density $D_r \cong 40\%$. In this study,

number of stress cycles (N) is expected to reach 1000 cycles in each sample during cyclic testing so as to observe the influence on sand dynamic properties. However, some samples cannot get N = 1000 cycles due to the error of DSS apparatus data acquisition system, as shown in Figure 6-10. It is inevitable to meet this trouble. Thus, the approximate value of G_S is taken from reading off the fitted curves of 4 points of various N.

In accordance with Figure 6-10, G_S increases with increasing N for a given shear strain amplitude (γ) and vertical stress (σ_v). It can be noticed from Figure 6-10(a) that the higher the γ, the lower the fitted curve of γ. Thus, G_S decreases with increasing γ for a given N. However, in Figure 6-10(b) and (c), the fitted curves of $\gamma = 1\% \; and \; 2\%$ cross together. G_S does not surely decrease when γ increases. As a result, the effect of γ on G_S is not able to be observed in Figure 6-10.

Figure 6-11 exhibits $G_S - \gamma \; relationship \; of \; RS - LS$ for $D_r \cong 40\%$. Owing to a slight flexibility provoked by mechanical linkage, it is impossible to preselect an exact shear strain amplitude for every test. Consequently, shear strain amplitudes of each test are a bit different from the desired γ, as shown in Figure 6-11. There is a decrease in G_S with increasing γ and decreasing σ_v for N = 10, as illustrated in Figure 6-11(a). It can also be noticed that the effect of σ_v on G_S seems to be small as σ_v gets higher. This is consistent with Silver and Seed (1971). Similar data and trends are obtained for tests conducted at N = 100 and 1000 in Figure 6-11(b) and (c).

The effect of N on $G_S - \gamma$ relationship for samples having $D_r \cong 40\%$ is shown in Figure 6-12. It is clear that the increase of N in a range of 10 to 1000 has small effect on secant shear modulus. This is in good agreement with Silver and Seed (1971) that the value of G_S seems to be similar after N = 10. This is the reason why many researchers would like to select N=10 to investigate the cyclic soil response.

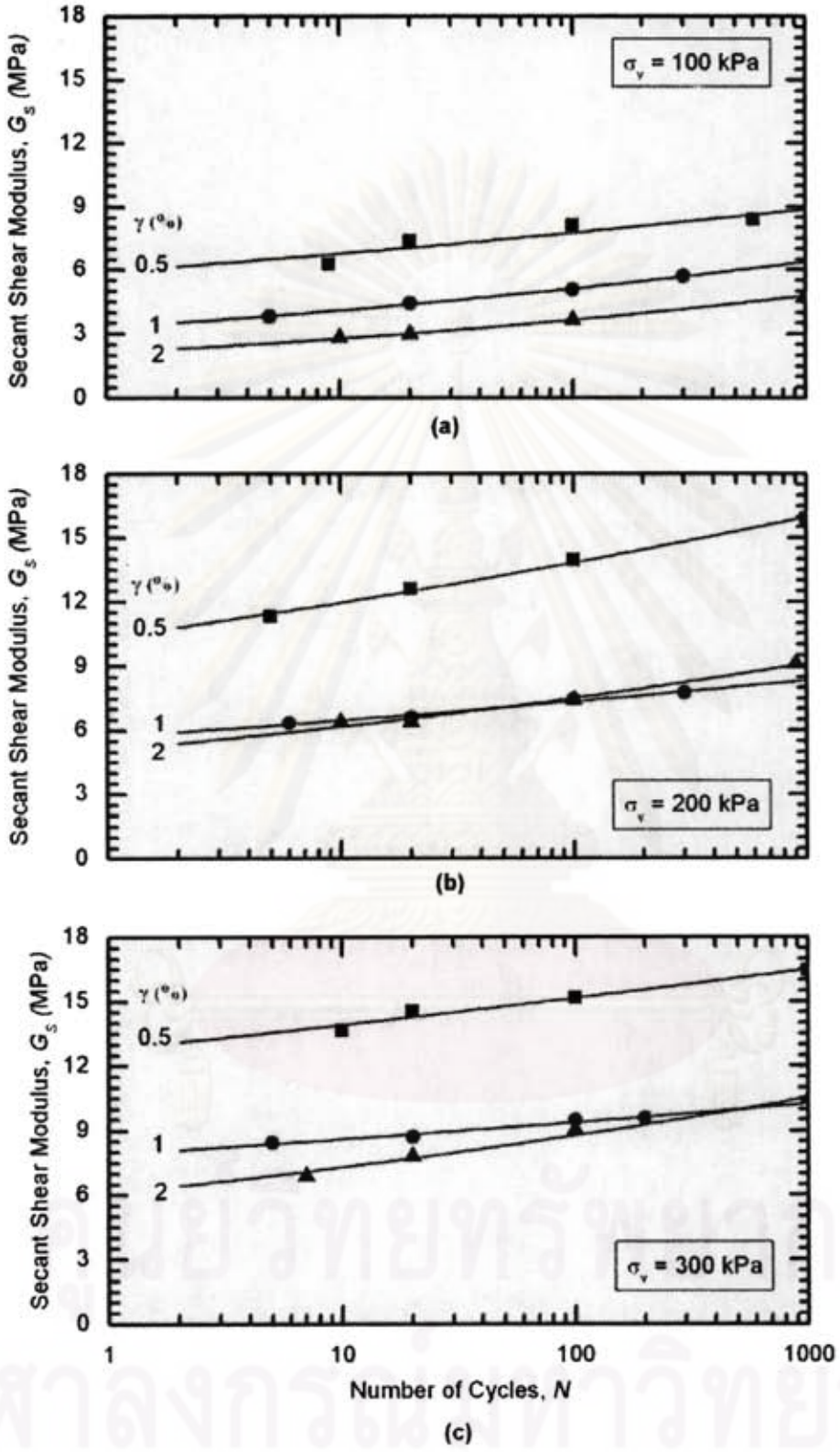

Figure 6-10 $G_S - N$ **relationship of RS-LS for** $D_r \cong 40\%$ $(e_0 = 0.53)$: (a) at $\sigma_v = 100\ kPa$; (b) at $\sigma_v = 200\ kPa$; (c) at $\sigma_v = 300\ kPa$

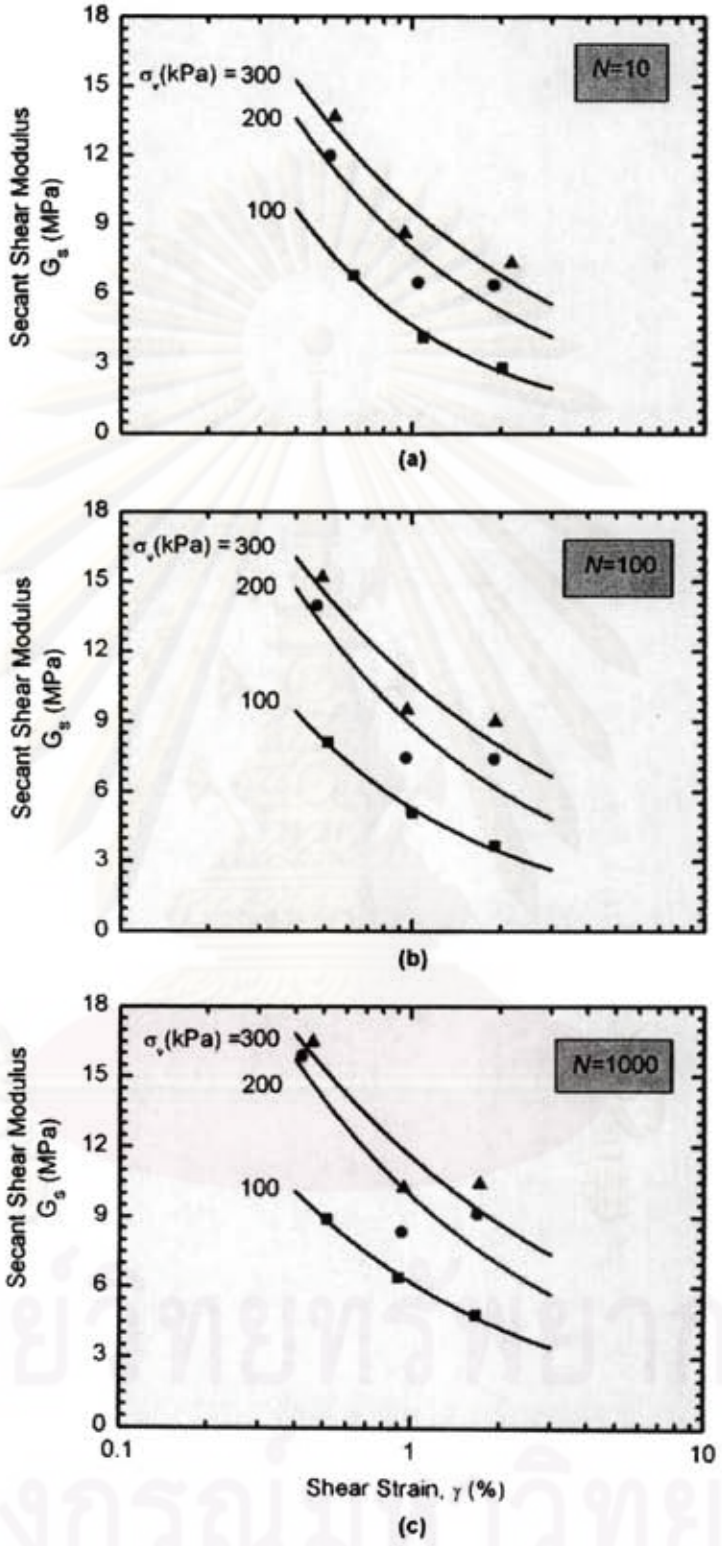

Figure 6-11 $G_S - \gamma$ *relationship of* $RS - LS$ **for** $D_r \cong 40\%$ $(e_0 = 0.53)$**: (a) at N = 10; (b) at N = 100; (c) at N = 1000**

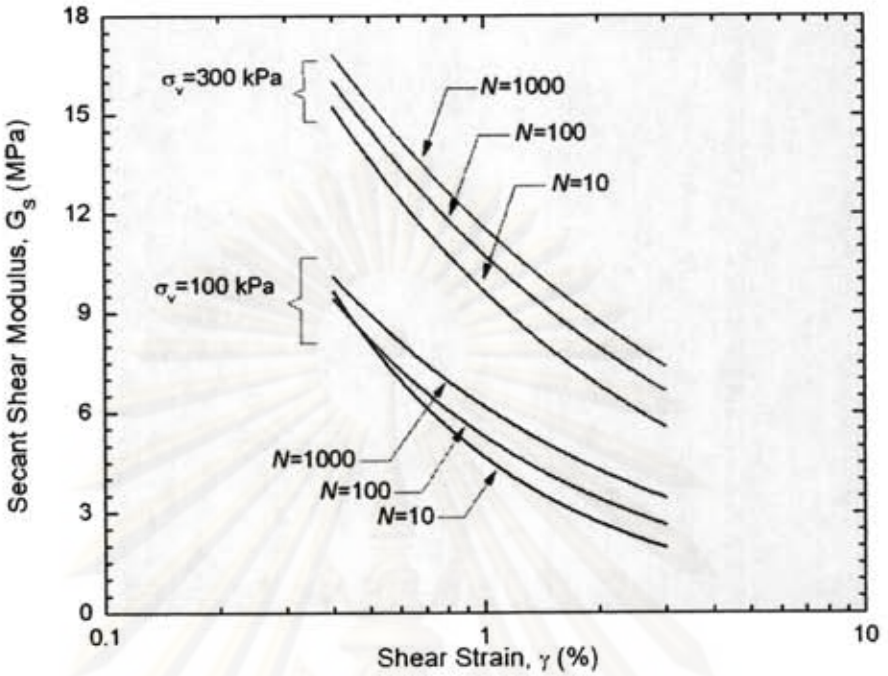

Figure 6-12 Effect of N on $G_S - \gamma$ relationship for $D_r \cong 40\%$ ($e_0 = 0.53$)

6.5.1.2 *River Sand in Case of Dense State*

Relationship between secant shear modulus (G_S) and number of cycles (N) for samples having relative density $D_r \cong 80\%$ is present in Figure 6-13. The similar trends are found as indicated in samples with $D_r \cong 80\%$. The value of G_S increases with increasing N for a given shear strain amplitude (γ) and vertical stress (σ_v). Figure 6-14 depicts $G_S - \gamma$ *relationship of* $RS - LS$ for samples with $D_r \cong 80\%$. There is a decrease in G_S with increasing γ and decreasing σ_v for N = 10, 100, and 1000. The effect of N on G_S – γ relationship for samples having $D_r \cong 80\%$ is illustrated in Figure 6-15. It is obvious that the increase of N in a range of 10 to 1000 slightly effect on secant shear modulus.

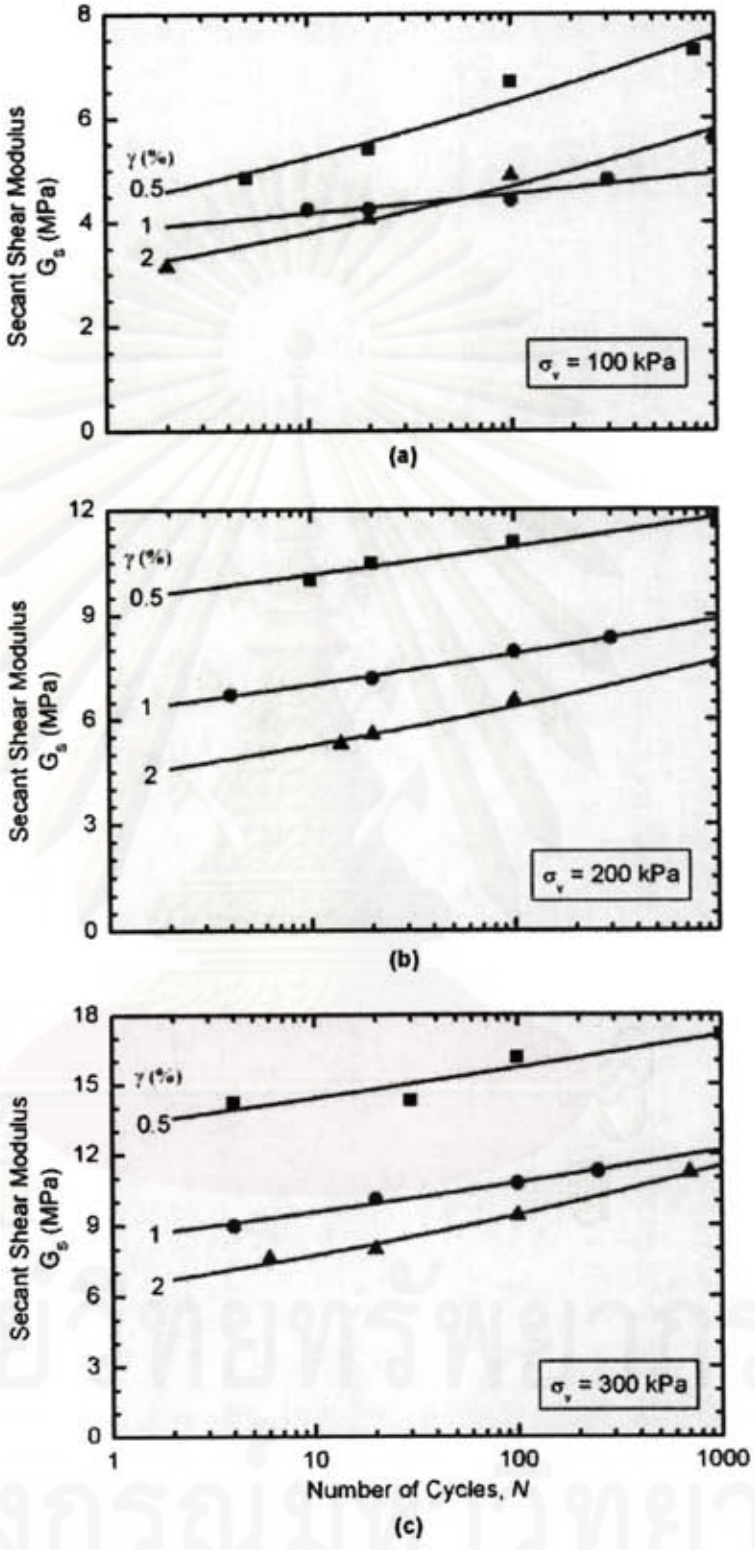

Figure 6-13 $G_S - N$ **relationship of RS-LS for** $D_r \cong 80\%$ $(e_0 = 0.44)$: (a) at $\sigma_v = 100\ kPa$; (b) at $\sigma_v = 200\ kPa$; (c) at $\sigma_v = 300\ kPa$

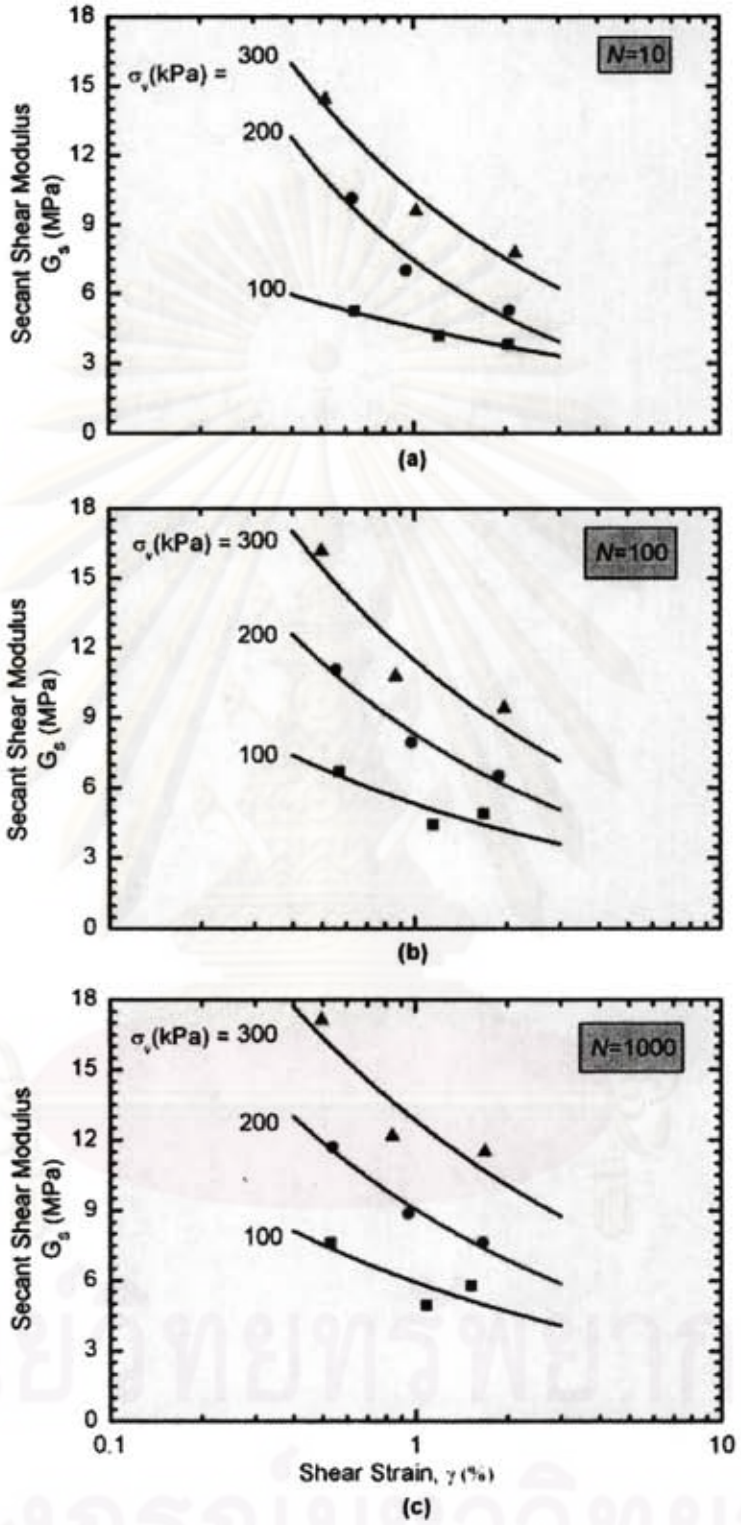

Figure 6-14 $G_S - \gamma$ ***relationship of*** $RS - LS$ **for** $D_r \cong 80\%$ $(e_0 = 0.44)$**: (a) at N = 10; (b) at N = 100; (c) at N = 1000**

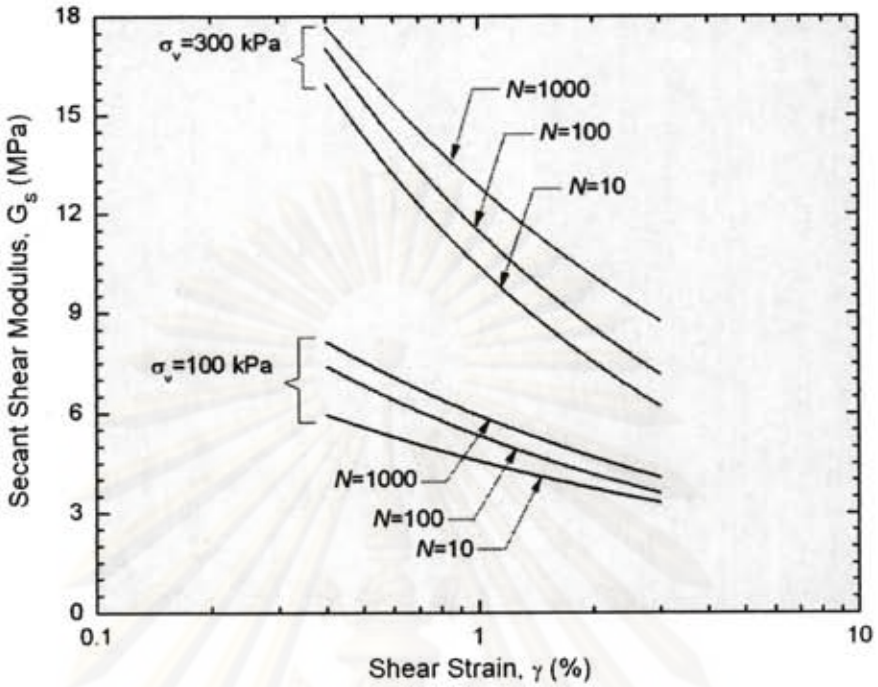

Figure 6-15 Effect of N on $G_S - \gamma$ relationship for $D_r \cong 80\%$

6.5.1.3 Comparision between G_S of RS-LS and RS-DS

The effect of D_r on $G_S - \gamma$ *relationship of RS* for different σ_v is shown in Figure 6-16. The solid curves and dot curves represent samples with $D_r = 40\%$ *and* $D_r = 80\%$, respectively. It can be seen that the trends of samples having $D_r = 40\%$ *and* $D_r = 80\%$ is similar for a given N. This tendency occurs in the entire range of vertical stress $\sigma_v = 100kPa$ *to* $300\ kPa$. Therefore, it can be concluded that the effect of D_r on G_S seem to be small if compared with other parameters such as σ_v *and* γ.

Figure 6-17 points out G_S plotted against σ_v on log-log scale for RS at different γ. On the left hand side, experimental data of cyclic drained DSS test is obtained from RS-LS; and on the right hand side, from RS-DS. It is evident from Figure 6-17 that relationship between G_S and λ can be expressed as a straight line on a log-log plot (Silver and Seed, 1971, Iwasaki et al., 1978, Seed et al. 1986, and Rollins et al., 1998). Such a relationship can be defined as

$$G_S = K_m \sigma_v^m$$

Where m = slope of line on the log-log plot and K_m = a constant

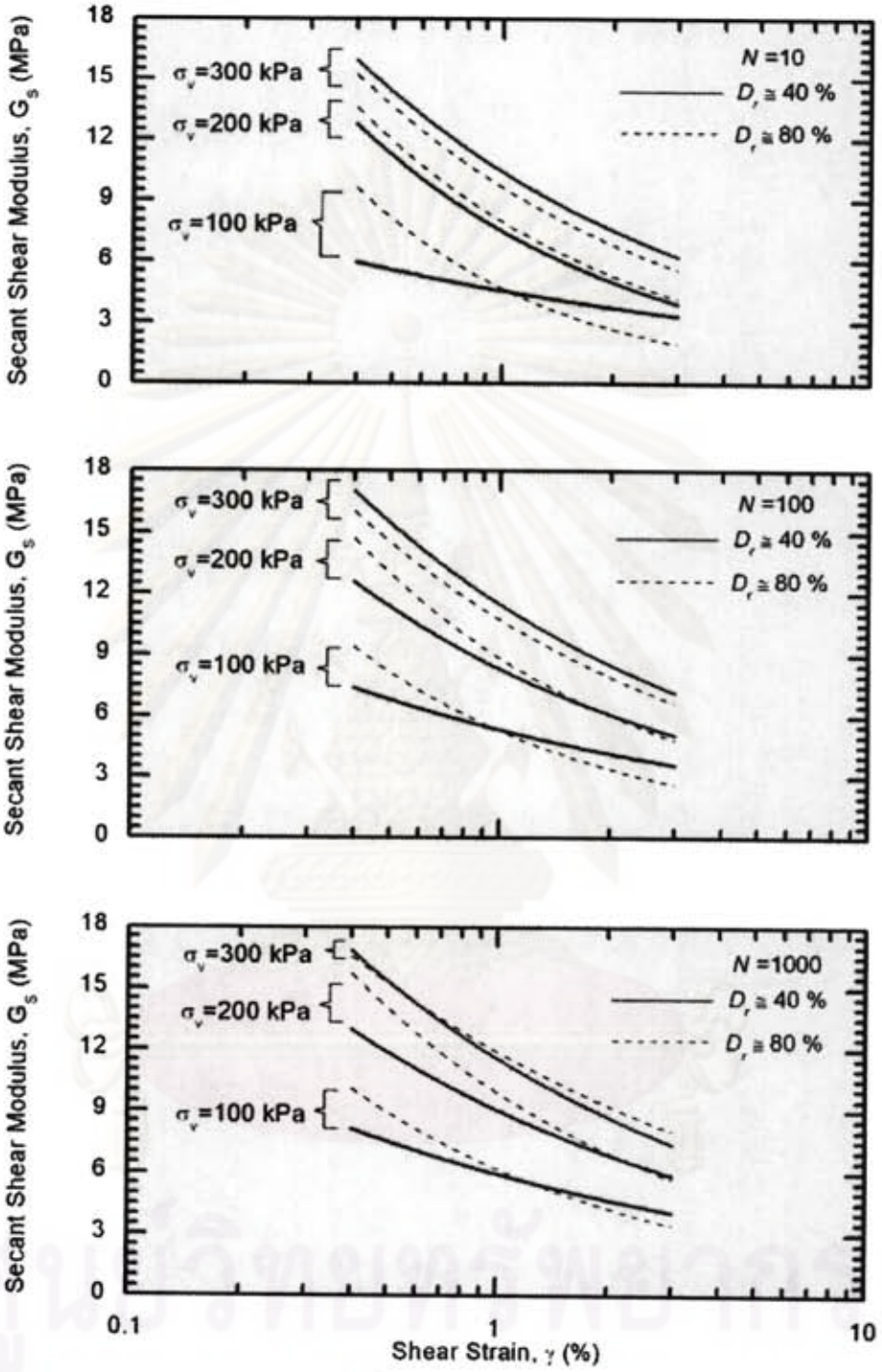

Figure 6-16 Effect of D_r on $G_S - \gamma$ *relationship of RS* for different σ_v

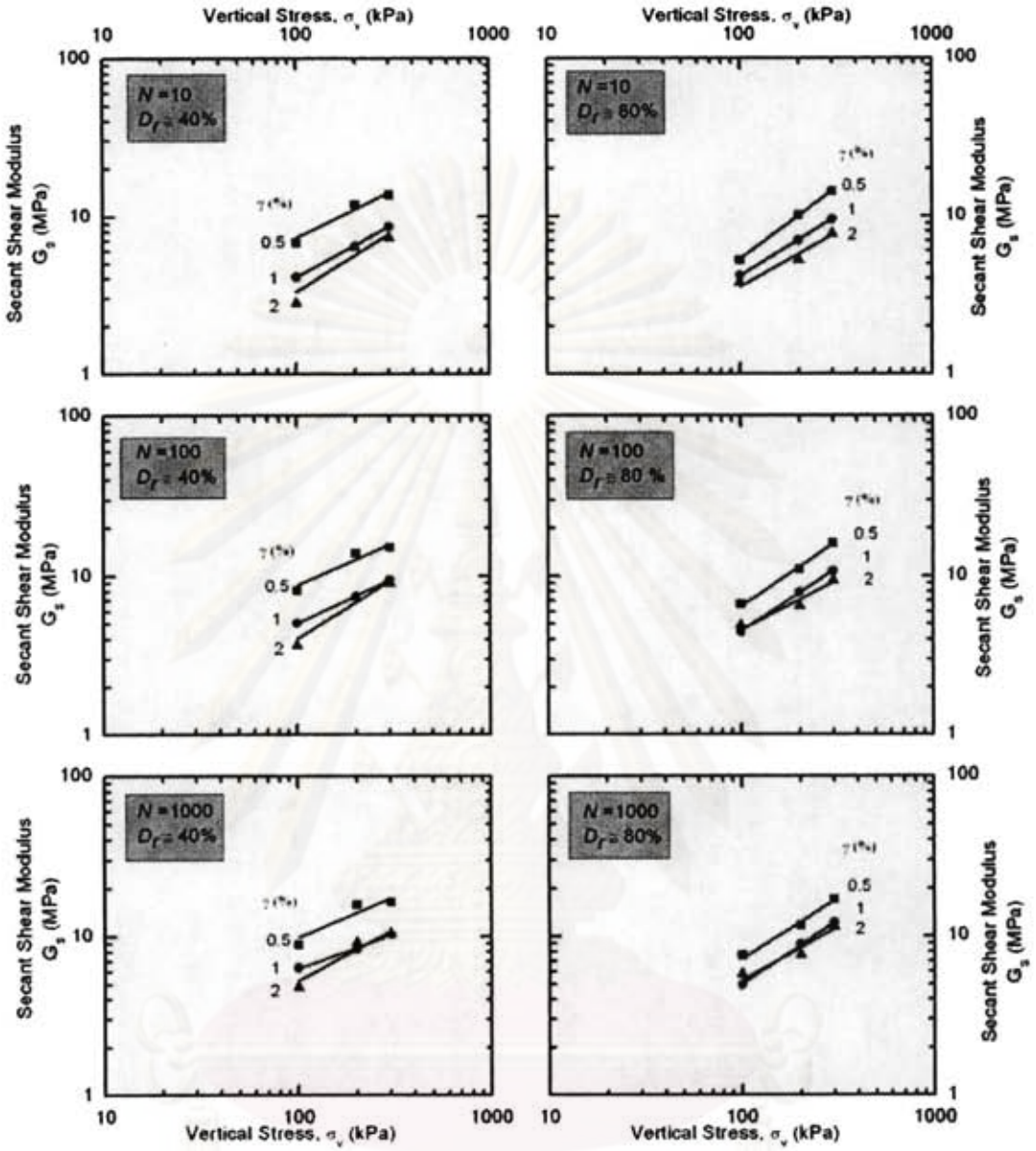

Figure 6-17 $G_S - \sigma_v$ *relationship at different* γ *and* D_r

In addition, from Figure 6-17, the effect of D_r on G_S for RS can also be observed in Figure 6-18. There is a slight difference between the trends with the same γ. This tendency occurs in the entire range of N. Thus, the effect of D_r does not significantly affect dynamic properties of Chiang Mai sand.

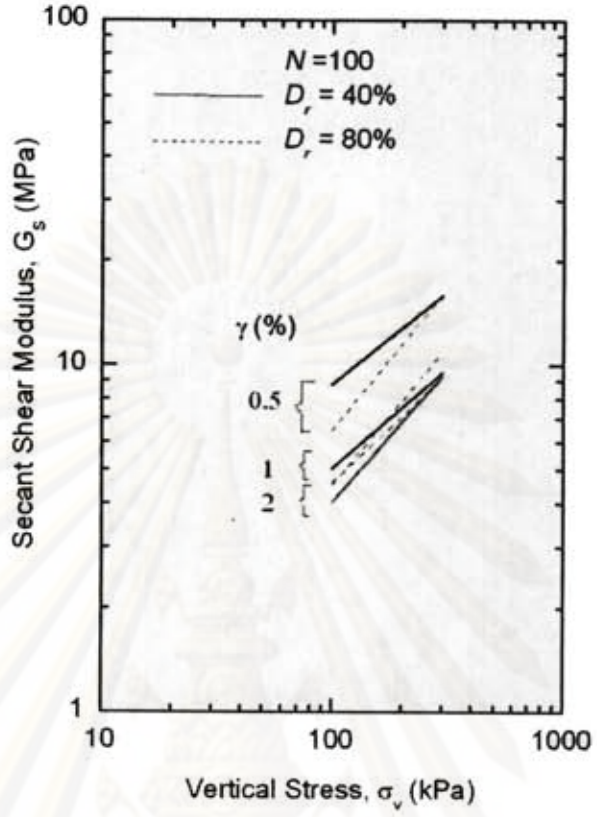

(a)

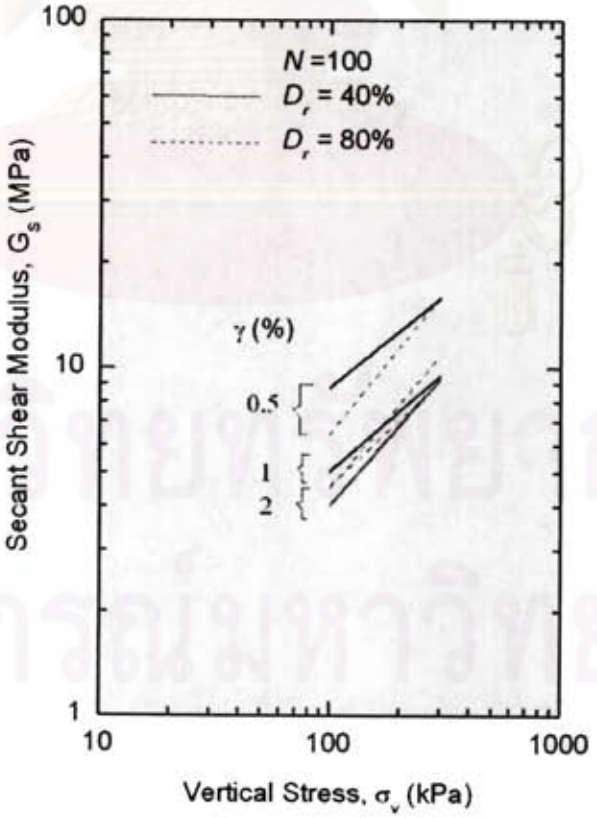

(b)

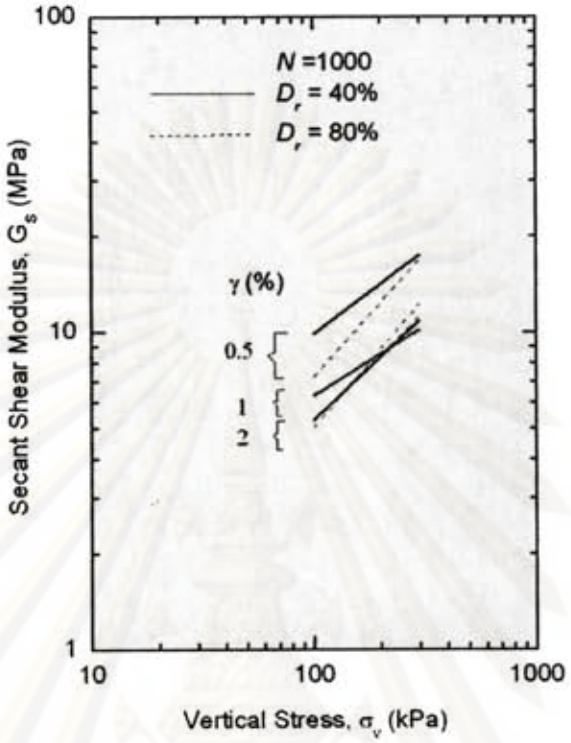

(c)

Figure 6-18 Effect of D_r on $G_S - \sigma_v$ relationship of RS

6.5.2 Damping ratio of RS: RS-D

After an interpretation of secant shear modulus from drained cyclic DSS test in foregoing section, the interesting results of viscous damping ratio will be interpreted and analyzed, based on previous researches (Silver and Seed,1971, and Vucetic et al., 1998). Comparison of these experimental results will be illustrated in following chapter.

Hysteretic damping ratio (λ) is plotted against number of stress cycles (N) in the simple shear test carried out at a relative density of D_r = 40%, as shown in Figure 6-19. Similar data and trends are found in Figure 6-20 plotted as λ versus N in samples having D_r = 80%. It can be seen that the value of λ decreases with increasing N for the range of vertical stress (σ_v) included in the test program.

The effect of D_r on λ-γ relationship at different σ_v for RS is illustrated in Figure 6-21 to 6-23. Although the experimental data are slightly scattered, these data strongly confirm that λ is likely to be independent of relative density, as proposed by Silver and Seed (1971). The cause of data scattering is probably because of the effect of plasticity index of sand (PI = 0), reported by Vucetic (1998). In addition, it can be observed that there is a decrease in λ with increasing γ in the entire range of σ_v selected in the research study.

Similar data plots from Figure 6-21 to 6-23 is summarized in Figure 6-24. The effect of σ_v on $\lambda - \gamma$ relationship of RS can be observed. It is obvious that for a given γ, calculated values of damping ratio (λ) decreases as vertical stress (σ_v) increases. Likewise, Figure 6-25 exhibits the summary of experimental results from Figure 6-21 to 23 by noticing the effect of N on $\lambda - \gamma$ relationship of RS. It can be concluded that λ decreases with increasing N in the entire range of σ_v. The tendency to reduce damping ratio is important for ground shaking analysis. It is usually convenient to use an average damping ratio in N = 10 according to various researchers (Iwasaki et al., 1978, Seed et al., 1986, Rollins, K. M. et al., 1998, Zhang, J., 2005).

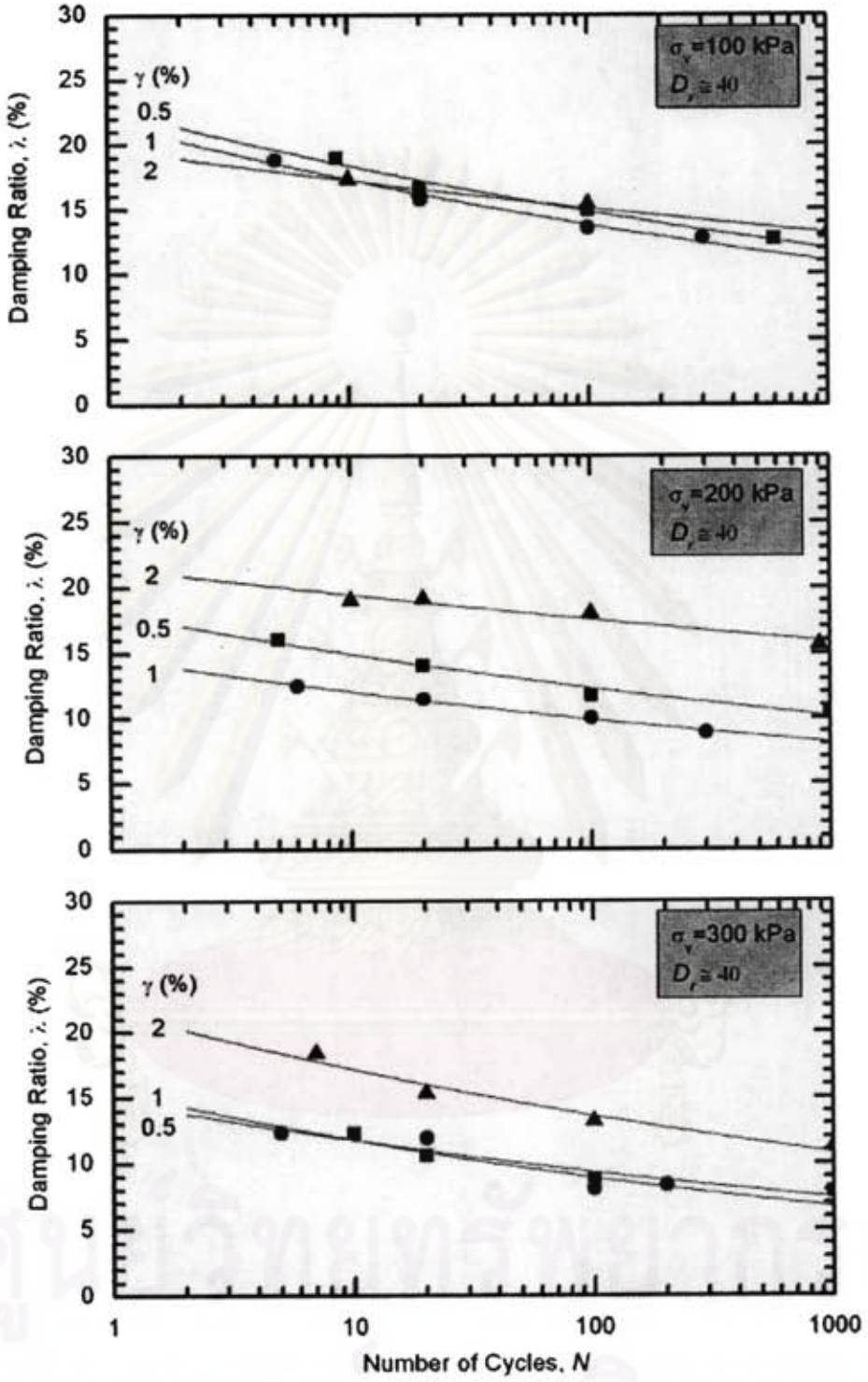

Figure 6-19 $\lambda - N$ **relationship of RS at** $D_r = 40\%$ $(e_0 = 0.53)$

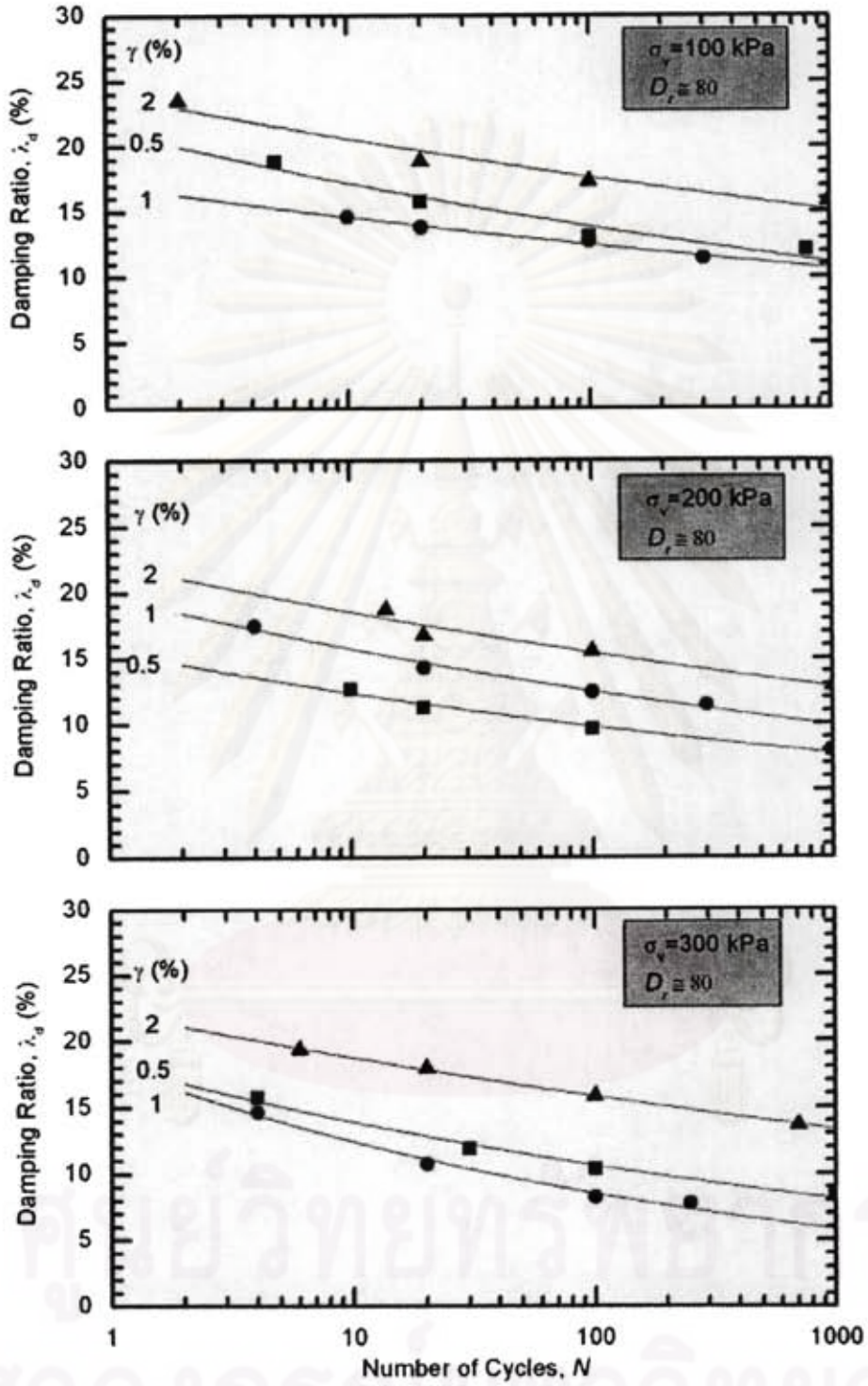

Figure 6-20 $\lambda - N$ **relationship of RS at** $D_r = 80\%$ $(e_0 = 0.44)$

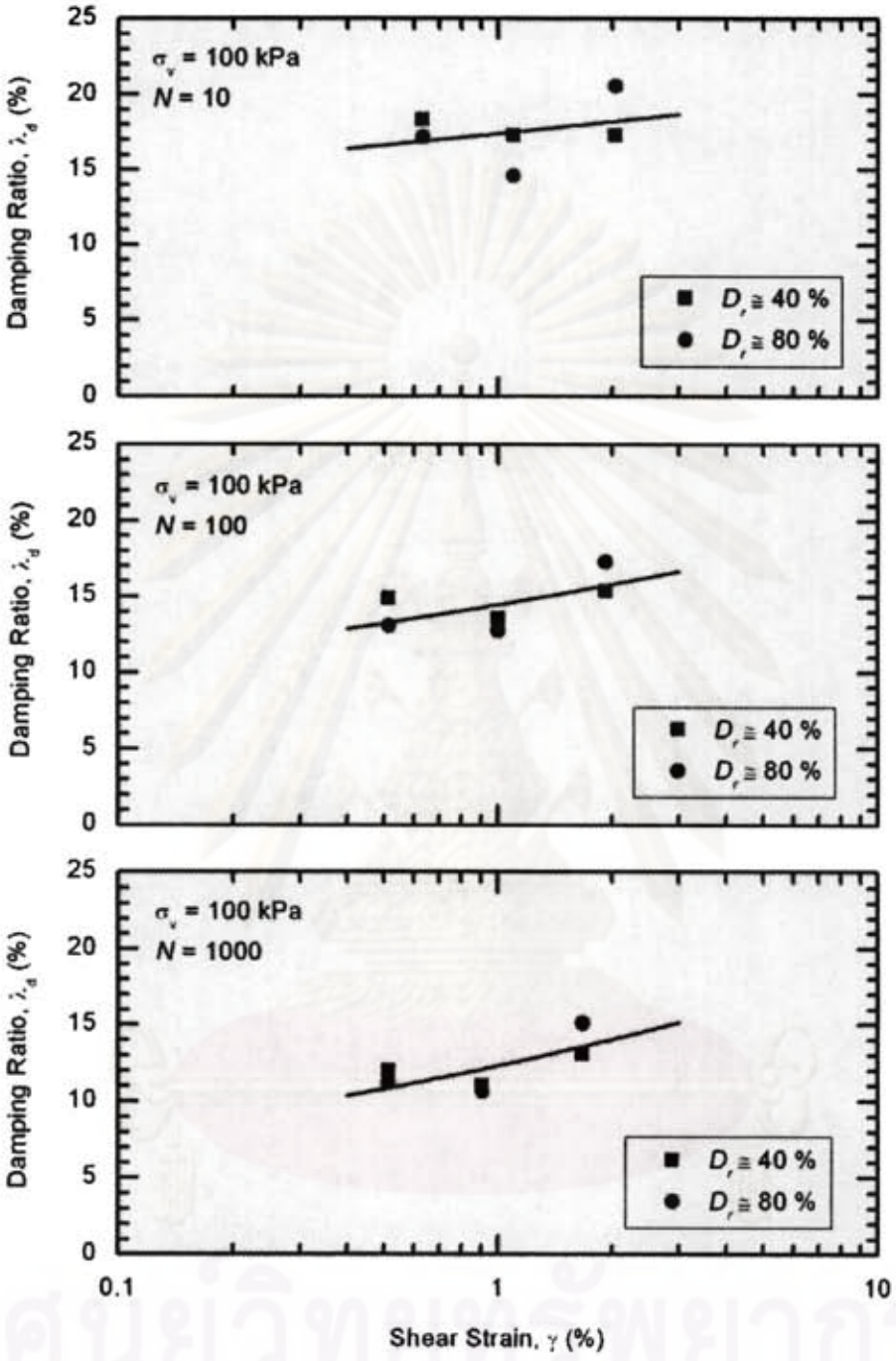

Figure 6-21 Effect of D_r on $\lambda - \gamma$ relationship of RS at $\sigma_v = 100\ kPa$

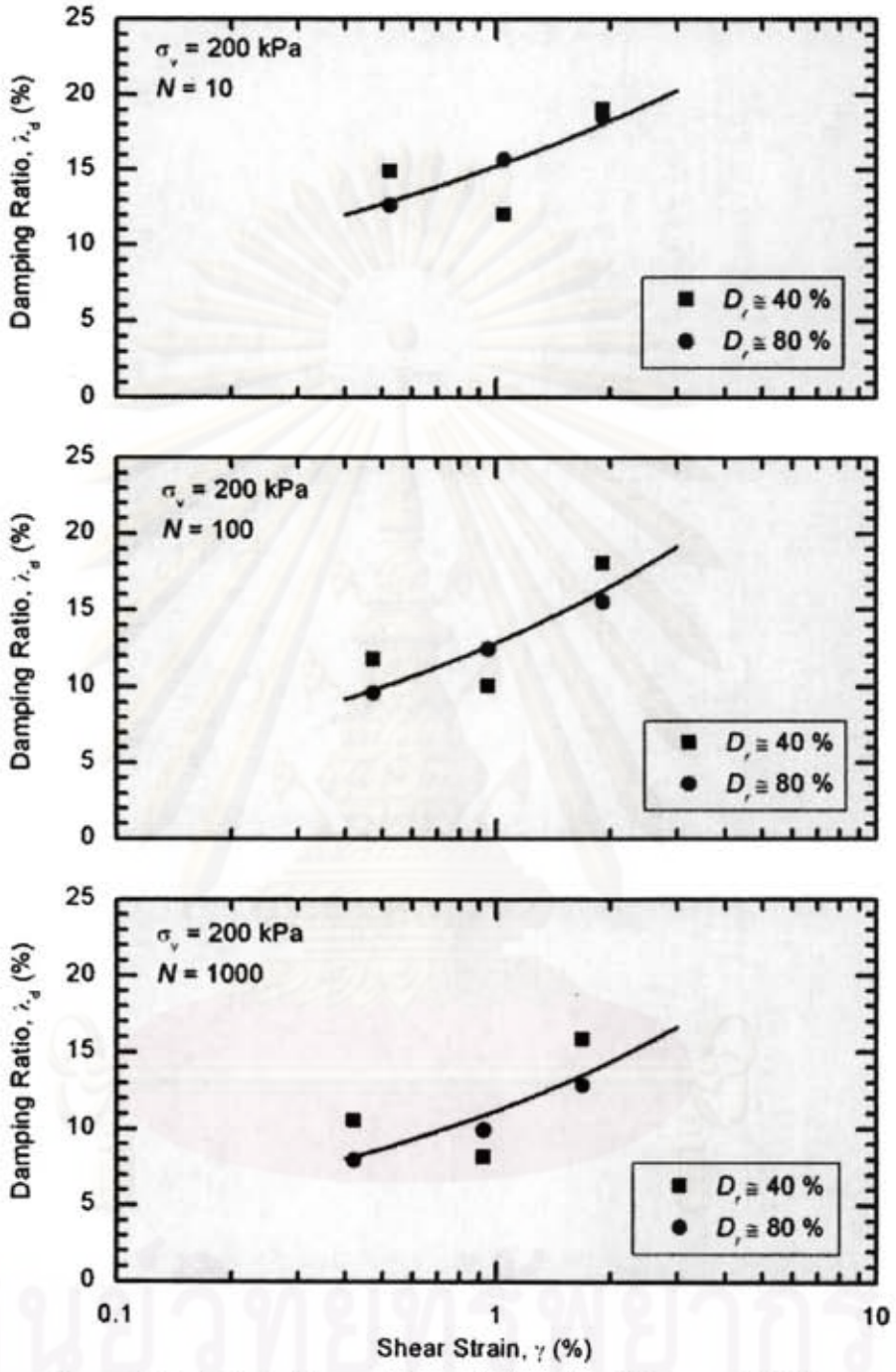

Figure 6-22 Effect of D_r on $\lambda - \gamma$ relationship of RS $\sigma_v = 200\ kPa$

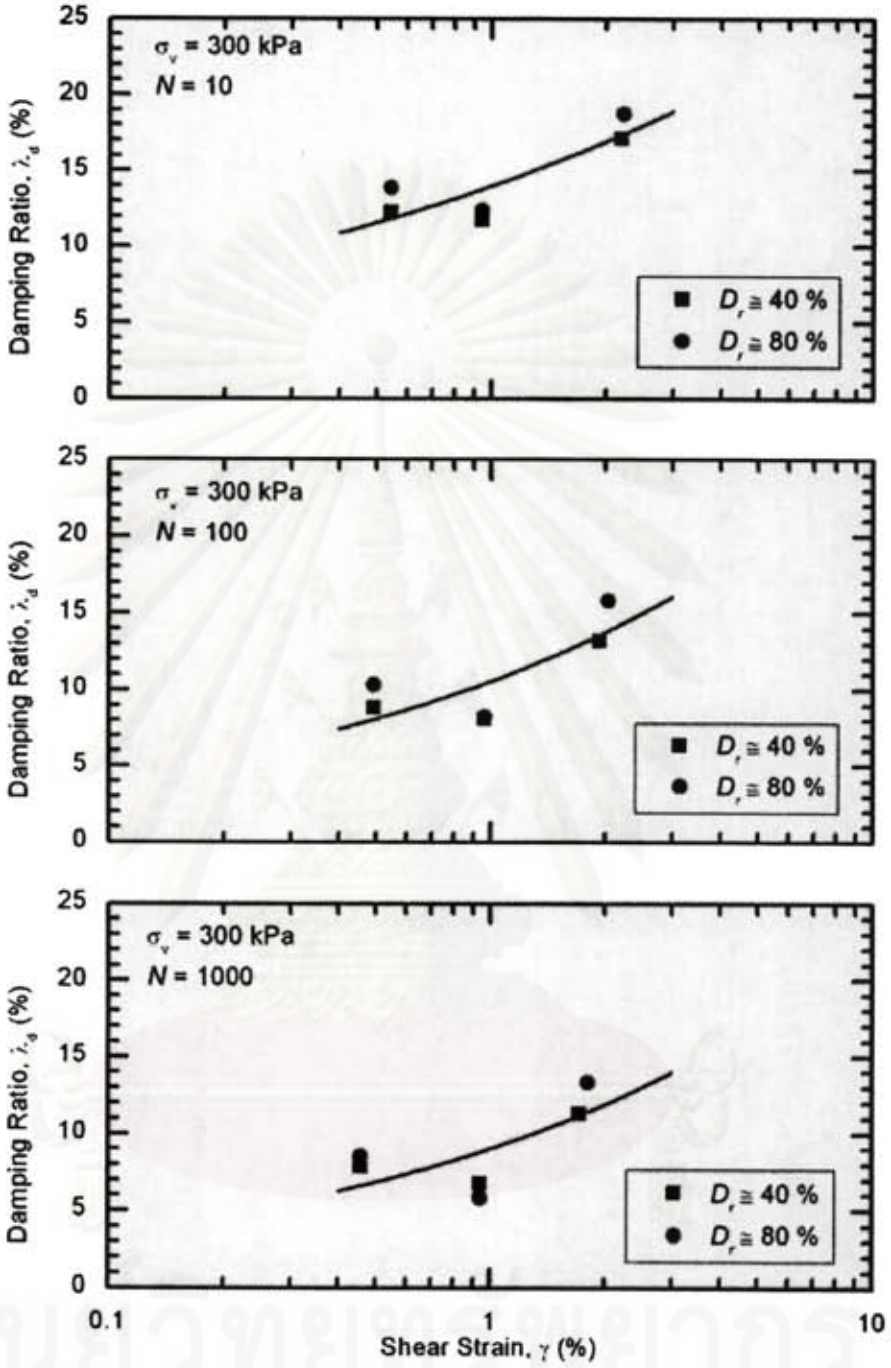

Figure 6-23 Effect of D_r on $\lambda - \gamma$ relationship of RS at $\sigma_v = 300\ kPa$

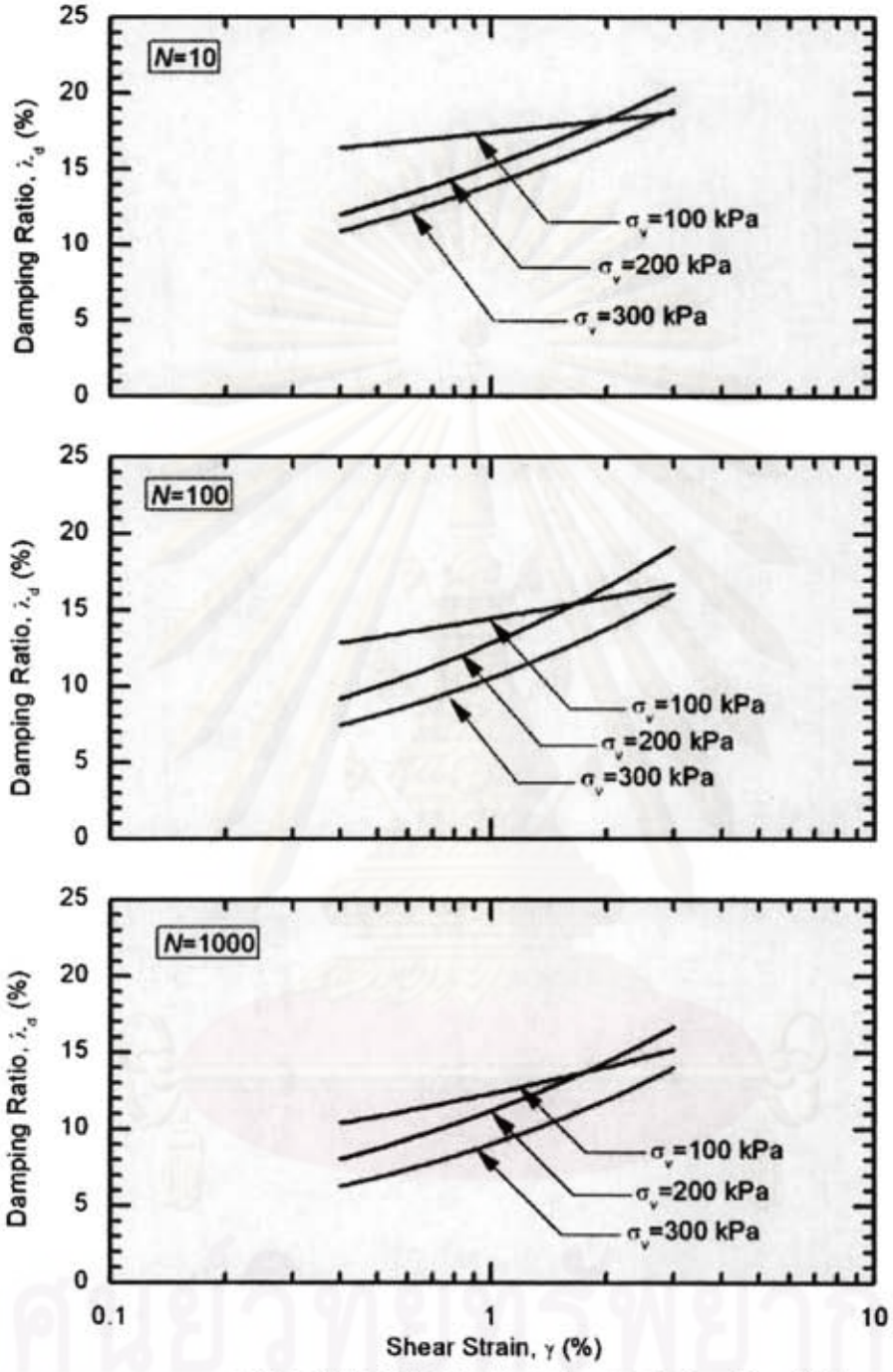

Figure 6-24 Effect of σ_v on $\lambda - \gamma$ relationship of RS

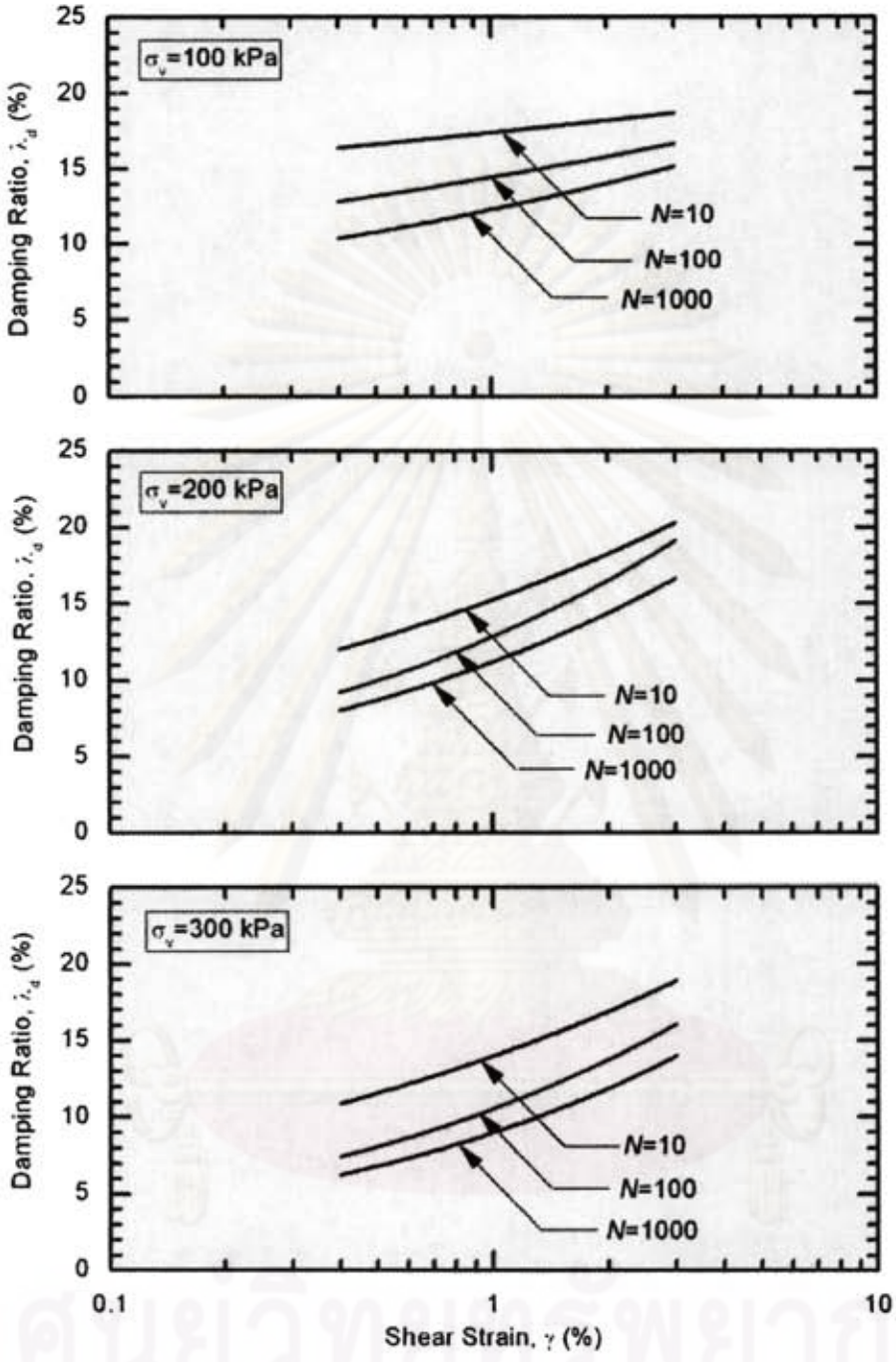

Figure 6-25 Effect of N on $\lambda - \gamma$ relationship of RS

CHAPTER VII

CONCLUSION AND RECOMMENDATION

7.1 Conclusion

This thesis research mainly aims to present an assessment of dynamic properties of Chiang Mai sand using cyclic direct simple shear test. Nevertheless, supplementary investigation of monotonic direct simple shear test is carried out to have more understanding of static response of Chiang Mai sand.

According to the experimental results from monotonic test in Chapter V, it can be inferred that:

1. Effective friction angle at critical state from River sand for loose state and dense state is found to be similar for the same test condition (e.g., drained or undrained).
2. Effective critical state friction angle from DSB test is similar to that from drained DSS test, but larger than that from undrained DSS test. It is consistent with previous researchers (Airey, D.W., 1985, and Atkinson et al., 1990).

On the other hand, in cyclic DSS test, relative density, vertical stresses, shear strain amplitude, and frequency are varied to observe their effect on sand dynamic properties. It can be concluded from the testing results that:

1. Secant shear modulus increases as number of stress cycles increases. However, damping ratio decreases with increasing number of cycles.
2. There is a decrease in shear modulus with increasing shear strain amplitude in the range of vertical stress used in the tested program. On the contrary, damping ratio increases with increasing shear strain amplitude.
3. It is evident from the interpretation in Chapter VI that the effect of relative density as well as number of cycles on dynamic properties of sand is found to be small, if compared to that of shear strain amplitude and vertical stress.
4. Dynamic properties of sands are likely to be significantly dependent of vertical stress and shear strain amplitude. Shear modulus increases with

increasing vertical stress. The value of hysteretic damping ratio decrease with increasing value of vertical stress.

5. Relationship between secant shear modulus and vertical stress can be expressed as a straight line on a log-log plot. This is in good agreement with Silver & Seed (1971), Iwasaki et al. (1978), Seed et al. (1986), and Rollins et al. (1998).

7.2 Comparison of Present study

While the measured secant shear modulus and damping ratio values obtained from DSS test are consistent in themselves, it is of interest to compare the testing results with values obtained by other investigators using different techniques. Such a comparison is shown in Section 7.2.1 and 7.2.1.

7.2.1 With Field Tests

As to previous investigations of SPT, Downhole test, and MASWM in Wat Chedi Luang at depth of approximately 15 m, in-situ maximum shear modulus can be figured out from Equation (2-1) to (2.4), as summarized in Table 7-1. It can be seen from Table 7-1 that maximum shear modulus value from Downhole test is the biggest and that from MASWM is the smallest. In chapter VI, the secant shear modulus from cyclic DSS test at $N = 10$ and $\gamma = 0.5\%$ for Wat Chedi Luang dense sand is found to be approximately equal to 15 MPa. If compared with three foregoing field test results of modulus, it is clear that the secant shear modulus value from present study is equal to 9.6% of that from SPT, 7.6% of that from Downhole test, and 11% of that from MASWM.

Table 7-1 Maximum shear modulus from three different field tests

Type of field tests	Shear wave velocity V_S (m/s^2)	N-Values	Maximum shear modulus G_{max} (MPa)
SPT		> 50	155
Downhole test	313		196
MASWM	261		136

7.2.2 With Laboratory Tests

Due to the lack of experimental data of dynamic sand properties in Chiang Mai, the tested sand will compared with Toyoura sand from Japan and Silica No. 20 sand from America.

Figure 7-1 exhibits the comparison of the present study data with previous study data on secant shear modulus (G_S) of sand at N = 10. The data of Chiang Mai sand from DSS test, Crystal silica No. 20 sand from NGI DSS test (Silver & Seed, 1971), and Toyoura sand from Torsional shear test (Iwasaki, 1978) are plotted as G_S versus γ. Grain size distribution curves of two latter sands are also shown in Figure B-5. It is obvious that G_S of the present study is noticeably smaller than that of previous researchers, as shown in Figure 7-1. The reason is that shear strain amplitude of 0.003% and 0.25 % used in TS and NGI DSS test of previous study is lower than that of 0.5%-2% performed in cyclic NGI DSS test of present investigation on Chiang Mai River sand. This is in consistency with Silver & Seed (1971).

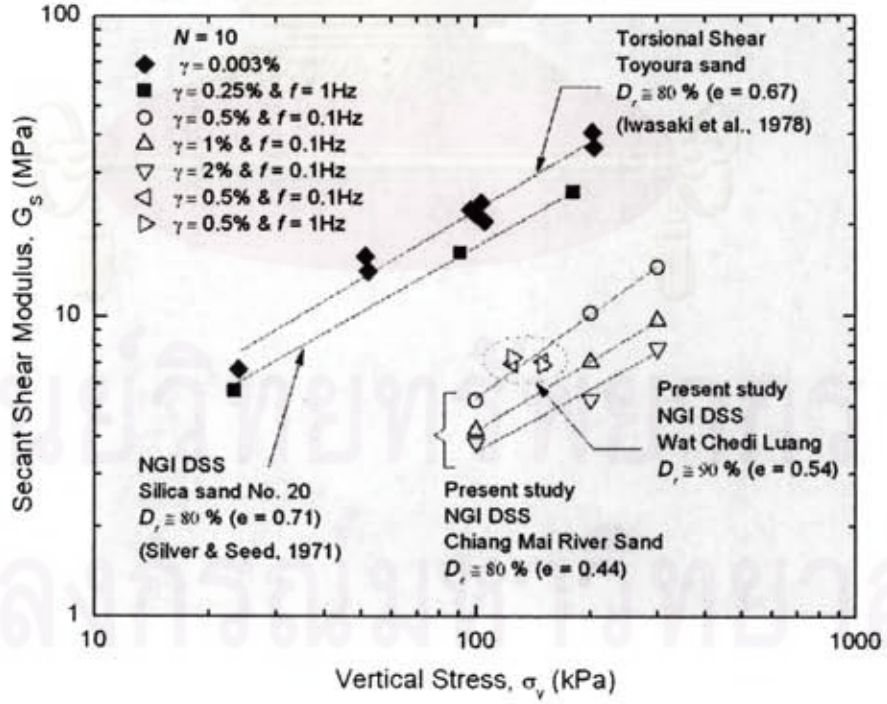

Figure 7-1 Comparison between secant shear modulus

In addition to comparison of shear modulus, data of 10 investigators on damping ratio are plotted in Figure 7-2. Seed et al. (1986) proposed the range of data for sand, for which the average solid line is presented by DSS data, and upper and lower bound dot lines are from various tests at $N = 10$. Damping ratio (λ) of all kinds of sands regardless of particle size and relative density will be in that proposed range. In accordance with experimental results plotted in Figure 7-2 as open triangle and rectangle symbols for RS and WS, respectively, they remain a bit lower than the lower bound of proposed data range for sands. This is in fair agreement with what Seed et al. (1986) suggested.

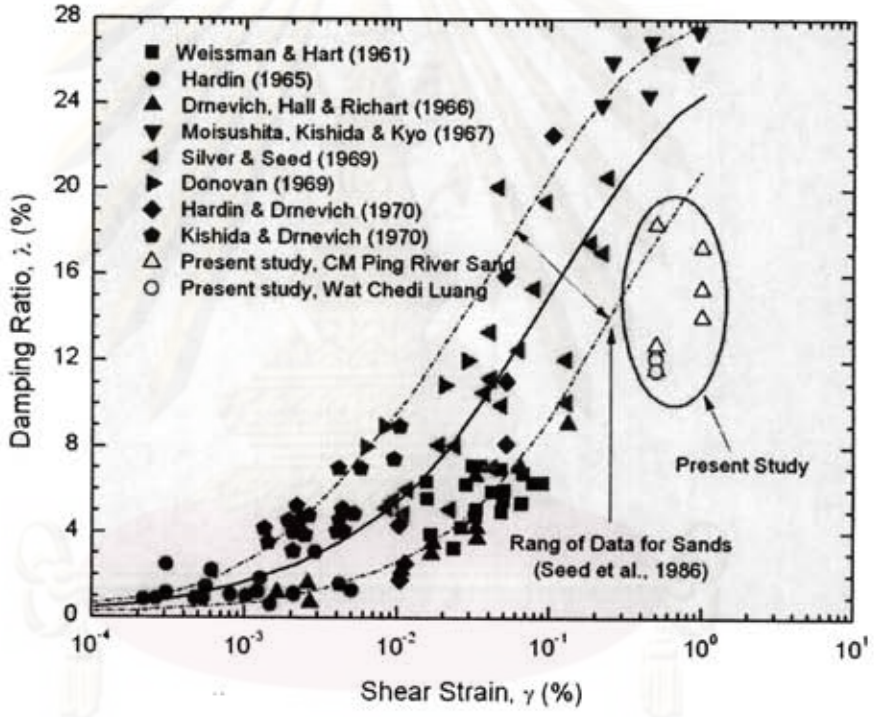

Figure 7-2 Comparison between damping ratio

7.3 Recommendation

As mentioned in previous chapter, the ability of modified cyclic NGI DSS apparatus to conduct the experiment in present study is limited. Only large shear strain amplitude higher than 0.5% can be used. It is impossible to perform the DSS test on small shear strain amplitude. Therefore, following researchers interested in DSS test should improve the DSS apparatus ability to carry out on small shear strain. Besides, the higher frequency should be varied to observe the effect on dynamic sand properties.

REFFERENCES

ASTM D422. (1998). Standard test method for particle-size analysis of soils. ASTM International, West Conshochocken.

ASTM D854. (1998). Standard test method for specific gravity of soils. ASTM International, West Conshochocken.

ASTM D4253. (1998). Standard test methods for maximum index density and unit weight of soils using a vibratory table. ASTM International, West Conshochocken.

ASTM D4254. (1998). Standard test method for minimum index density and unit weight of soils and calculation of relative density. ASTM International, West Conshochocken.

ASTM D2487. (1998). Standard practice for classification of soils for engineering purposes (Unified Soil Classification System). ASTM International, West Conshochocken.

ASTM D3080-98. (2006). Standard test method for direct shear test of soils under consolidation drained conditions. ASTM International, West Conshochocken.

ASTM D6528-00. (2006). Standard test method for consolidated undrained direct simple shear testing of cohesive soils. ASTM International, West Conshochocken.

Bassett, R. H. (1967). The behavior of granular materials in the simple shear apparatus. Ph. D. thesis, University of Cambridge.

Bjerrum, L. & Landva, A. (1966). Direct simple shear tests on a Norwegian quick clay. Geotechnique 16(1): 1-20.

Budhu, M. (2007). Soil mechanics and foundations. Jonh Wiley & Sons, Hoboken.

Carter, J. P., Airey, D. W., & Fahey, M. (2000). A review of laboratory testing of calcareous soils. Proc. 2nd Int. Conf. Engng Calcareous Sediment Bahrain 2: 401-431

Castro, G. & Poulos, S.J. (1977). Factors affecting liquefaction and cyclic mobility. Journal of the Geotechnical Engineering Division, ASCE 106(GT6): 501-506.

Duku, P. M., Stewart, J. P., Whang, D. H. & Yee, E. Y. 2008. Volumetric strains of clean sands subject to cyclic loads. J. Geotech. Geoenviron. Eng. 134(8): 1073-1085.

Iwasaki, T., Tatsuoka, F. & Takagi, Y. (1978). Shear moduli of sands under cyclic torsional shear loading. Soils Found. 18(1): 39-56.

Kokusho, T., Tohma, J., Yajima, H., Tanaka, Y., Kanatani, M., and Yasuda, N. (1994). Seismic response of soil layer and its dynamic properties. Proc., 10th world Conf. on Earthquake Engrg 11: 6671-6680.

Palasri, C. & Ruangrassamee, A. (2008). Relations among shear wave velocity, SPT N-value and undrained shear strength of soil in Bangkok and the north of Thailand. Proc., 14th National Convention on Civil Engineering (14th NCCE), Nakhon Ratchasima, Thailand: 83-88

Peacock, W.H. & Seed, H. B. (1968). Sand liquefaction under cyclic loading simple shear conditions. J. SMFD, Proc. ASCE 94(SM3): 689-708.

Porcino, D., Caridi, G. & Ghionna, V. N. (2008). Undrained monotonic and cyclic simple shear behavior of carbonate sand." Geotechnique 58(8): 635-644

Rollins, K. M., Evans, M. D., Diehl, N. B. & Daily III, W. D. (1998). Shear modulus and damping relationships for gravels. J. Geotech. Geoenviron. Eng. 124(5): 396-405.

Roscoe, K. H. (1953). An apparatus for the application of simple shear to soil samples. Proc., 3rd International Conference on Soil Mechanics and Foundations Engineering, Zurich 1: 186-191.

Roscoe, K. H. (1970). The influence of strains in soil mechanics. Tenth Rankine Lecture. Geotechnique 20(2): 129-170.

Seed, H. B., Wong, R. T., Idriss, I. M. & Tokimatsu, K. (1986). Moduli and damping factors for dynamic analysises of cohesionless soils. J. Geotech. Engrg., ASCE, 112(11), 1016-1032.

Seng, S. & Boonyatee, T. (2008). Application of multichannel analysis of surface wave to shallow site investigation for subsoil in Thailand. Master thesis, Chulalongkorn University, Thailand.

Silver, M. L. & Seed, H. B. (1971). Deformation characteristics of sands under cyclic loading. J. SMFD, Proc. ASCE 97(SM8): 1081-1098.

Vaid, Y. P., Stedman, D., & Sivathayalan, S. (1999). Influence of specimen-reconstituting method on the undrained response of sand. Geotech. Testing J. 22(3): 187-195

Vucetic, M. (1993). Cyclic Threshold Shear Strains of Sands and Clays. Research Report, UCLA Dept. of Civil Engineering.

Vucetic, M., Lanzo, G. & Doroudian, M. (1998). Damping at small strains in cyclic simple shear test. J. Geotech. Geoenviron. Eng. 124(7): 712-728.

APPENDICES

APPENDIX A

Table A-1 Soil profiles of Wat Chedi Luang subsoil in Chiang Mai (KEC boring log report)

Soil Types	Depth (m)	Unit Weight (t/m^3)	Water Content (%)	SPT N-value
Crust	0 - 1	2.04	12	28
Stiff Clay	1 - 2.5	2.08	16.67	13
Medium Sand	2.5 - 6	2.06	12.67	25
Very Stiff Clay	6 - 13	1.95	22	26
Very Dense Sand	13 - 21.4	2.06	15.2	>50

Table A-2 Correction factors for rod length, sampler type, and borehole size (Skepton, 1986)

Correction factor	Item	Correction factor
	Rod length (below anvil)	
	$\geq 10m$	1
η_R	6-10m	0.95
	4-6m	0.85
	3-4m	0.70
	Standard sampler	1.0
η_S	U.S sampler without liners	1.2
	Borehole iameter:	
	65-115mm	1.0
η_B	150mm	1.05
	200mm	1.15

Table A-3 Correlation of N, N60, γ, Dr, and $\emptyset'$ for coarse-grained soils (Budhu, 2007)

N	N_{60}	Compactness	$\gamma(kN/m^3)$	D_r (%)
0-4	0-3	Very loose	11-13	0-20
4-10	3-9	Loose	14-16	20-40
10-30	9-25	Medium	17-19	40-70
30-50	25-45	Dense	20-21	70-85
>50	>45	Very dense	>21	>85

APPENDIX B

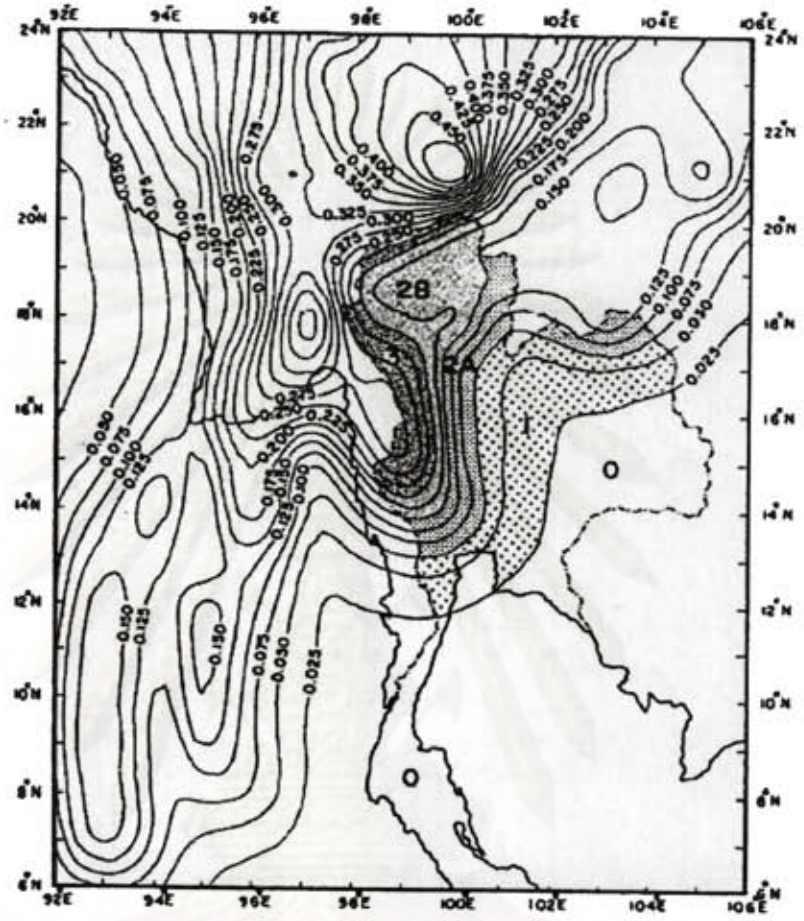

Figure B-1 Seismic source zones in Thailand and vicinity (Nutalaya et al. 1985).

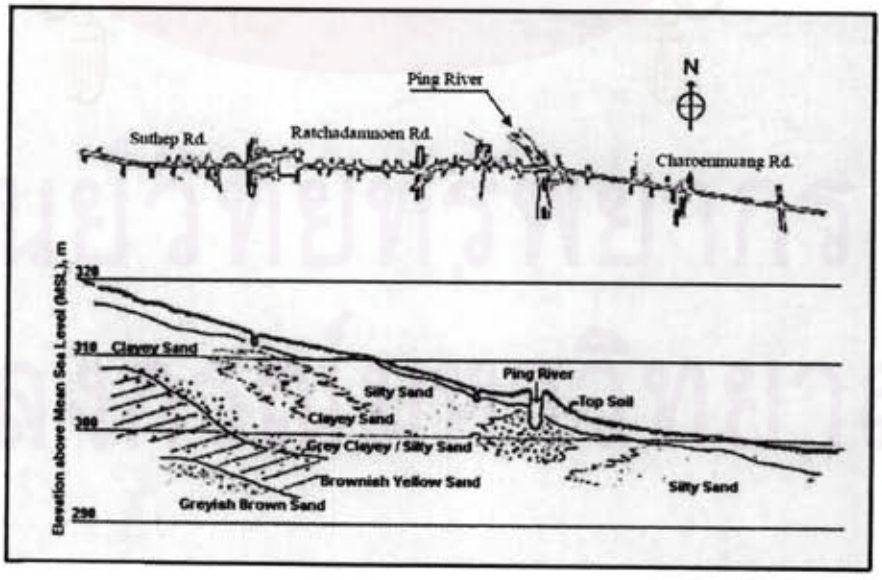

Figure B-2 Typical subsoil section in Chiang Mai Province (modified from Anantasech and Thanadpipat, 1985)

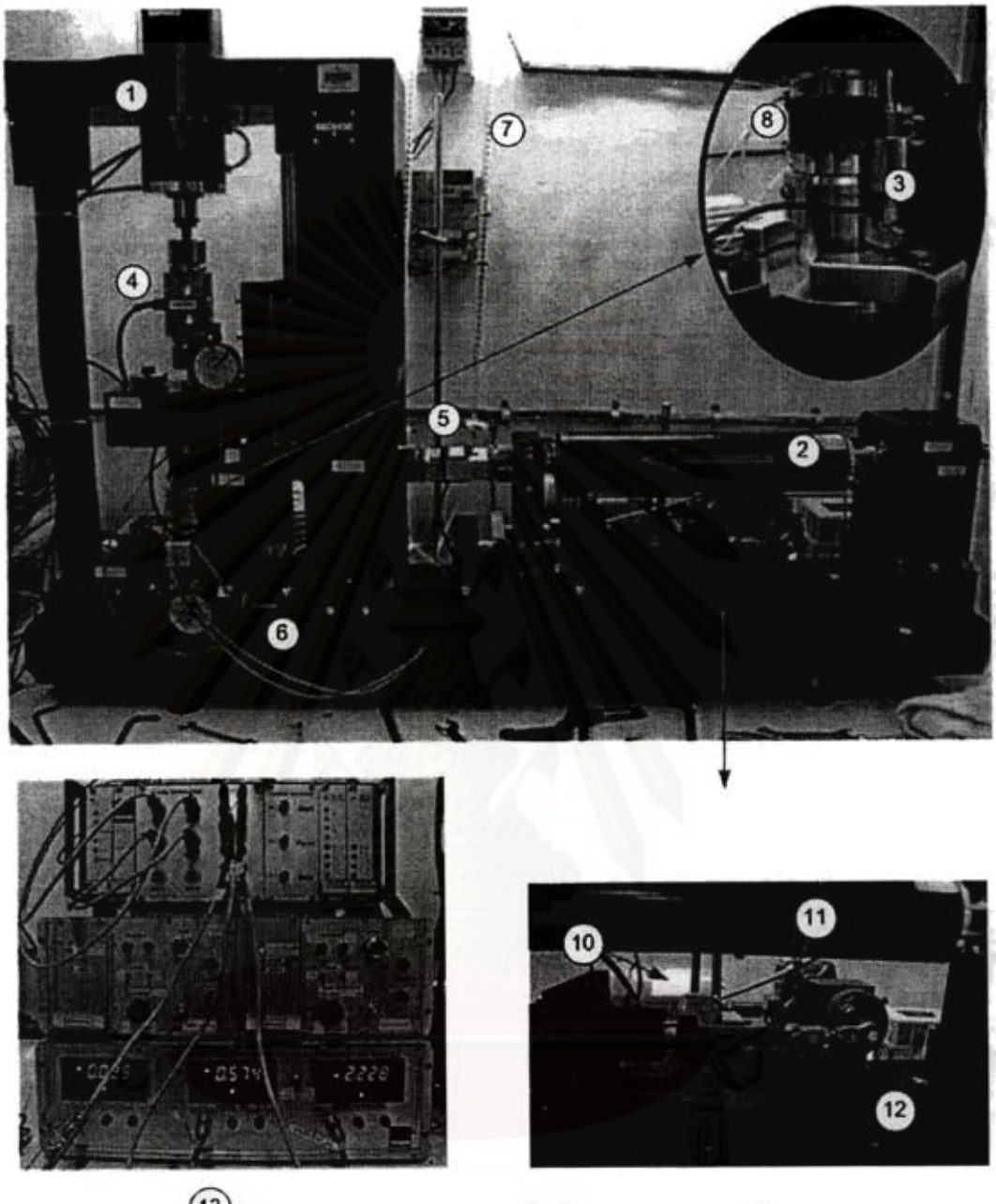

Figure B-3 Detail of DSS apparatus

1. Vertical load cell
2. Horizontal load cell
3. LVDT
4. Vertical force tranducer
5. Horizontal force tranducer
6. Horizontal diagauge
7. Water Burette
8. Specimen placed in DSS apparatus
9. A set of cyclic motors
10. Motor
11. Motor gear
12. E-motor
13. Data acquisition system

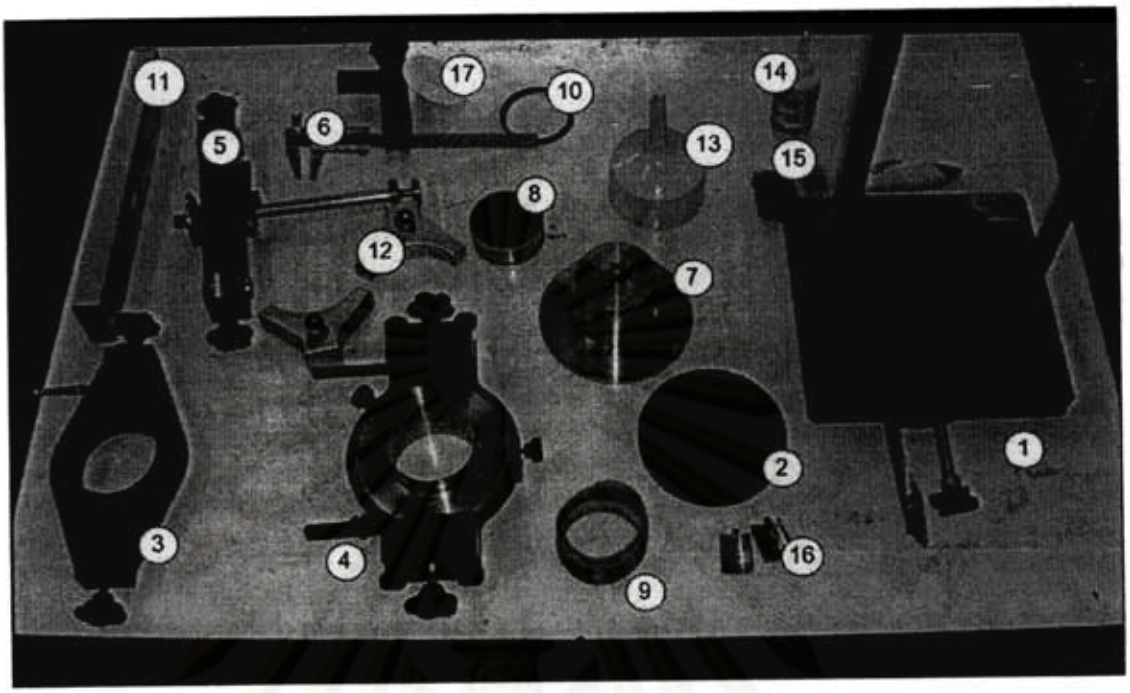

Figure B-4 Trimming tools of DSS apparatus to prepare samples

1. Turntable
2. Dummy pedestal
3. Membrane expander yoke
4. Cutter yoke
5. Top yoke
6. Meter
7. Sample pedestal
8. Filter holder with porous stone
9. Reinforced rubber membrane
10. O-ring
11. Level
12. Nuts fixing sample pesdestal
13. Funnel
14. Oil
15. Brush
16. Nuts fixing sample pesdestal with bottom filter holder
17. Porous paper

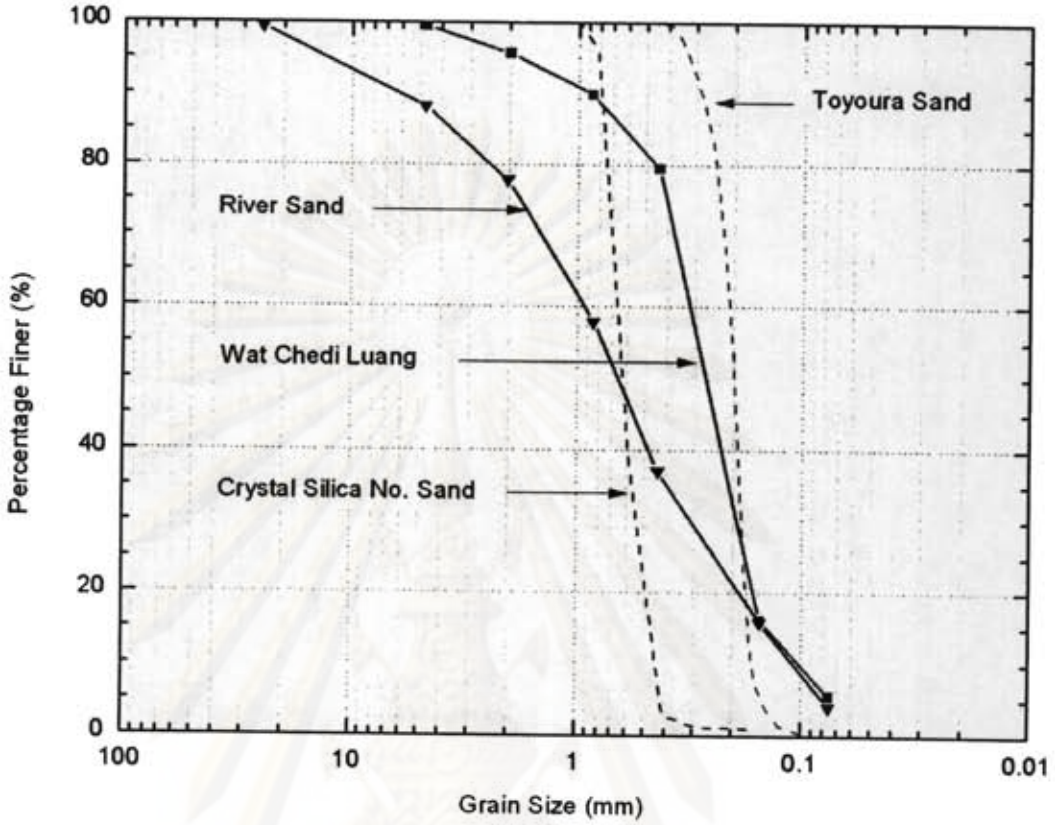

Figure B-5 Grain size distribution curves of tested soils

BIOGRAPHY

Soksan Thay

Soksan Thay was born on July, 07 1984 in Pursat Province, Western part of Cambodia. After he finished high school at Pursat High School in 2002, he took the university entrance and passed the exam to study Bachelor's degree of Civil Enigeering at Institute of Technology of Cambodia (ITC) for 5 years. During the last year of his degree, he applied for the scholarship to study Master's Degree Program under support of AUN/SEED-Net (JICA). Shortly, after his successful graduation in June 2007, he attained the scholarship award for further study in Master's program in Civil Engineering department at Chulalongkorn University, Thailand. He already submitted two proceedings: the 14th National Convention on Civil Engineering (14th NCCE) and the 22nd KKCNN Symposium, Thailand. This thesis is a partial fulfillment of the requirements for the degree.